UCLouvain

École polytechnique de Louvain

Introduction to the Thermal Behavior of a CubeSat

Author: **Julien Defauw**
Supervisors: **Marc Bekemans, Antoine Delille**
Readers: **Hervé Jeanmart, Caroline Leroi**
Academic year 2018–2019
Master [120] in Electro-mechanical Engineering

Remerciements

Premièrement, je voudrais spécialement remercier Aerospacelab pour leur collaboration avec l'UCLouvain qui a permis à ce mémoire de voir le jour. En particulier, je remercie fortement Antoine Delille pour m'avoir guidé durant cette période. Il fut l'œil expert sur mon travail.

Ensuite, pour m'avoir pris en tant que mémorant, je souhaite exprimer ma gratitude envers mon promoteur M. Beckemans, professeur à l'EPL à l'UCLouvain. Il a non seulement été à l'origine de l'approche choisie dans ce travail, mais il m'a également fourni de nombreux conseils qui se sont révélés très utiles.

Au-delà de l'aide technique, j'ai aussi profité d'un soutien moral de la part de mes amis et ma famille. Ils ont toujours été présents et ont indéniablement participé à la mise à terme de ce mémoire. Je tiens à remercier mon frère Thomas pour avoir passé ce dernier mois à mes côtés, lui aussi ayant un mémoire à rédiger, il fut toujours très positif, mais aussi mon frère Louis, ma future belle-sœur Céline et ma sœur Leia pour avoir relu ce travail et permis de pouvoir présenter un travail plus soigné, et enfin mes parents qui ont été aux petits soins durant cette période.

Enfin, je ne pourrais pas clôturer ces remerciements sans en adresser à toutes les personnes qui furent présentes pour moi tout au long de mon cursus d'ingénieur civil. Des remerciements ne sont qu'un petit geste à la vue de l'ampleur de leur soutien. Merci.

Contents

Introduction **1**

1 One Node Analysis of an Object in Earth Orbit **7**

1.1 How Cold Is Space? A Matter of Equilibrium 8

1.2 Earth Orbit of a CubeSat 11

1.3 Sun Effect: Daytime and Eclipse 13

1.4 Earth Contribution on the Incoming Flux 15

1.4.1 Earth InfraRed Emission (Earth IR) 16

1.4.2 Albedo Flux 17

1.4.3 Overall Incoming Heat Flux 19

1.5 Calculation of the Temperature of the Sphere over Time 21

1.6 Internal Dissipation Addition Influence 24

1.7 Application of a Coating: What is the Effect? 28

1.8 One-Node Analysis Parameters Discussion 33

1.8.1 LTAN and Scale Effect 33

1.8.2 Equilibrium Temperature during Daytime and Eclipse 35

1.8.3 Optical Properties Considering Solar Panels 37

1.8.4 Altitude Variation 38

1.9 Comparison between Sphere and Cube 39

1.10 Conclusion 45

2 CubeSat Architecture and Thermal Requirements **47**

2.1 CubeSat Subsystems 47

2.1.1 Primary Structure 49

2.1.2 Electric Power System (EPS) 49

2.1.3 Attitude Determination and Control System (ADCS) 54

2.1.4 Communication Subsystem (COM) 56

2.1.5 On-Board Computer (OBC) 57

2.1.6 Payload 58

2.2 Temperature Requirements Summary 59

2.3 Thermal Control System (TCS) 60
2.3.1 Coatings 60
2.3.2 Radiators 61
2.3.3 Thermal Links 63
2.3.4 Sunshield 64
2.3.5 Heat Storage 65
2.3.6 Heaters and Cryocoolers 65
2.3.7 TCS Approach for CubeSat 66
2.4 CubeSat Configuration 67
2.5 Power Budget 68
2.6 Mass Budget 73

3 Study Case 75
3.1 Study Case Model Architecture 75
3.2 Thermal Nodal Model Theory 80
3.3 Internal Heat Transfers: Radiation versus Conduction 82
3.4 Study Case Thermal Model 87
3.5 Simulation Results 90
3.5.1 Energetic Analysis 90
3.5.2 Temperature Analysis 92
3.5.3 Temperature Requirements 94
3.5.4 Heat Flows Analysis 100
3.6 Nodal Model Discussion 104
3.7 Conclusion 107

Conclusion 109

Appendix 111

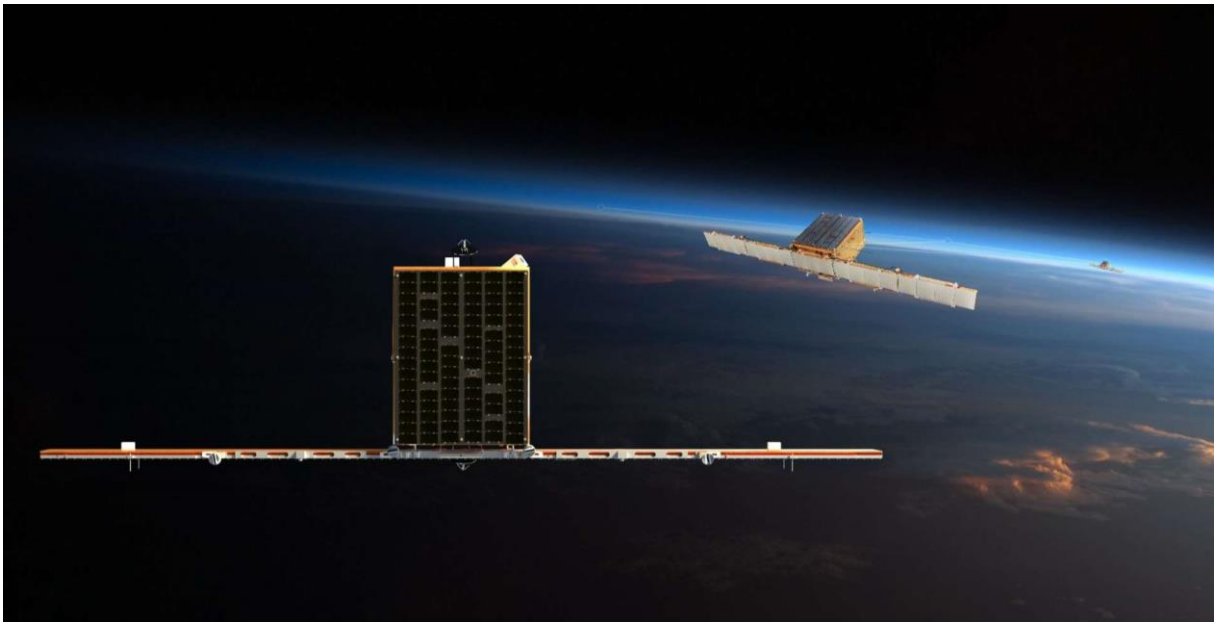
Bibliography 116

Introduction

The unknown world of space has always fascinated humans. For thousands of years, we have been elaborating theories that could help us grasp the phenomena that take place into space. It is only recently that we have been able to "conquer" space by sending the first artificial satellite into orbit, Sputnik 1, in the second half of the 20th century. Since then, we have sent more sophisticated satellites, such as the Hubble Space Telescope or the International Space Station, which are still in orbit. We have built numerous satellites harvesting all kind of data for scientific purposes such as a satellite landing on another planet or catching sight of beyond with telescopes. Nevertheless, this does not represent the main purpose of artificial satellites. Most of them orbit around Earth and are used for earthly needs such as observation or communication.

Scientists have quickly noticed that most space missions could be directed by smaller satellites than conventional ones. Smaller satellites are lighter and need less power, it makes them less expensive. As economic viability is a crucial criterion in our current development model, small satellites have become more and more present. Most small satellites have a mass of a few kilograms and are called nanosatellites.

The first two nanosatellites, TUBSAT-N and TUBSAT-N1, were developed by the Technical University of Berlin for a communication mission and launched in 1998. It is 15 years later, with the reduction of the launch and components costs, that the production of nanosatellite exploded. Today, more than a thousand of them have been placed into orbit and about 700 are still in orbit. This industry is still in expansion with over 3000 nanosatellites forecasted to be launched in the future 6 years [1] [2] (Figure 0.1).



https://www.futura-sciences.com/sciences/definitions/petit-satellite-microsatellite-196/

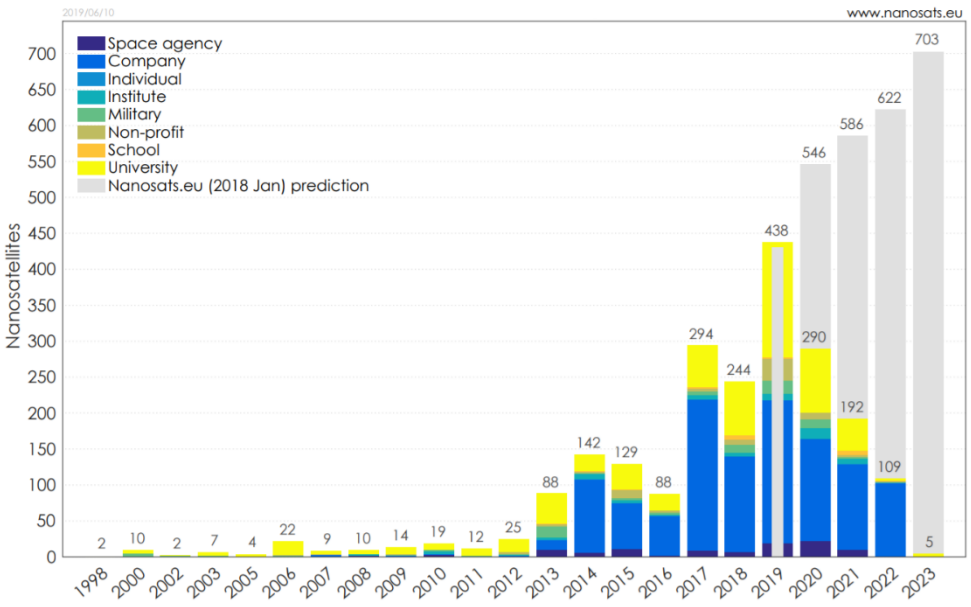


Figure 0.1 - Nanosatellite launches by organizations

Nanosatellites have revolutionized the accessibility to space. In the past, only a handful of entities, such as NASA and ESA, were able to launch artificial satellites into space. As for now, any university or startup has the possibility to have its own nanosatellite orbiting Earth.

CubeSat

More than 90% of nanosatellites are cube-shaped, hence their appellation of CubeSats [1]. They follow normalized dimensions and are defined by the standard CubeSat unit, namely a cubic structure measuring 10x10x10cm (1U). For example, a 3U CubeSat is a satellite with dimensions of 30x10x10cm, in other words, made of three standard CubeSat units. Most CubeSats are nanosatellites (1 to 10kg) but it does restrain some to be picosatellites (100g to 1kg) or microsatellites (10 to 150kg). In general, 1 unit corresponds to a mass of minimum 1kg. From the different existing dimensions (Figure 0.2), the 3U design is the most common, although, the 6U is becoming more and more present in the commercial field.

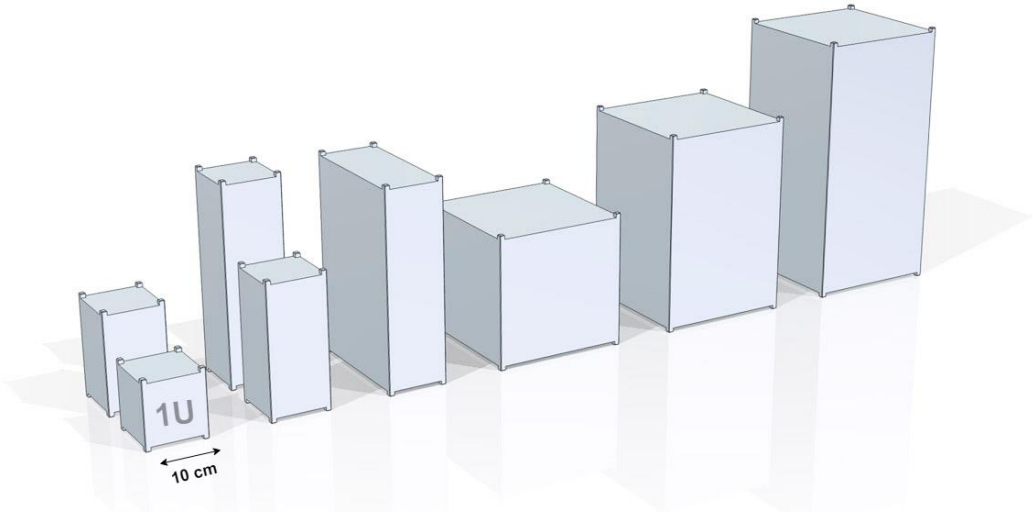


Figure 0.2 - CubeSat standard sizes (from 1U to 16U) [1]

This simple shape is meant for standardization. It opens up the commercialization of standard components, or Commercial-Off-The-Shelf (COTS) components, thereby considerably cutting the cost of engineering and development in comparison with conventional satellites. In addition, while a conventional satellite requires between 5 and 15 years from identifying the need to placing it into orbit, a CubeSat can take less than 8 months. [3]

Small satellites can carry out the same tasks as conventional satellites, of course, the features differ but are sufficient for multiple applications. CubeSat applications can be gathered in different categories:

- **Earth observation**: Earth observation or imaging missions basically consist of observing the Earth. It can consist of collecting data for scientific or commercial purposes such as environmental monitoring, meteorology or map-making. It can also harvest data for military purposes. This type of military missions is carried by intelligence satellites, most known as spy satellites.
- **Communication**: Small satellites are used to relay communications and to develop networks on a global scale. This category includes geolocation and the development of the Internet of Things (IoT).
- **Scientific applications**: Small satellites can board a payload with scientific purposes such as space observation programs, interplanetary missions, in orbit systems testing or biomedical researches.
- **Technology demonstration**: The mission involves the first flight and validation of a new technology to increase its Technology Readiness Level (TRE).
- **Education**: Some CubeSats are designed by universities. They have as main purpose to propose a concrete case as an educational tool for its students and researchers. We can cite the SwissCube from EPFL in Lausanne, the OUFTI from ULiège or the LUNA from UCLouvain.

The main application of CubeSats is Earth observation. It represents nearly half of the missions of all CubeSats ever launched. While educational and technology demonstrations missions have always taken a fair share of the missions (more than 30% together), the communication ones are increasing each year. As for the scientific applications, they approximatively comprise 10% of CubeSats.

Thermal Requirements

Like us, humans who must remain close to room temperature to survive, any component must remain inside its specific temperature range to properly work, depending on its function. Consequently, any satellite must remain in specific temperature ranges to operate as desired and avoid the overheating or sub-cooling of its components.

The case of satellites is unusual. The first reason is the harsh environment that is space. The second is the impossibility to replace the broken components.

The thermal behavior of the satellite is therefore of great interest and must be analyzed before launching the satellite into orbit. For small satellites, this concern is critical. Indeed, a lower mass implies a lower thermal inertia which intensifies temperature variations. Moreover, being small, space and power available for the thermal control are reduced. It makes it more difficult to meet the thermal requirements. The TCS (Thermal Control System) gathers all the means to make it possible.

Work Approach

This work aims to introduce the thermal behavior of a CubeSat to anyone with a scientific mind and an interest in space. In a greater extent, this type of satellites is chosen to represent small satellites in general.

Before launch, any CubeSat is deeply analyzed to theoretically meet the thermal requirements for any situations that it could encounter. This is realized through numerical simulations which are very useful tools for thermal analyses. However, such analyses, whatever their accuracy, are only applicable for specific missions and cannot be extrapolated to other uses.

The approach of this work aims to be as global as possible in order to be applicable to most CubeSats. The purpose is to get away from highly accurate simulations and try to understand the global thermal behavior of a typical CubeSat. For simulations, MATLAB codes will be used with the objective to simplify what more complicated software packages do.

Thereby, this paper is will present some simplifications for the sake of comprehension.

First of all, we must know the basics of the thermal considerations for an object orbiting Earth. The thermal environment is quite different than our daily environment and it should be properly introduced along with the thermal behavior of an orbiting object. The first part of this work will cover this in the form of a one-node analysis, going from a simple sphere in the deep space to a more detailed description. A one-node analysis means that the satellite is considered as one thermal node, or in other words, as a small isothermal body.

The second part describes the layout and the components of a CubeSat. It is a general overview that details their features such as their operating principles, performances, and energy consumptions. In particular, a portrait of the existing methods for thermal control is drawn up. The underlying goal is to establish the thermal requirements of a typical CubeSat and present the techniques to satisfy them. Along with them, the power and mass budgets of the satellite are discussed. The whole constitutes the starting point of the third part of this work.

The third and last part is the completion of this work as it brings together the knowledge of the first chapter and the technical elements of the second in a thermal analysis of a CubeSat. This analysis takes the form of a study case. This study case sets up the most typical mission, the observation of Earth, and analyzes its thermal behavior. It does so with a simplified thermal model that reflects the guidelines of the whole approach: generality and comprehension.

The logic of the work is summarized by Figure 0.4:

- **First chapter: one-node thermal analysis**. The reader is invited to grasp the thermal behavior associated with a sphere in orbit around the Earth. From this simplified analysis, one smooth temperature profile comes out.
- **Second chapter: presentation of the satellite**. The sphere is now turned into a CubeSat, the one-node system becomes a more complex one. Main features and thermal requirements are presented.
- **Third chapter: study case**. The first two chapters are merged together into the thermal analysis of a typical CubeSat. From this combined analysis, multiple temperature profiles come out.

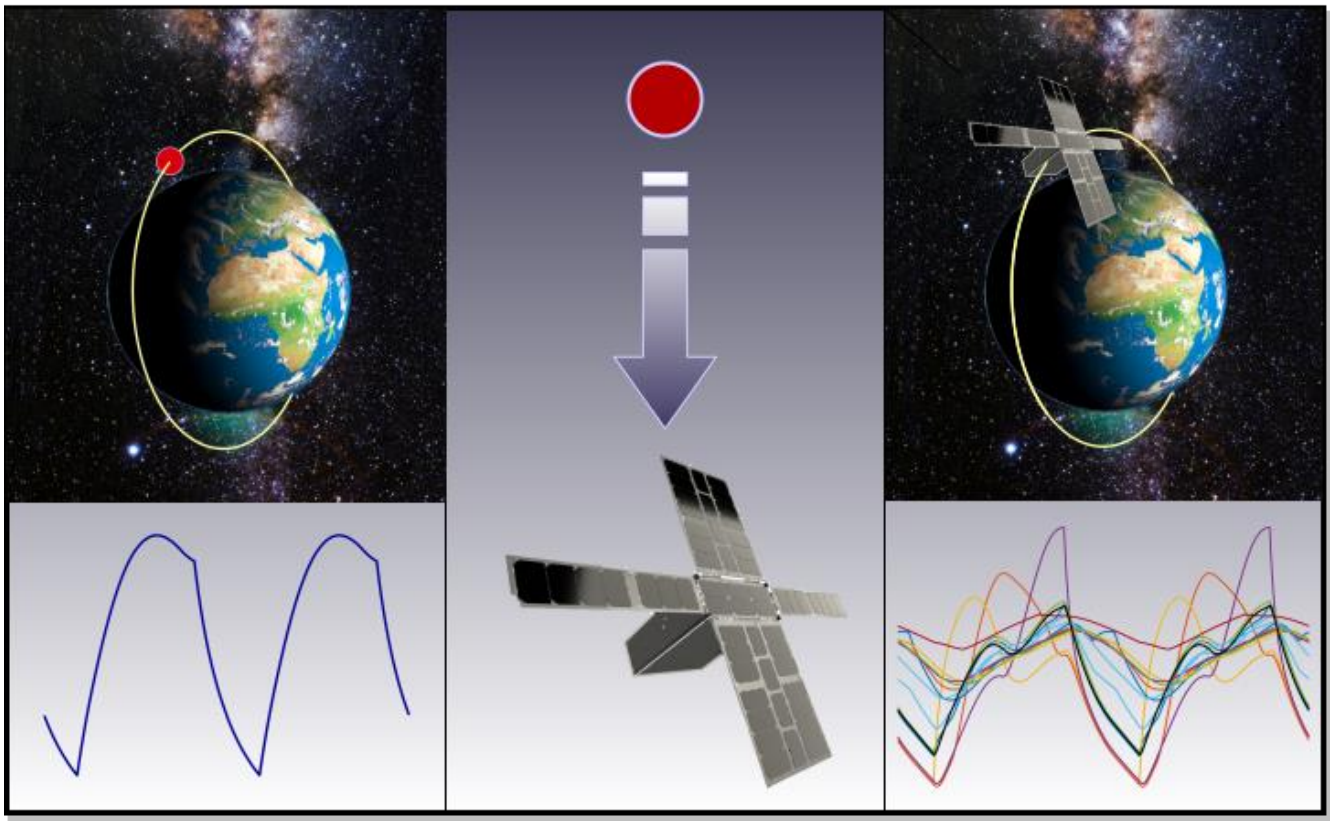


Figure 0.3 - Outline of the work

1 One Node Analysis of an Object in Earth Orbit

This chapter presents a thermal analysis of a body in orbit around Earth. Step by step, the different incoming heat fluxes, the internal dissipation of the satellite and its physical properties will be considered. This has been written with the desire of making it easily understandable and intuitive. It is why it mainly focuses on a sphere-shaped body as it is the simplest shape, only converting it into a cube at the end of the chapter.

A thermal one-node analysis can be visualized by an electrical one-node model, as shows Figure 1.1. The sphere is represented as the node S and the parameter of interest is its temperature T_s. The thermal model can be represented as an electrical model where the temperature T corresponds to the voltage, the heat flux Q to the currents and the thermal capacity C to the electrical capacity.

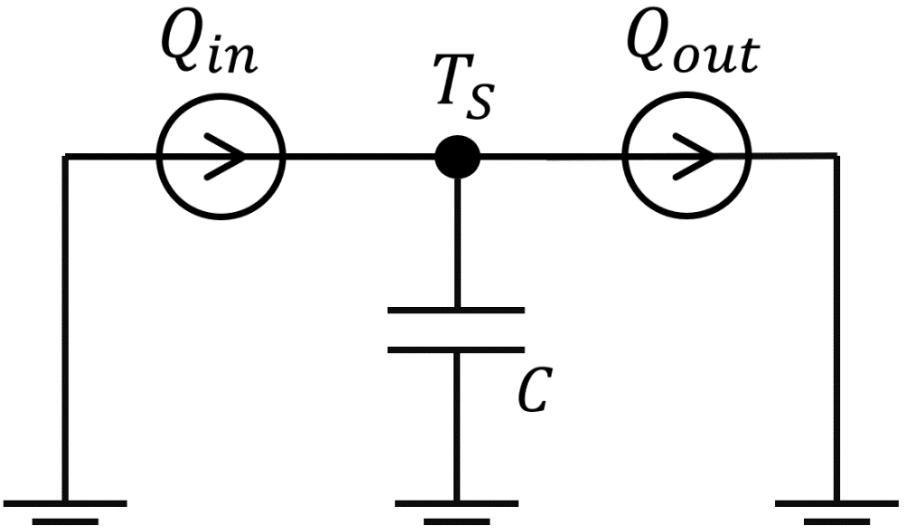


Figure 1.1 - One-node thermal model of an object orbiting around Earth

This simple model is at the center of this chapter. Each section has for purpose to bring relevant considerations to it.

1.1 How Cold Is Space? A Matter of Equilibrium

For starters, the first question anyone should ask is: How cold is space?

Actually, it is a nonsense question because deep space has no temperature. The temperature is a state-related to the internal energy, internal energy implies matter, therefore we need matter to talk about temperature. Well, let us put an object in deep space, how cold will it be?

In deep space, away from any energy source, there is still the cosmic microwave background radiation, these radiations have been permeating the entire universe since the dawn of time. Thanks to this small amount of energy, the object will tend to reach a temperature of 2.7K, just above absolute zero.

Let us now consider a homogenous opaque sphere. If we place it in deep space, it would reach 2.7K, but what would happen if we place it in an orbit around the Sun at Earth distance?

We consider that the sphere only sees the Sun, it constitutes thus the only heat source that can affect it. There are three main ways to heat up an object: convection, conduction and radiation. The two firsts, convection and conduction, rely on molecular interactions to transfer heat from one body to another. The sphere is in space, an environment without matter, therefore, heat cannot be transferred from the Sun to our sphere neither by convection nor by conduction. Only radiations can transfer heat in a vacuum medium, it represents therefore the only heat transfer between an object in space and its surroundings.

Radiative heat transfers are exchanges of small energy quanta, called radiations. One body emits radiations, another absorbs them: a radiative heat exchange happened. Radiations travel through any medium until it is absorbed or reflected by a body. If reflected, it rebounds on the body and changes of direction. If absorbed, it releases its energy to the body. For example, when we face the shining Sun, the light we see is simply radiations emitted that we absorb, the absorbed radiations release their energy to us and warm us up.

In our case, the Sun emits radiations and the sphere will either absorb or reflect them, if it reflects them all, the sphere won't receive any heat and then won't warm up, if it absorbs them all, the sphere will get all the energy the Sun can give. The sphere considered is opaque which means that radiations cannot pass through it, there is no transmission ($\tau = 0$). Figure 1.2 shows the different reactions of an incident radiative flux G that encounters a surface.

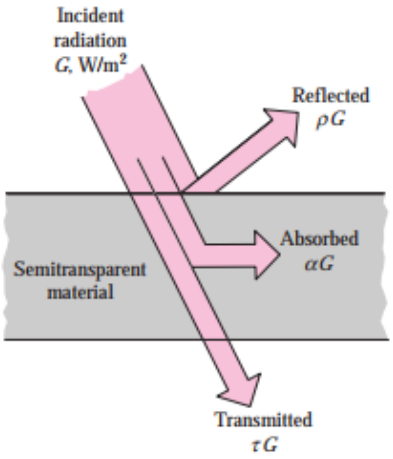


Figure 1.2 - Radiative absorption [114]

In fact, not only the Sun but anything above 0K emits radiations. The radiation emission depends on the temperature of the body. Figure 1.3 displays the emission intensity of an ideal thermal body, called a black body, for different temperatures. The Sun's average surface temperature is 5777K and its spectrum is represented by the yellow curve, the maximal intensity of the emitted radiations corresponds to wavelengths in the visible range, it is why the Sun appears bright to us. Colder bodies, e.g. everyday life items, emit infrared radiations, they are not visible to us but still carry energy. The total heat flux emitted

by a body is the sum of the intensity at every wavelength, in other words, it is the integral of the curves in Figure 1.3. It is clearly observable that this total heat flux intensity increases with the temperature.

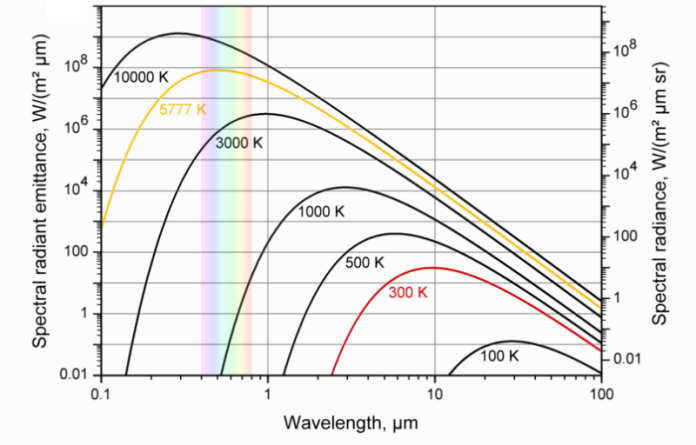


Figure 1.3 - Black body spectrum [111]

Coming back to our sphere, on the one hand, it absorbs the heat from the Sun, on the other hand, it emits heat as well. As said, the emitted radiation or outgoing heat flux increases with the body temperature, while the incoming heat flux from the Sun is constant. It means that at a given temperature, the outgoing and incoming fluxes are balanced, this temperature is called equilibrium temperature. The equilibrium temperature is the temperature that an object tends to reach in a stable state.

The ability to absorb or emit radiations is defined by the absorptivity, α, and the emissivity, ϵ, which are coefficients ranging from 0 to 1, an absorptivity or emissivity of 1 corresponds to a maximal absorption or emission. Black bodies are ideal thermal bodies with absorptivity and emissivity of 1. These coefficients are determined by the surface optical properties of the body. Figure 1.4 shows the same sphere covered with different coatings, each having a specific absorptivity and emissivity, and its associated equilibrium temperature.

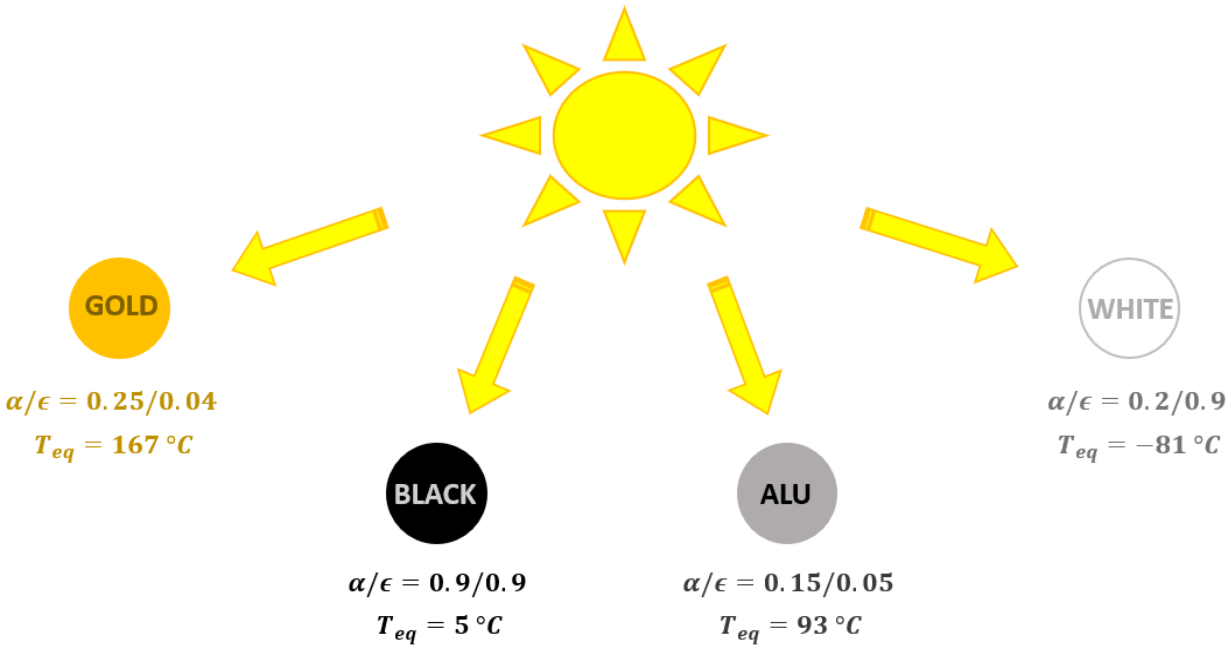


Figure 1.4 - Equilibrium temperature of different homogeneous spheres at Earth-Sun distance

The four coatings represented in Figure 1.4 are respectively gold coating, black paint, aluminum foil and white paint. The difference between their equilibrium temperatures is huge and it is only due to the coating applied on the body.

With this basic consideration, we can apprehend the thermal problematic that can encounter satellites.

To compute the equilibrium temperature of a body we need to go through some basic equations.

The first is the emissive power or exitance E , this is a power per unit of external area which is described by the Stefan-Boltzmann equation,

$$E = \sigma \epsilon T^4 \left[\frac{W}{m^2}\right]$$

With σ the Stefan-Boltzmann constant, ϵ the emissivity and T the temperature of the body in Kelvin.

The irradiance G is the radiant flux received by a surface per unit area. The irradiance from a surface i to a surface j is,

$$G_{ij} = F_{ij} E_i \left[\frac{W}{m^2}\right]$$

With E_i, the emissive power of surface i[1] and F_{ij} the associated view factor. The view factor F_{ij} is the factor that applies the reduction of power from the power emitted by i to the power received by j, in simple words, it is the way surface i views surface j.

The power absorbed by the surface is then equal to

$$Q_{in} = q_{in} A = \alpha G A \ [W]$$

With α the absorptivity of the receiving surface A and q_{in} the incoming heat flux absorbed per unit area. The absorbed power, Q_{in}, is simply the irradiance multiplied by the surface and the ability to absorb this irradiance. As for the emitted power, it is equal to,

$$Q_{out} = E A_{out} = \epsilon \sigma T^4 A_{out}$$

Near Earth, a body will receive from the Sun an irradiance, called solar constant E_s, of [4]

$$E_s = 1367 \left[\frac{W}{m^2}\right]$$

Which corresponds to the irradiance coming from a black body at 5780K at a distance of 1 AU[2]. A black body is an idealized thermal body with optical properties of $\alpha = \epsilon = 1$.

The equilibrium temperature is computed via the energy balance of the sphere. This is the temperature at which the incoming and outgoing powers are equal.

$$Q_{in} = Q_{out} \iff \alpha E_s A_{in} = \epsilon \sigma T_{eq}^4 A_{out}$$

A_{in} corresponds to the equivalent surface receiving the solar rays, for a sphere, it is its cross-section πR^2. A_{out} corresponds to the external surface, for a sphere it is $4\pi R^2$.

The equilibrium temperature of a sphere illuminated by the Sun at Earth distance is

$$T_{eq} = \left(\frac{\alpha}{\epsilon} \frac{E_s}{4\sigma}\right)^{\frac{1}{4}}$$

For an object only affected by the Sun, the equilibrium temperature is only depending on the optical properties of its coating.

A point to note is that emissivity and absorptivity depend on the wavelength of the emitted or absorbed radiation, α is denoted as the solar absorptivity (wavelengths from 0.3 to 3µm), ϵ as the infrared (IR)

[1] In this equation the radiosity is approximated by the emissive power which is totally valid for the Sun.

[2] AU = Astronomical Unit = 849 597 870 700 km, the average distance between the Sun and the Earth

emissivity (wavelengths from 3 to 50µm). The absorptivity of any material at far IR wavelengths can be approximated as its emissivity therefore $\alpha_{IR} = \epsilon_{IR} = \epsilon$.

1.2 Earth Orbit of a CubeSat

Let us now describe the orbit around Earth that a CubeSat follows. We want our sphere to behave as a typical CubeSat would, following thus the same orbit.

An object in orbit around Earth rotates in an elliptic path. Small satellites usually orbit in Low Earth Orbit (LEO), at this altitude range, this elliptic path can be approximated as a circle.

As shown in Figure 1.5, the orbit with this approximation is defined by

- its altitude H compared to Earth surface. (or semi-major axis (a on the figure) diminished by Earth radius)
- its inclination i which is the angle between the orbital plane and the reference plane (in this case the equatorial plane).
- its longitude of ascending node Ω, the ascending node is the intersection between the equatorial and orbit planes. Ω is the angle between a reference direction γ and the node line. The node line is the intersection between the orbital plane and a reference plane.

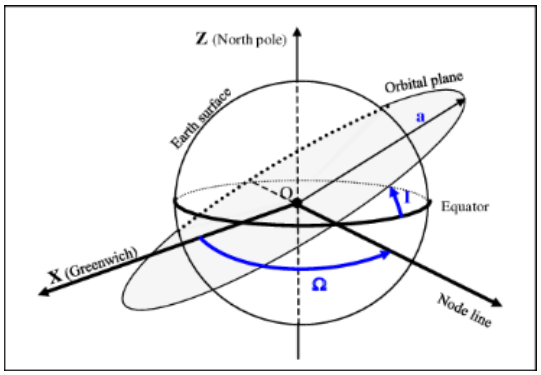


Figure 1.5 - Orbit parameters [113]

The true anomaly θ is the angular position of the satellite on its orbit. It starts at $\theta = 0°$ on the equatorial plane, intersects again the equatorial plane on the other side of the Earth at $\theta = 180°$ and ends its revolution around Earth at $\theta = 360°$.

Most small satellites, in particular, the Earth observation ones, follow a Sun-Synchronous Orbit (SSO).

Let us remind that the Earth is not a perfect sphere but an ellipsoid, the Earth is flattened at its poles and bulges at the equator. The effect is very limited, e.g. the Earth is still rounder than a pool ball, but it is sufficient to significantly affect LEO orbits. The non-homogeneity of the Earth's gravitational field will affect the orbital plane by making it rotate around Earth's axis. A judicious choice of inclination and altitude will make the orbit plane rotate 360° in one year. At this altitude and inclination, the angle between the orbital plane and the mean Earth-Sun axis is constant throughout the year, it implies a constant relationship with the Sun. The orbit is said to precess through one complete revolution each year, or about 1° a day. In other words, a satellite that follows an SSO always passes over the Earth at the same mean solar time, it stays in the same time zone (or its opposite one when passing over the other side of Earth). On Figure 1.6, an SSO in green is compared to a motionless orbit in red.

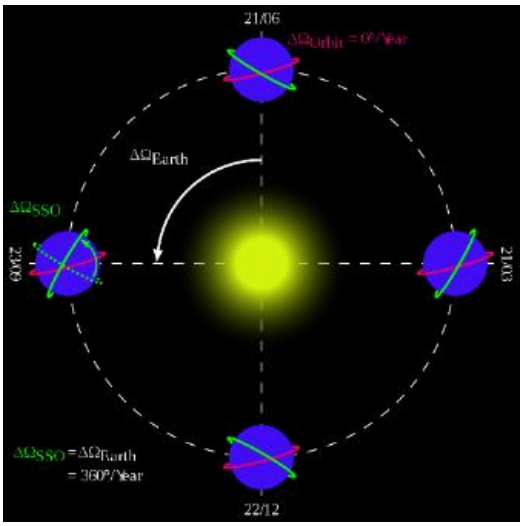


Figure 1.6 - Sun-Synchronous Orbit (SSO)

As said before an orbit is described, among others, by the longitude of its ascending node Ω, since an SSO remains on the same time zone, it is customary to talk of Local Time of Ascending Node (LTAN).

Typical SSO's are orbits of LTAN 12:00 or LTAN 10:30, which means the SSO is maintained on noon/midnight or 10:30am/pm time zone. Their altitude ranges between 470 and 650 km with the majority flying at 500 km (Figure 1.7). It represents a small part of the LEO range which includes all altitudes under 2000 km.

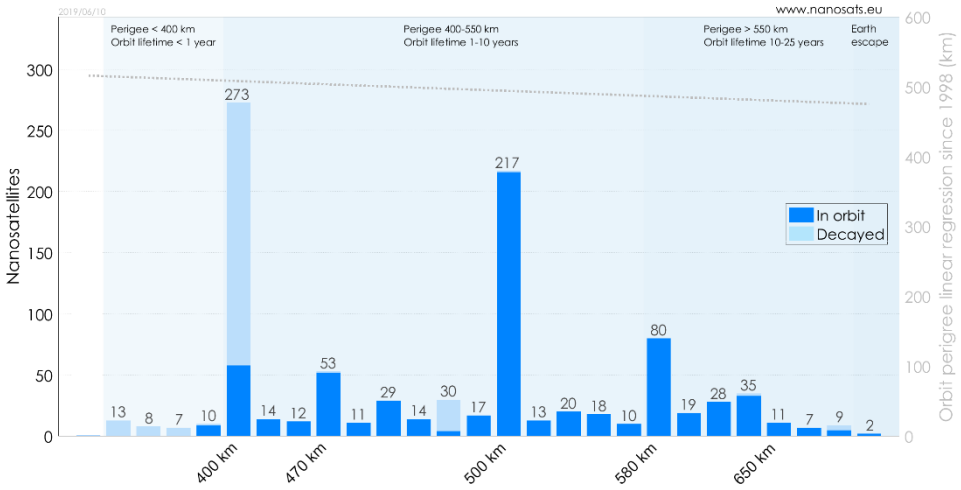


Figure 1.7 - Classification of the nanosatellites by their orbit altitude, modified from [1]

The upper and lower bound of their typical altitude is set for practical reasons. The satellite at the end of its life must eventually reenter the atmosphere and disintegrate inside so as not to become another debris in space. At 800 km of altitude, this phenomenon occurs after 25 years while at 550 km, it does after 10 years. On the contrary, a low altitude means a higher drag caused by the Earth's atmosphere, at 400 km, the orbit lifetime is about one year.

In the rest of the chapter, the default altitude is set at 600 km, the effect of its variation is not significant considering the narrow range, it will be discussed in section 1.8.4.

For SSO's, the inclination and the altitude are linked, when a CubeSat is described, its altitude is given, and its inclination is implied (it remains close to 98°). The reference direction γ is the sub-solar direction, direction from the center of the Earth to the Sun, this direction is changing throughout the year, rotating 360° in the inertial frame of the Sun. The reference plane is the ecliptic, plane parallel to solar rays and to the course of the Earth, and that cuts the Earth in its center. Instead of Ω, for SSOs, we will call β the angle between the reference direction and the node line. The LTAN and the β angle are two ways of representing the same angle. The LTAN is used as the definition of the orbit, β for the mathematics. β varies in]0; 90°] for LTAN]0:00; 6:00] and]-90; 0°] for LTAN]6:00; 12:00]. The relationship is linear, for example, an SSO of LTAN 3:00 will correspond to an angle $\beta = 45°$.

The orbital period increases with the altitude, in our case, it is between 94 and 97 minutes for the prementioned altitude interval, 470 to 650 km.

1.3 Sun Effect: Daytime and Eclipse

Let us now take the same sphere as before and make it follow an SSO. The sphere has now two states. The first is when it is illuminated by the Sun, called the illuminated phase or daytime. The second is when it is in the shadow of the Earth and it does not see the Sun, called the eclipse.

The main source of incoming heat flux is the Sun. It is why during the illuminated phase, the sphere warms up until it reaches the eclipse at what point it starts to cool down until it sees the Sun again and so on. The temperature experienced by the sphere is thus periodic.

The solar flux is constant, but the sphere is not exposed to it during eclipses. The solar flux that reaches the sphere, or incoming heat flux from the Sun G_s, is affected by the factor F_{ecl},

$$G_s = F_{ecl} E_s$$

With E_s the solar constant and F_{ecl} the eclipse factor, $F_{ecl} = \begin{cases} 0 \text{ if eclipse time} \\ 1 \text{ if daytime} \end{cases}$.

The position of the sphere on its orbit is described by the angle θ, starting at $\theta = 0°$ at the illuminated intersection of the ecliptic and orbital plane. The angle θ_{ecl} corresponds to the beginning of the eclipse and characterizes it. This angle is shown in Figure 1.8. The factor F_{ecl} is equal to 1 for $\theta < |\theta_{ecl}|$ and 0 otherwise.

Figure 1.8 displays two SSOs LTAN 12:00 illuminated by the Sun from the left, the first (solid red line) at an altitude H, the second (dashed red line) at a higher altitude H'. The first sphere has an angular position θ and is moving towards the angle θ_{ecl} at what point the eclipse, represented by the black area, begins. It can be seen that the first sphere will enter the eclipse zone at a smaller critical angle than the second sphere, Figure 1.8 highlights the influence of the altitude of the sphere on the eclipse duration.

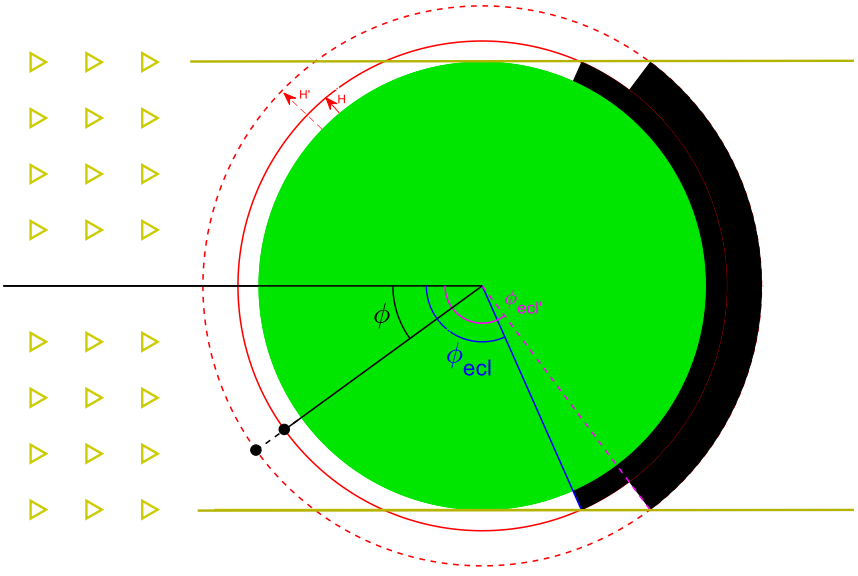


Figure 1.8 – Altitude influence on the eclipse duration

Another point of view is taken in Figure 1.9, the solar rays are going in and the ecliptic is represented by the black line. Four Sun-synchronous orbits, with increasing β angle, are drawn, from the blue SSO with $\beta = 5°$ (or LTAN 0:20) to the red one with $\beta = 90°$ (or LTAN 6:00). The dashed part of the line is the eclipsed part of the orbit (behind the Earth), it is observable that the eclipse time decreases as the β

angle increases until the red SSO which is always illuminated by the Sun. The illuminated to total time ratio will increase with β, until β reaches its critical angle, β_{max}, at what point there is no more eclipse.

Figure 1.9 also compares the orbit true inclination of 98° (on the left) to its approximation of 90° (on the right), which fits the true inclination. This approximation will be useful as it simplifies the model and will be used by default for the most part of this chapter.

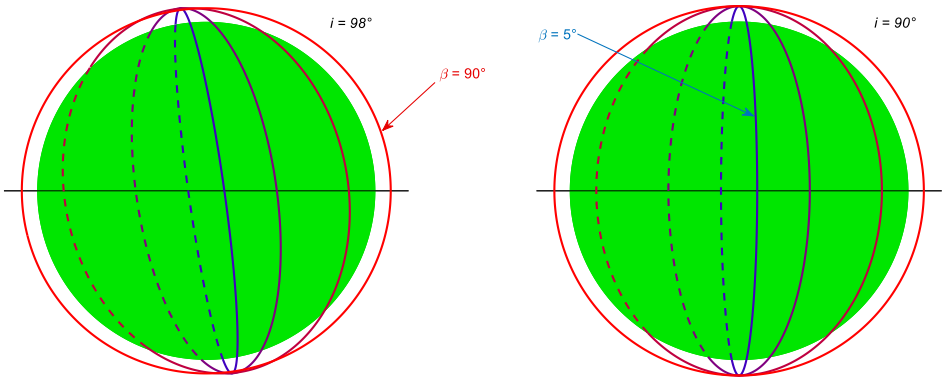


Figure 1.9 - Beta angle influence on the eclipse

With the approximation of perpendicular inclination (see Figure 1.9), only two parameters can influence the eclipse time, the altitude H and the angle β. By basic geometry, the eclipse angle θ_{ecl} is equal to

$$\theta_{ecl} = \pi - \text{acos}\left(\frac{\sqrt{h^2 - 1}}{h\,cos(\beta)}\right)$$

With $h = \frac{R_e + H}{R_e}$, R_e being the Earth radius and H the altitude of the sphere from Earth's surface.

The β angle at which there is no more eclipse, β_{max}, can be calculated by simple trigonometry

$$\beta_{max} = \text{asin}\left(\frac{1}{h}\right)$$

The eclipse factor is now defined as,

$$F_{ecl} = \begin{cases} 0 \; if \; \theta \geq |\theta_{ecl}| \\ 1 \; if \; \theta < |\theta_{ecl}| \end{cases}$$

The minimum θ_{ecl} corresponding to the maximum eclipse time occurs at $\beta = 0°$ and is equal to

$$\theta_{ecl,min} = \pi - \text{acos}\left(\frac{\sqrt{h^2 - 1}}{h}\right) = \pi - \text{asin}\left(\frac{1}{h}\right)$$

It gives $\theta_{ecl,\text{min}} = 114°$. The minimum ratio illuminated/total time is equal to $\frac{\theta_{ecl,\text{min}}}{180°} = 0.63$ or about 2 thirds of the time. So, at maximum eclipse time, the sphere is illuminated twice the time as shadowed, the minimum eclipse time corresponds to a $\beta > \beta_{\text{max}}$ where the sphere is always illuminated.

The mean eclipse factor, $\overline{F_{ecl}}$ is included in the interval,

$$\overline{F_{ecl}} = [0.63; 1] \qquad \text{for } \beta = [0; > \beta_{\text{max}}] \qquad \text{With} \quad \beta_{\text{max}} = 65°$$

Therefore, the average incoming solar flux is

$$G_s = [861; 1367] \left[\frac{W}{m^2}\right] \quad \text{for } \beta = [0; > 65°]$$

The impact of the LTAN of the sphere is huge and can reduce by up to 40% of the incoming heat from the Sun.

Figure 1.11 shows the solar incoming heat flux in yellow during three revolutions around the Earth for $\beta = 0°$, in gray are displayed the eclipse times. The dashed line corresponds to the mean value of the flux over the orbital period. This situation represents the maximal eclipse time with a ratio of about 1/3 of the orbital period and the minimum mean solar heat flux.

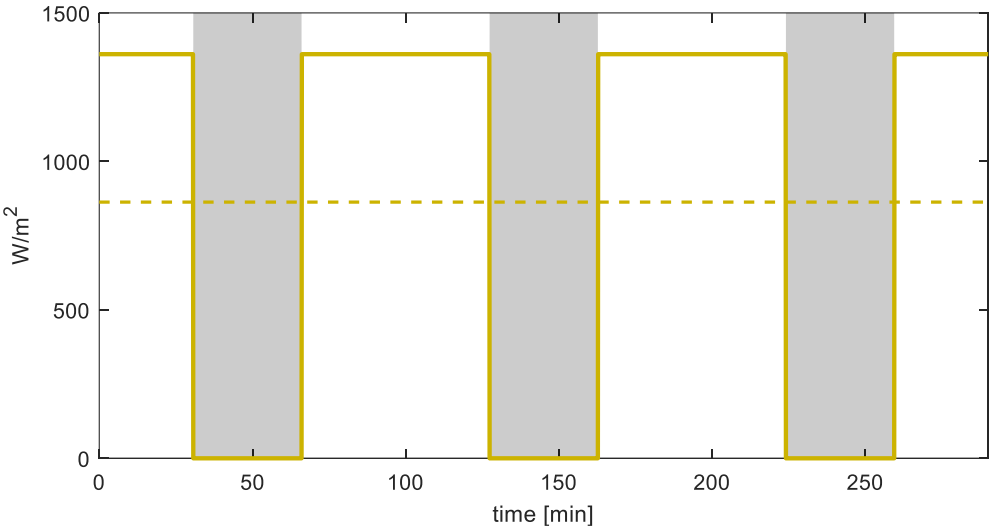


Figure 1.10 - Solar flux intensity evolution during 3 orbits

1.4 Earth Contribution on the Incoming Flux

Not only the Sun but also the Earth emits a heat flux that will reach the sphere. There are two types of Earth radiations: InfraRed radiation flux (IR) and albedo flux. Figure 1.12 presents those external fluxes along with the solar flux.

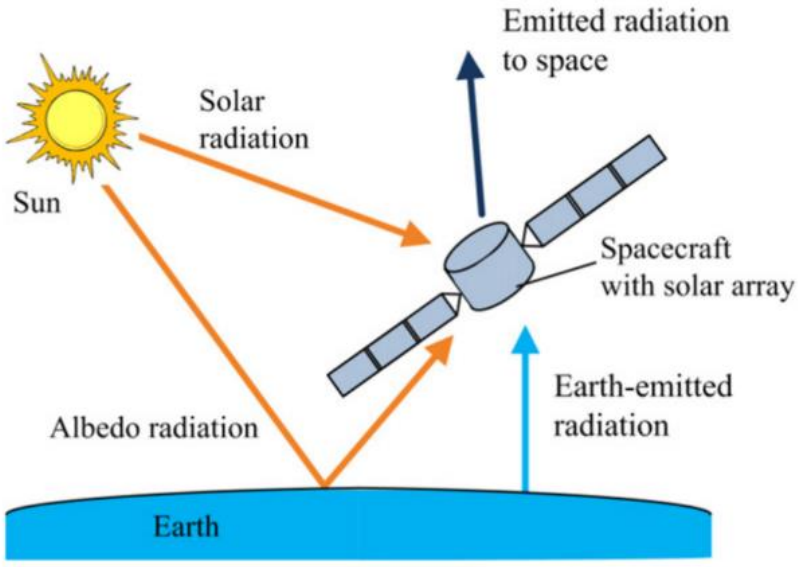


Figure 1.11 - External incoming heat fluxes [108]

1.4.1 Earth InfraRed Emission (Earth IR)

The Earth emits radiations and due to its lower temperature than bright stars, the emitted radiations are not visible but concentrated in the IR wavelengths (see Figure 1.3). The IR radiation will come as a heating flux to the sphere. The radiations emitted by the Earth are displayed in Figure 1.13 as a function of their wavelength, it does not follow a black body curve but the overall heat flux emitted is the same as a black body at 255K [4].

The Earth can therefore be modeled as it was, giving an emission of

$$E_e = \sigma T_e^4 = 240 \left[\frac{W}{m^2}\right]$$

We call $G_{e,h}$ the flux reaching the altitude of the sphere,

$$G_{e,h} = F_{e,h} E_e$$

Not to be mistaken with the incoming flux, or flux that reaches the surface of the sphere, which is

$$G_e = F_e E_e$$

With E_e the Earth radiation emission.

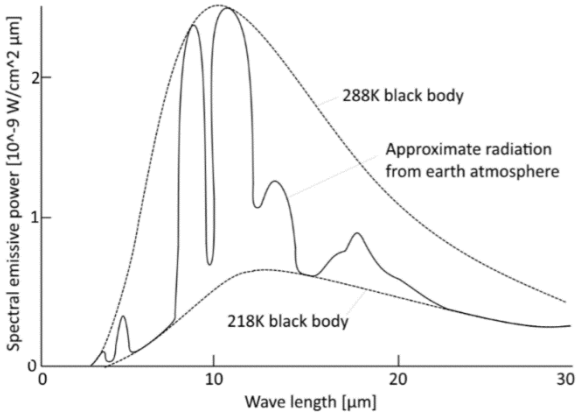


Figure 1.12 - Earth IR emission [4]

$F_{e,h}$ derives simply from the energy conservation principle, the Earth is considered as an isotropic flux emitter, therefore,

$$F_{e,h} = \frac{4\pi R_e^2}{4\pi (R_e + H)^2} = \left(\frac{R_e}{R_e + H}\right)^2 = \frac{1}{h^2}$$

F_e is the view factor from the sphere to the Earth.

The view factor between two spheres, F_{s-s}, in the case of a small to a very large sphere, is, [5]

$$F_{s-s} = \frac{1}{2}\left(1 - \sqrt{1 - \frac{1}{h^2}}\right)$$

With $h = \frac{R_e + H}{R_e}$, R_e being the Earth radius and H the altitude of the sphere from Earth's surface (Figure 1.14).

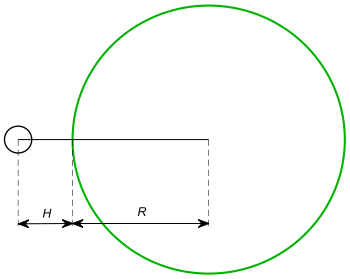


Figure 1.13 - Sphere to sphere view factor

F_{s-s} is the view factor per unit of external area ($4\pi r^2$). To have the same units as the solar flux, we are interested in the view factor per unit of cross-sectional area (πr^2), therefore,

$$F_e = 4F_{s-s} = 2\left(1 - \sqrt{1 - \frac{1}{h^2}}\right)$$

Actually, F_e tends to $F_{e,h}$ as the ratio h gets larger. It is logic since, as the sphere gets away from the Earth, its spherical shape, from the Earth, is more and more seen as a plate.

For an altitude of 600 km,

$$F_e = 1.19$$

The fact that F_e is greater than 1 means than the sphere gets more radiations than a plate of the same radius at the surface of the Earth. The IR incoming flux is then,

$$G_e = 285 \left[\frac{W}{m^2}\right]$$

We remind that it is a flux per unit of cross-sectional area. While the IR flux reaching such a height is

$$G_{e,h} = 200 \left[\frac{W}{m^2}\right]$$

This contribution is notably lesser than the solar flux, but it is not negligible at all, especially for the fact that this flux reaches the sphere even during eclipses.

1.4.2 Albedo Flux

The light emitted by the Sun is in part reflected on the surface of the Earth, hence its illuminated side. The reflected light is called the albedo flux. This flux is characterized by the albedo coefficient of the Earth, a, which is the reflectivity of the Earth, it is linked to the solar flux by

$$G_a = a\, F_a\, E_s$$

With E_s the solar constant and F_a the view factor associated to the albedo flux.

The factor a depends on the location on Earth where the solar rays reflect. It has an average value of 0.3. The actual value of a can go from 0.07 over uncloudy regions of tropical oceans to 0.9 over the Antarctic in 25 minutes [6]. However, thanks to the thermal inertia of the sphere (notion detailed in section 1.5), these rapid variations can be averaging without much affecting the thermal behavior of the sphere.

The view factor F_a consists of 2 terms, the first considers the distance from the Earth and is logically equal to F_e, the second considers the influence of the location of the sphere F_{loc}. Indeed, the factor F_{loc} considers the fact that the sphere at the subsolar point will get more albedo flux than the sphere at any other location.

$$F_a = F_e\, F_{loc}$$

As shown in Figure 1.15, the sphere location on its orbit influences the received flux from Earth albedo. In this figure, the black line points towards the Sun on the left, the black circle is the ecliptic, the sphere is the black bullet, and its orbit is the red line of LTAN defined by the angle β. The green line is the ground trace of the orbit. The albedo effect is represented by the yellow line which is a solar ray that reflects on the Earth surface and reaches the sphere of angular position θ.

The solar ray is reflected at an angle ϕ, this angle is the absolute angular position of the sphere, the angle formed by the Sun, the center of the Earth and the sphere. ϕ corresponds to the resultant angle of β and θ. A reflected ray loses intensity the more the angle of incidence deviates from perpendicularity due to the increase of the area of incidence for the same flux intensity. For LEO orbits, the flat-planet model is a good assumption. If the sphere is at an absolute angular position ϕ, it will get an albedo irradiance $E_{\mathrm{a,max}}\cos(\phi)$, with $E_{\mathrm{a,max}}$ the albedo irradiance at subsolar point. This effect is represented by the location factor F_{loc}.

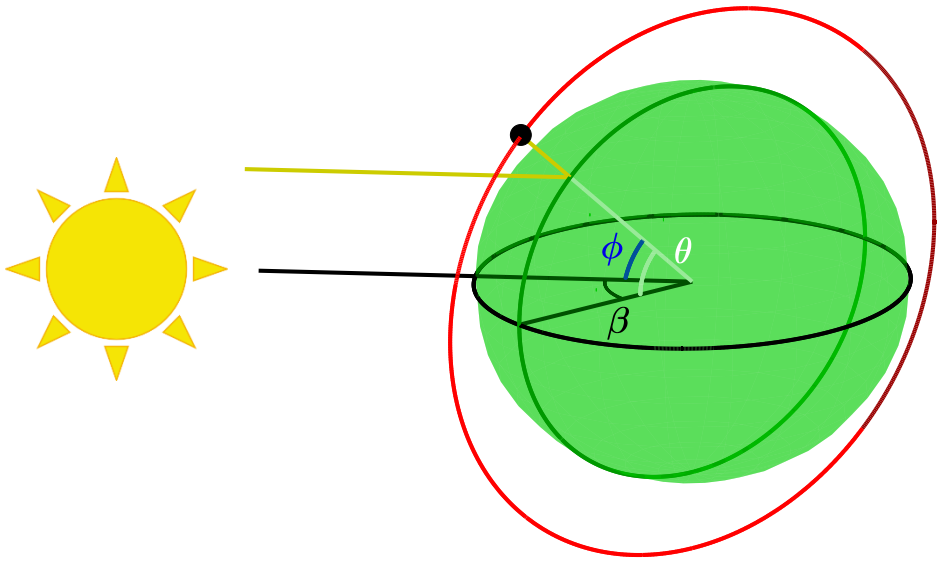


Figure 1.14 - Sphere position influence on the albedo flux

Using the spherical law of cosines and the approximation of perpendicular inclination ($i \cong 90°$), $\cos(\phi) = \cos(\theta)\cos(\beta)$ where θ is the sphere angular position in its orbit and β the orbit solar angle, F_{loc} can be approximated as

$$F_{loc} = F_{\theta,\beta} F'_{ecl} = \cos(\beta)\cos(\theta)\ F'_{ecl}$$

This approximation is very simplistic but has for convenience to be intuitive, the actual albedo view factor is difficult to evaluate and requires empirical expressions (one is detailed in Appendix A). In this form of F_{loc}, F'_{ecl} is equal 1 for $\theta \leq |90°|$ and 0 otherwise, it prevents F_{loc} from being negative. It is not accurate because for a position between 90° and θ_{ecl}, the sphere is still illuminated by the albedo flux. However, the albedo flux is very small for those angles, we consider it negligible in order to keep a simple expression for F_{loc}.

The final simplified expression of the albedo flux is,

$$G_a = a\, F_e \cos(\beta)\cos(\theta)\ F'_{ecl}\, E_s$$

In Figure 1.16 is shown the albedo flux G_a over time for one revolution. The curve is displayed for different β angles. Since the flux is proportional to its cosine, it strongly depends on the β angle value.

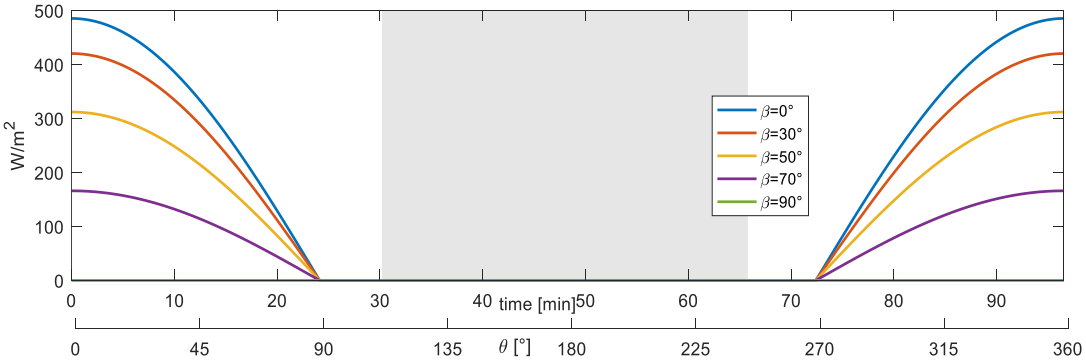


Figure 1.15 - Albedo flux throughout the orbit for different β angles

The mean value of the location factor, $\overline{F_{loc}}$, is

$$\overline{F_{loc}} = \frac{1}{2\pi}\int_{-\frac{\pi}{2}}^{\frac{\pi}{2}} \cos(\beta)\cos(\theta)\ \mathrm{d}\theta = \frac{1}{\pi}\cos(\beta)$$

Its maximum value occurs for $\beta = 0°$, $\overline{F_{loc,\max}} = \frac{1}{\pi} \approx 0.32$

With a view factor F_e of 1.19 (see section 1.4.1), the maximum mean albedo factor, $\overline{F_a}$, is

$$\overline{F_{a,\max}} = 0.38 \quad \rightarrow \quad \overline{F_a} = [0,0.38] \qquad \text{for } \beta = [90; 0°]$$

The mean incoming heat flux from Earth albedo is therefore included in

$$\overline{G_a} = [0; 154]\ \left[\frac{W}{m^2}\right] \quad \text{for } \beta = [90; 0°]$$

1.4.3 Overall Incoming Heat Flux

The three incoming fluxes are compared on Figure 1.17 on the basis of their mean value during one revolution in function of β (solar, Earth IR and albedo fluxes, respectively in blue, red and yellow). On the left, each heat flux is displayed. On the right, the total incoming flux is divided in its different sources, Sun, Earth IR and Earth albedo. Its minimum occurs at $\beta = 0°$ while its maximum occurs at $\beta = \beta_{\max}$.

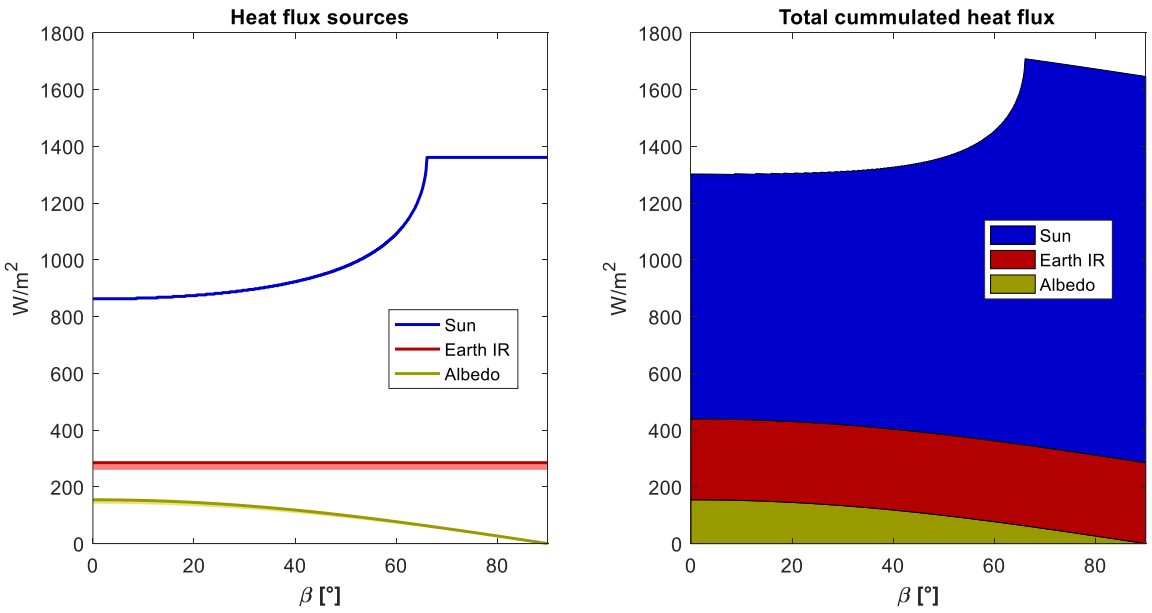


Figure 1.16 - mean external fluxes intensity in function of β

The main and obvious observation to be made is that the Sun provides the main incoming radiations by far, the second is that the IR flux gives more heat to the sphere than the albedo flux. The evolution of the solar flux with β is caused by the eclipse time varying with β. The eclipse time drops rapidly when β approaches $\beta_{\max}$ at what point there is no more eclipse, giving the maximum value for the solar flux.

Figure 1.17 is useful to have an idea of the relative importance of the different external fluxes.

The overall incoming heat flux per unit area is

$$G_{in} = G_s + G_e + G_a = F_{ecl}E_s + F_eE_e + a\,F_a\,E_s \left[\frac{W}{m^2}\right]$$

G_{in} is plotted in Figure 1.18 as a function of its orbital position and its LTAN or β angle on the left, on the right is shown the projection of G_{in} for $\beta = 0°$ with a detail of the fluxes G_s, G_e and G_a.

It can be observed that despite that the mean value of IR flux is twice the one of albedo flux at $\beta = 0°$, this last flux can have superior values for small θ's.

The overall incoming flux is comprised in,

$$G_{in} \in [285;\ 2130] \left[\frac{W}{m^2}\right] \quad \text{for } \beta < \beta_{\max}$$

The absorbed heat flux is named q_{in} in [W/m²] and Q_{in} in [W], small q for power per unit area and capital Q for power will be used throughout the paper.

$$q_{in} = \alpha\, G_{in} \left[\frac{W}{m^2}\right] \qquad Q_{in} = A\, q_{in} = \alpha\, A\, G_{in}\ [W]$$

With α, the absorptivity of the sphere and A its cross section.

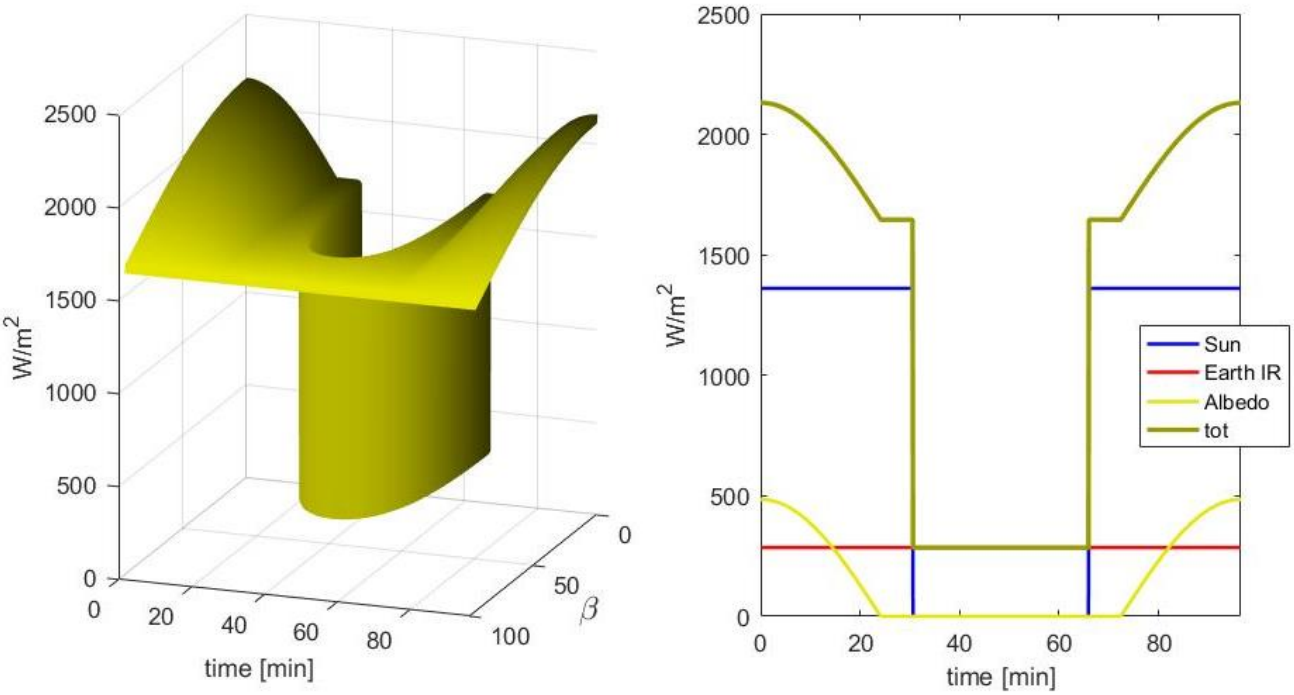


Figure 1.17 - total external heat flux over one orbit in function of β (left) and for $\beta = 0°$ (right)

1.5 Calculation of the Temperature of the Sphere over Time

Now that we have the incoming heat fluxes, we are interested in the temperature of the sphere.

The temperature of an object in space depends on many parameters such as its mass, external area or internal specific heat. To compute the sphere temperature, it is necessary to impose these parameters, which makes the analysis less general. Nevertheless, it is still interesting not for the exact temperatures reached but to have an idea of the temperature curve shape or the size of the temperature range.

The method to calculate the temperature is simply a power balance. Our sphere is considered as being one node, therefore, at each instant, the difference between incoming and outgoing fluxes must correspond to the variation of internal energy. In equation, it gives

$$m\,c\frac{\mathrm{d}T}{\mathrm{dt}} = \sum Q = Q_{in} - Q_{out}$$

With Q_{in} the incoming flux and $Q_{out} = \sigma\,\epsilon\,A_{out}\,T^4$ the emitted flux with T the temperature of the sphere of mass m and specific heat c. The thermal capacity C in [J/K] is equal to mc.

This equation was illustrated in Figure 1.1.

The specific heat, or specific thermal capacity, c of a material is defined as the amount of energy that must be supplied to raise the temperature of one kilogram of material by one degree, its unit is [J/kgK]. The specific heat depends on each material, but some similarities can be made, for example, water has a high specific heat while metals usually have low ones.

But what does it mean to have low or high thermal capacity?

We know from section 1.1 that for a constant flux, the temperature reached does not depend on the thermal capacity of the body. The thermal capacity determines the rate at which the material will warm up or cool down, not its equilibrium temperature. Intuitively, the term capacity is well chosen. Indeed, the heat flux charge the capacity until it is full at what point the equilibrium temperature is reached. The larger the capacity, the longer it takes for an equivalent flux to fill it, the longer it takes for the equilibrium temperature to be reached. For example, our sphere filled with water will warm up about ten times more slowly than if it were filled with iron of equivalent mass.

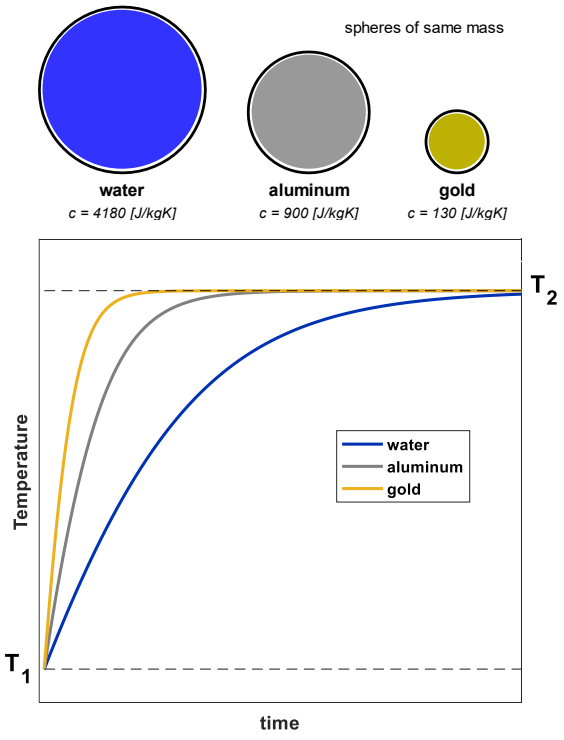


Figure 1.18 - Thermal inertia effect on temperature variation

The term thermal inertia, defined as the resistance to any change in temperature, is directly linked to thermal capacity and thus to the specific heat of the material. An object is said to have a high thermal inertial if its temperature slowly reacts to heat flux variations, it means that its thermal capacity is also high (and vice versa for low thermal inertia).

Let us visualize this idea: we consider three spheres of the same mass, one made of water, one of aluminum and one of gold. For the same mass, the spheres do not have the same dimensions due to their different densities, they are shown at scale in Figure 1.19. It is

considered that they are all covered with a black coating. Starting from a temperature T_1, the spheres are suddenly exposed to the same incoming flux which sets a new equilibrium temperature T_2. Figure 1.19 depicts the transition between T_1 and T_2. As the thermal inertia increases (from yellow to blue), the time to reach T_2 increases.

This example also serves as a reminder of section 1.1: the equilibrium temperature does not depend on the size of the object, only on its shape, this consideration will be discussed again in section 1.8.2.

Aluminum is also shown in Figure 1.19 because it is the most common material sent in space. It is why, for the future temperature representations in this chapter, we will use aluminum as default material for the sphere.

By resolving the balance equation, one can draw the temperature evolution of the sphere.

The temperature evolution at the beginning will depend on the initial conditions, it is why the temperature is displayed from the point where it reaches a stable state. It means that it is displayed from the point where it is not influenced by the initial conditions anymore but only by the heat fluxes. These are the thermally stable conditions. This has been done in Figure 1.20 for three revolutions. The three revolutions taken are thermally stable revolutions, which means the temperature is periodic, that happens after orbiting for a little time.

For plotting purpose, we have set the sphere as having a mass, radius and specific heat respectively of 0.5 [kg], 0.1 [m] and 900 [J/kgK] (aluminum). In addition, the sphere has the properties of a black body and follows an SSO 12:00 at 600km. Such a sphere is the default design for all temperature graphs of the chapter. It is important to note that it does not correspond to the mass of a typical CubeSat. It rather corresponds to the mass of its frame. The mass is lowered in the intent to reveal in a more visual way the specific effects of the thermal behavior of an object in space. It is actually a better approach because it accustoms the reader with drastic temperature variations which match the temperature of individual parts of a CubeSat. If the mass was higher, the temperatures would be damped which is not representative. This consideration will be brought out by the last chapter (section 3.6).

Figure 1.20 shows the temperature evolution of the sphere over time. In addition, it compares the temperature evolution in yellow for the overall flux (from the Sun and the Earth) and in red for the solar flux (only from the Sun), pointing out the non-negligible effect of the fluxes from the Earth (IR and albedo).

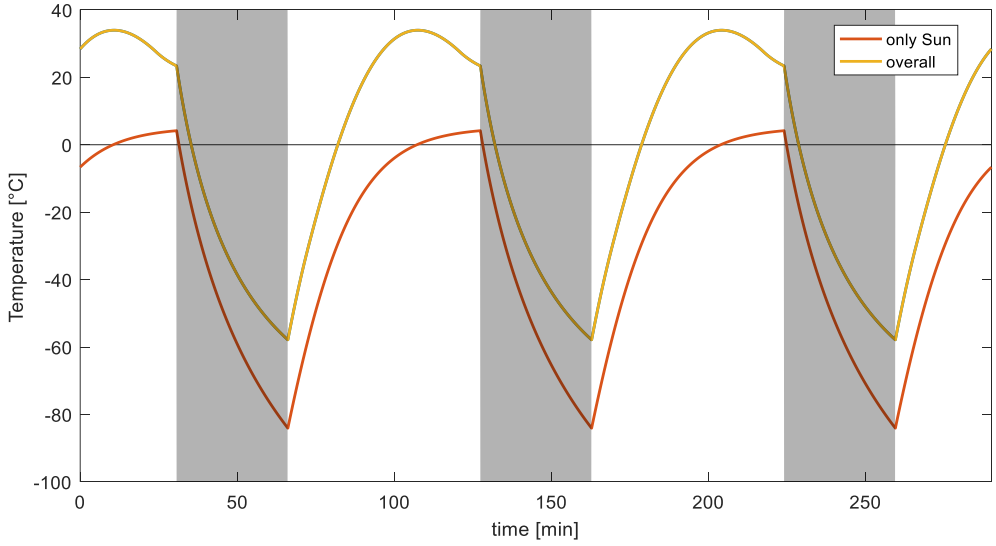


Figure 1.19 - Temperature evolution of a black-body sphere in SSO 12:00 at 600 km

The eclipse periods are represented by the gray areas. As one can expect, the temperature decreases at the beginning of an eclipse until the illuminated period starts again at what point the temperature starts to increase and so on.

As said, the effect of the Earth (IR + albedo) is not negligible, the sphere will be obviously warmer at any instant since the incoming flux is larger. Moreover, the temperature profile will be affected too due to the irregular albedo flux intensity, the peak temperature does not occur right before the eclipse anymore. Those results have to be carefully considered since the temperature evolution depends on the physical properties of the sphere such as the mass or thermal conductivity. The temperature curve of a sphere with other physical properties would be somewhat different, but the trend is the same which makes it interesting to analyze.

In the continuity of Figure 1.19, Figure 1.21 shows the same three black painted spheres now orbiting around Earth[3]. Their temperature evolutions are much different. The equilibrium temperature during eclipse being extremely low, none of the spheres has time to reach it. However, the lower the thermal inertia, the closer it gets to its equilibrium and thus the lower the temperature at the end of the eclipse. For illuminated periods, the golden sphere reaches its equilibrium while the water sphere does not have enough time. In short, the higher the thermal inertia, the lower the temperature fluctuations.

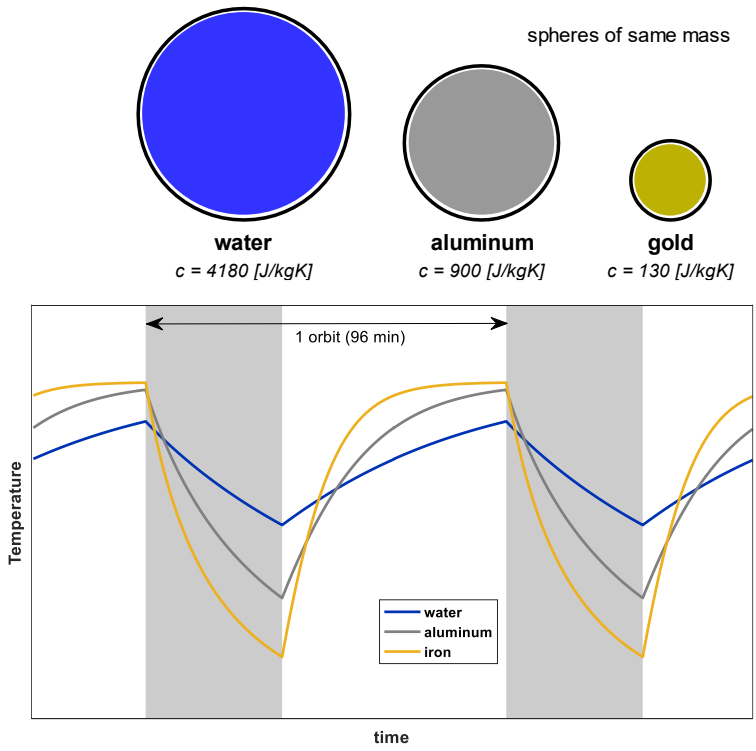


Figure 1.20 - Thermal inertia effect on orbital temperature

Another aspect of the thermal inertia variation is its influence on the mean temperature of the sphere. Indeed, on the one hand, the time to reach the upper equilibrium temperature (during daytime) is longer than the time to reach the lower one (during eclipses), and on the other hand, the equilibrium is reached faster with higher thermal inertia. These facts imply a slightly higher mean temperature as the thermal inertia increases.

[3] For visual sake, only the solar flux has been considered.

1.6 Internal Dissipation Addition Influence

We have analyzed the external fluxes reaching a lonely sphere trapped in its orbit around Earth, we will in this section equip this sphere with internal electrical devices that dissipate energy.

Heat Fluxes Balance

The only way to transfer heat from the sphere to its surroundings is by radiative means, the amount of heat emitted, or outgoing heat flux is equal to

$$Q_{out} = \sigma \, \epsilon \, A_{out} \, T^4$$

ϵ is the emissivity of the external surface A_{out} of temperature T.

When the sphere has reached thermally stable conditions (periodicity of its temperature), the incoming flux must be balanced by the emitted flux. Indeed, the temperature being the same at the beginning and the end of the revolution, the overall flux received and emitted must balance each other by energy conservation.

Figure 1.22 plots these considerations, the green and black lines are the external and emitted heat fluxes (Q_{in} and $-Q_{out}$), the total flux ($Q_{in} - Q_{out}$) is represented by the blue line. Q_{in} does not depend on the sphere temperature while Q_{out} does, its absolute value increasing with temperature. It is this total flux that will affect the temperature value (red line). Indeed, when the total flux is positive, the temperature rises, on the contrary, when it is negative, the temperature drops. By energy conservation, the mean value of the total flux must be null.

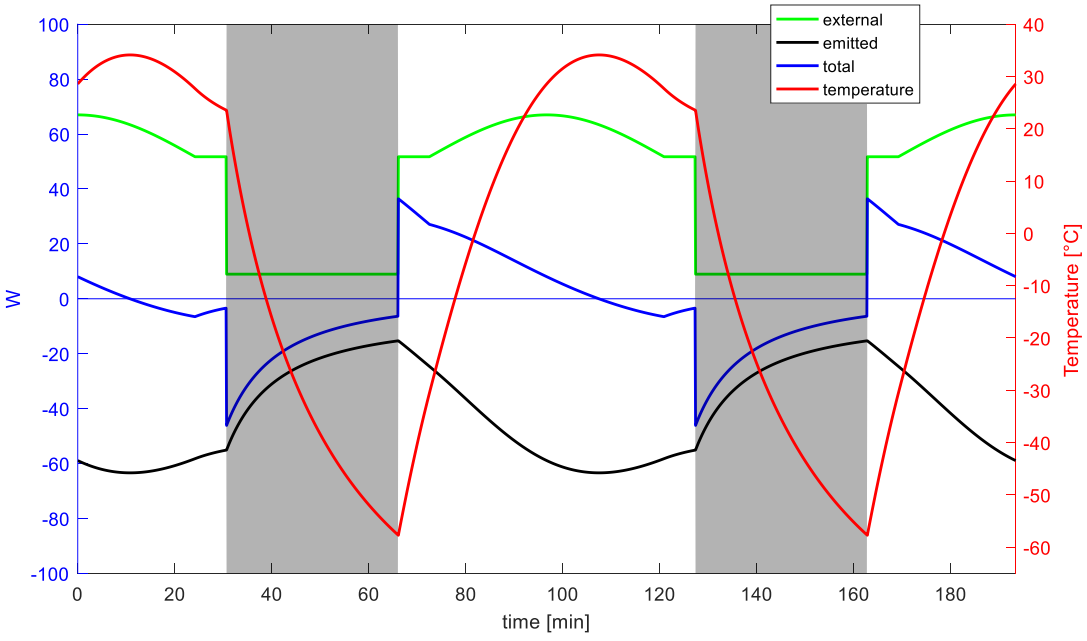


Figure 1.21 – Received and emitted fluxes contributions to total flux and temperature of the sphere

This graph corresponds to the situation of the default sphere with no internal power dissipated, the red curve is the same as the yellow one in Figure 1.20.

Internal Dissipation Addition

If an electrical device is added inside the sphere, for example, a communication system, it will need electricity to work. But the efficiency will never be of 100% and some of the electrical energy will be dissipated as heat. For the case of a communication system, a part of the electrical energy will be sent as electromagnetic waves towards the Earth and the rest of the energy will inevitably be dissipated as heat. It is why, by adding an electrical device, it results in adding a heat power source. The balance equation becomes

$$m\,c\frac{\mathrm{d}T}{\mathrm{dt}} = \sum Q = Q_{in} - Q_{out} + Q_{int}$$

With Q_{int} the internal heat dissipation in [W].

But how does this increment Q_{in} influence the temperature?

Since Q_{out} is proportional to the temperature to the power of 4, the latter equation is differential, and it is not easy to see the impact of the addition of Q_{int}. We will thus make some assumptions to answer this question.

Let us call T and T', the temperature of the sphere without and with internal dissipations. The following system is obtained,

$$m\,c\frac{\mathrm{d}T}{\mathrm{dt}} = Q_{in} - Q_{out}$$
$$m\,c\frac{\mathrm{d}T'}{\mathrm{dt}} = Q_{in} - Q'_{out} + Q_{int}$$

The difference between Q_{out} and Q'_{out} is assumed to be somewhat constant, which implies that the evolution of the temperature remains similar for T and T', that is to say that $\frac{\mathrm{d}T}{\mathrm{dt}} \cong \frac{\mathrm{d}T'}{\mathrm{dt}}$, thus

$$Q_{in} - Q_{out} \cong Q_{in} - Q'_{out} + Q_{int} \quad \rightarrow \quad Q_{int} \cong |Q'_{out}| - |Q_{out}| = \sigma\,\epsilon\,A_{out}\,(T'^4 - T^4)$$

An increment Q_{int} will therefore induce an increment in the temperature to the power of 4.

$$T'^4 \cong T^4 + \frac{Q_{int}}{\sigma\,\epsilon\,A_{out}}$$

This relationship allows us to say that an increment Q_{in} will have a greater impact on the temperature the more this one is low.

Figure 1.23 is identical to Figure 1.22 on two subplots (fluxes are above and temperatures are below) where the cases with and without internal dissipation are displayed respectively in solid and dashed lines. For this graph, an internal dissipation Q_{int} of 5 [W] has been added, it corresponds to the difference between Q_{in} (dashed green line) and Q'_{in} (solid green line). Our assumption of constant increment for Q'_{out} seems plausible in view of the similarity of the solid and dashed blue lines.

An interesting comparison in the bottom graph of this figure is the red and the magenta lines. The first is the temperature plotted via the differential balance equation, the second is the temperature approximated via the above equation, it is observed that the approximation fits the actual temperature.

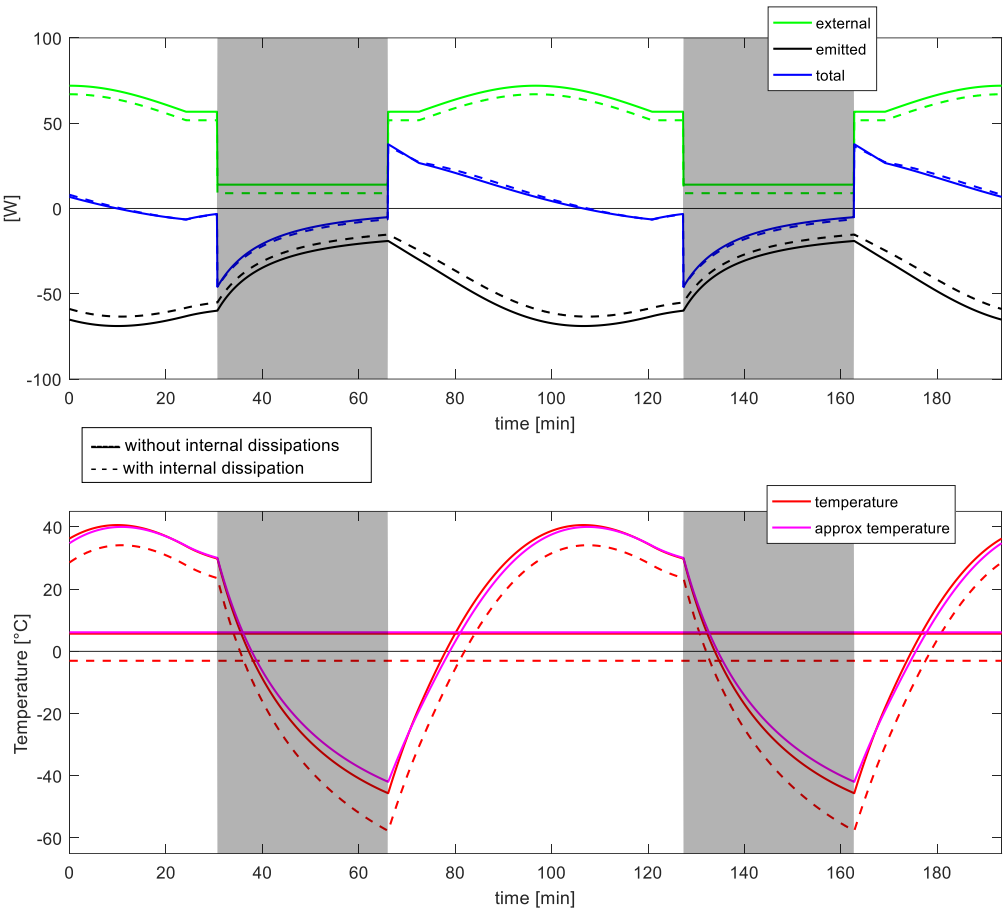


Figure 1.22 - Internal dissipation effect on fluxes and temperature

By calculation by hand, from the latter equation and with some plausible assumptions[4], the mean value of the temperature with internal dissipation T' is

$$\frac{Q_{int}}{\sigma \epsilon A_{out}} = T'^4 - T^4 \cong 4\, T_m^3\, \Delta T \cong 4\, T^3\, \Delta T$$

$$\Delta T = \frac{Q_{int}}{4\, T^3\, \sigma \epsilon A_{out}} \quad \rightarrow \quad \Delta \bar{T} \cong \frac{Q_{int}}{4\, \bar{T}^3\, \sigma \epsilon A_{out}}$$

From this approximation, Figure 1.24 depicts the impact of Q_{int} on the mean temperature of the sphere: the temperature increase ΔT in function of the temperature of the sphere with no internal dissipation $\bar{T}$ (or T_{avg}). Q_{int} varies from 0 [W] (blue line) to 20 [W] (red line) by increment of 2 [W]. As expected, the impact is greater the lower the initial temperature is, to a factor 2 between $T = -40$ and 40°C.

[4] The first one is valid for a ΔT smaller than 50K, 0.6% of difference $\Delta T = 50°C$ at $T_m = 50°C$ (mean temperature). The second one assumes a negligible difference between $\frac{1}{T^3}$ and $\frac{1}{\bar{T}^3}$.

The appealing point of this approach is that it does not depend on the mass of the sphere nor its shape but only on its external area and average emissivity. In addition, this analysis is quite accurate. This approximation for the mean temperature increase in function of the internal dissipated power is validated in Appendix B through a comparison with a simulated 6U CubeSat (study case proposed in chapter 3).

We must point out that an average of 20 W of internal dissipation for such a small sphere is a very large amount and is plotted for reference only.

This approach has allowed us to have a more intuitive understanding of the impact of internal dissipation inside an object in space. For the rest of the chapter, the temperature will be calculated from the differential balance equation.

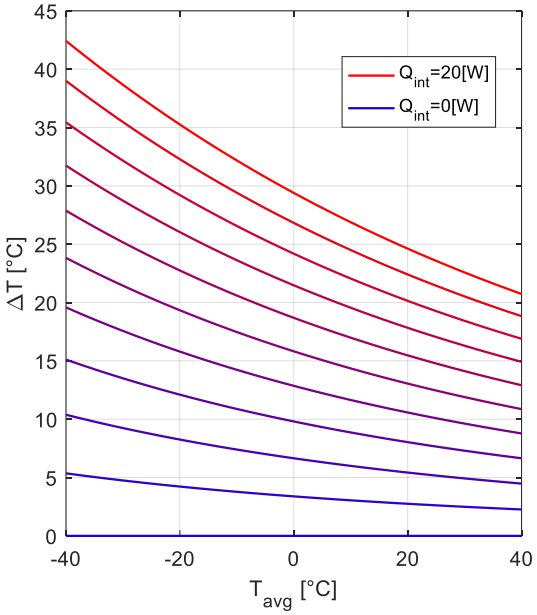


Figure 1.23 - Influence of internal dissipation on mean temperature

Non-Constant Internal Heat Dissipation

The internal dissipation profile is determined by the consumption profile of internal electrical devices. Constant consumption has been considered in the last section, in this one, we will see the effect of non-constant consumption.

Let us imagine our sphere equipped with an internal device whose sole purpose to dissipate heat. This device can operate at any time. The first thought would be to operate the device during cold periods, thereby, warming up the sphere.

This implementation is an active thermal control of the sphere. By consuming power at key moments of the orbit, the sphere can be prevented to reach too low temperatures. It is an active control, opposed to a passive one, due to its consumption of energy for control. It has the drawback of needing energy but the advantage of being adaptive.

Figure 1.25 depicts the temperature curve of the sphere to which an internal electrical device has been given the instruction to switch on when a specific temperature is reached. In this case, the critical temperature is -40°C and the power delivered by the internal device is 12 W. Those specific numbers are not of importance, they just serve the purpose of visual help.

This section has introduced the active thermal control by the use of internal dissipation, a judicious consumption profile of a load can regulate the temperature and prevent too low temperatures to be reached. This topic will be further discussed in the following chapters.

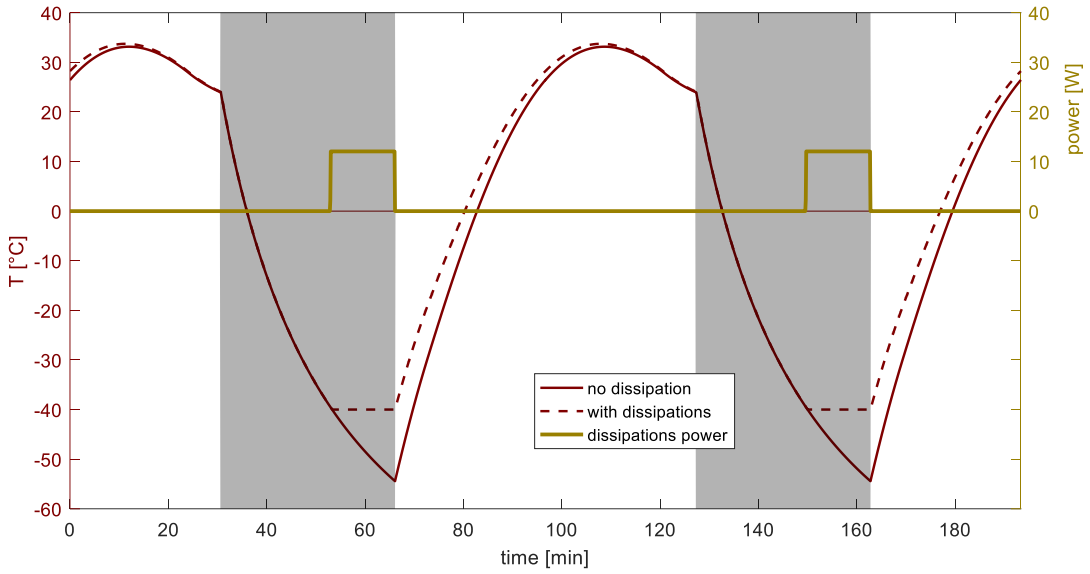


Figure 1.24 - Temperature evolution with thermal control via non-constant internal dissipation

1.7 Application of a Coating: What is the Effect?

In this subsection, our sphere, considered as a black body up to now, is covered with a coating. As shown in section 1.1, the coating can have drastic effects on the sphere temperature, but how exactly does it affect the sphere?

Optical Properties of a Surface

The optical properties of the external surface of the sphere are its absorptivity α and its emissivity ϵ. The first represents its ability to absorb heat, the second, its ability to emit heat. A black body is an ideal thermal body that absorbs and emits the maximum amount of heat possible, it is the reference ($\alpha = \epsilon = 1$). Gray bodies are bodies that have lowered abilities to do so, they are thus defined by an absorptivity and emissivity ranging from 0 to 1. The incoming and emitted heat, Q_{in} and Q_{out} are,

$$Q_{in} = \alpha\, A_{in}\, G_{in} \quad \text{and} \quad Q_{out} = \sigma\, \epsilon\, A_{out}\, T^4 \quad [W]$$

With G_{in} the incoming heat flux seen by the surface A_{in} and α and ϵ, the absorptivity and emissivity of the external surface of the sphere $\mathbf{A}_{out}$. As said in section 1.1, the emissivity and absorptivity depend on the wavelength of the emitted or absorbed radiation, α is denoted as the solar absorptivity (wavelengths from 0.3 to 3µm), ϵ as the infrared (IR) emissivity (wavelengths from 3 to 50µm). The absorptivity of a material at far IR wavelength can be approximated as its emissivity therefore $\alpha_{IR} = \epsilon_{IR} = \epsilon$.

Figure 1.27 shows the mean temperature of our sphere equipped with an external coating with different optical properties α and ϵ (respectively on y and x-axis). This figure points out that two different sets of (α, ϵ) can lead to a difference in mean temperature up to more than 200°C.

Figure 1.27 is drawn for $\beta = 0°$ and physical properties of the studied sphere.

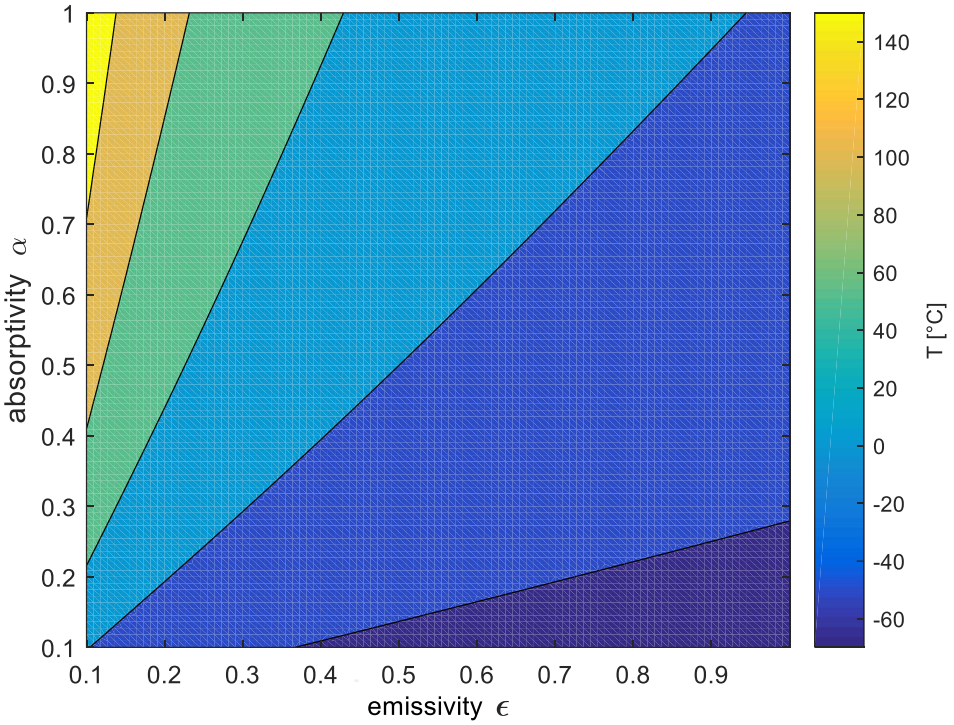


Figure 1.25 - Influence of the optical properties on the mean temperature of the sphere

The lower value of absorptivity and emissivity is set at 0.1 because, for an $\alpha = 0$, the temperature would quickly approach 2.7K (for zero internal dissipation) which is the equilibrium temperature of the deep space as it only emits heat while never absorbing any. For an $\epsilon = 0$, the mean temperature would never reach an equilibrium and tend to the infinity as it only receives heat without releasing any. Those two cases have no practical meaning.

It is also seen in Figure 1.27, that for a constant ratio α/ϵ, the mean temperature tends to be the same, this fact was already presented in section 1.1.

If only the ratio determines the mean temperature, does the actual value of absorptivity and emissivity matter?

In a thermally stable state, the absorbed flux must equal the emitted one over one revolution. During the illuminated phase, the sphere will absorb more flux than it will emit, the temperature will thus increase. During the eclipse, the sphere will emit more flux and its temperature will drop. The two phases must balance each other but it does not inform us about the amount of heat balanced. It is the actual values of absorptivity and emissivity that will. Indeed, the greater those values, the greater the absorbed and emitted fluxes and therefore the more extreme the temperature reached. This can be seen in Figure 1.26, the ratio α/ϵ is constant and equal to 1, the value of absorptivity and emissivity varies from 1 (black line) to 0.1 (red line). The fluctuations decrease with those values as the sphere absorbs and emits less and less heat.

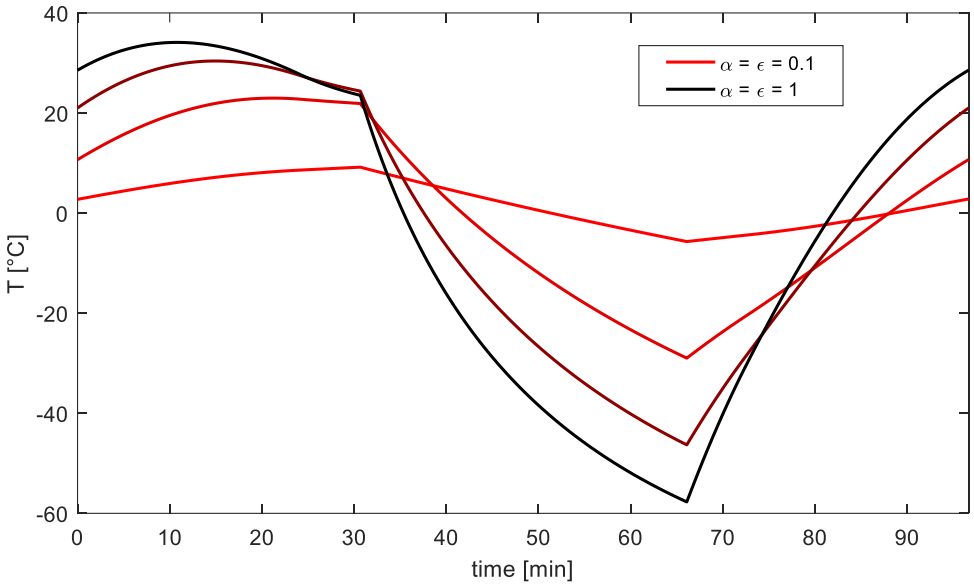


Figure 1.26 - Temperature evolution for different optical properties of same ratio

In conclusion, the ratio of the optical properties is important to determine the mean temperature of the sphere, and the actual value of the optical properties will influence the temperature fluctuations.

Solar Panels as Coating

Let us now consider an electrical device inside our sphere. For the sphere to provide electricity to its internal electrical device, it needs a power source. In space, the most available energy source is the Sun, and solar panels are the means to convert it into electricity. It is not the only technology that can provide energy to the sphere, but it is the most efficient in terms of power to mass ratio.

The efficiency of a solar panel η is defined as the ratio of the maximum power produced at 25°C, $(VI)_{\max}$, divided by the input solar energy,

$$\eta = \frac{(VI)_{\max}}{E_s A_{sc}}$$

With E_s the solar constant and A_{sc} the frontal area covered by solar cells, the frontal area is the equivalent area that is perpendicular to the solar rays. Most efficient solar cells, used for aerospace technologies, have about 30% of efficiency or $\eta = 0.3$. Solar panels are assemblies of solar cells connected through wires; the solar cells do not make the entire surface of the solar panel. The packing factor F_{sp} is thus introduced; it is the ratio of effective cell area to panel area.

On Figure 1.28, the energy balance of the incident solar flux G_s on a solar panel is depicted. A part of the flux is reflected ($\rho\, G_s$), the other part is absorbed and converted into a thermal flux (q_{th}) and electricity (q_{elec}). The electricity is used by internal devices and ends up being dissipated as heat (q_{diss}) or sent out of the sphere (q_{ext}) in another form (electromagnetic waves, heat, etc.). The heat will warm up the sphere resulting in a larger radiative emission (q_{out}), this completes the energy cycle.

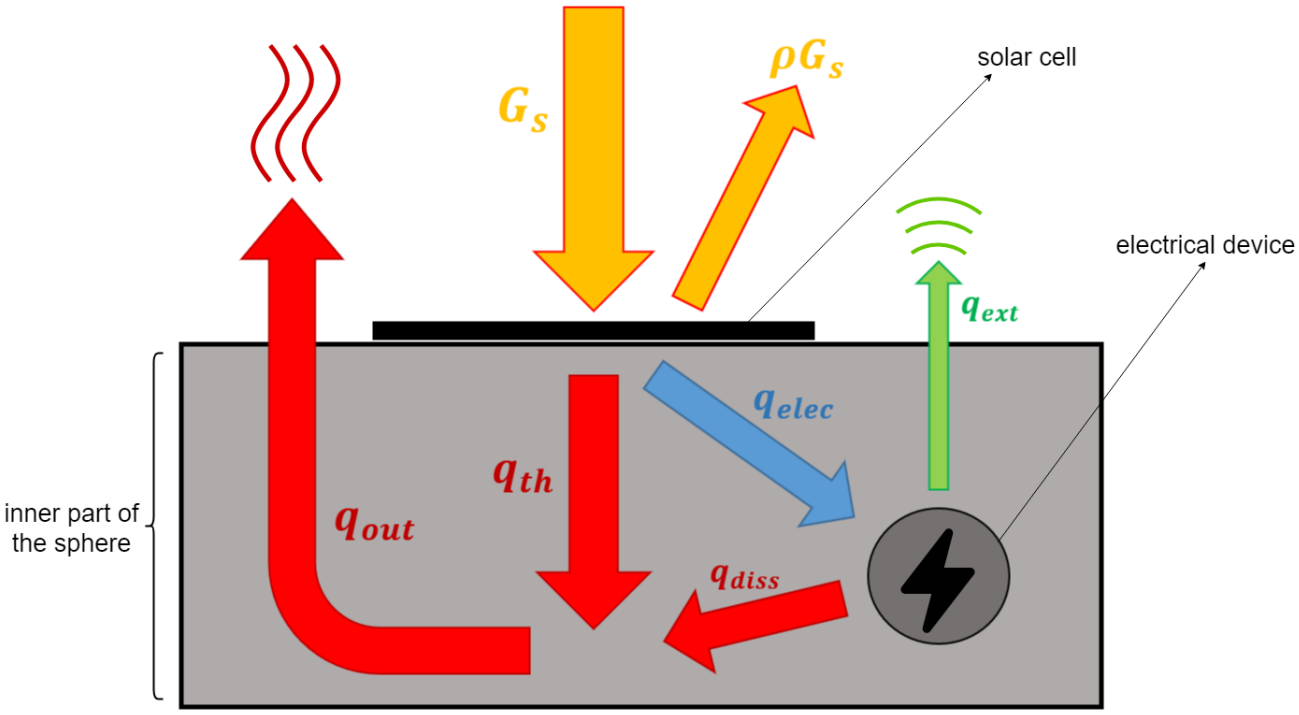


Figure 1.27 - Solar flux power balance through the sphere

By energy conservation and radiative absorption,

$$G_s = \rho\, G_s + \alpha\, G_s = \rho\, G_s + q_{th} + q_{elec}$$

$$\alpha\, G_s = q_{th} + q_{elec} = \alpha_{th} G_s + \alpha_{elec}\, G_s \quad \rightarrow \quad \alpha = \alpha_{th} + \alpha_{elec} \text{ with } \alpha_{elec} = F_{sp}\eta$$

With α the total absorptivity of the solar panel, α_{th} its thermal absorptivity and α_{elec} its electrical absorptivity. The latter corresponds to the efficiency of the panels which is the efficiency of the cells multiplied by the packing factor. Solar panels are placed on the outer surface and will thus serve as a partial coating for the sphere with thermal absorptivity α_{th} when the solar panels are producing electricity. Indeed, when they are not operational, no electricity is produced, their absorptivity is thus α and not α_{th}.

The typical absorptivity of a solar cell α is 0.75 and the typical packing factor of solar panels F_{sp} is 0.8 [5]. It makes a thermal absorptivity of operational solar panels α_{th} of 0.51.

After being produced, what happens to the electricity?

A substantial part of the incoming flux is transformed into electricity, q_{elec}, through photovoltaic modules. It is then directly used by the electrical device or stored in a battery. The battery storage will then provide electricity when it is needed.

Afterward, except for the devices that send out energy such as communication devices or propulsion engines ($q_{ext} \neq 0$), most internal devices will eventually dissipate their energy as heat. It is a consequence of energy conservation. A simple example is a moving electric car: 1 unit of electricity is used to rotate the motor which activates the wheels, converting the electrical energy into mechanical energy. An important fraction of the initial energy is already dissipated as heat in the transfer. The remaining energy used to rotate the wheels will dissipate as heat by friction with the air and the ground. If the car accelerates and gains kinetic energy, it will be dissipated as heat through the brakes when the car stops. In the end, the entire initial unit of electricity is dissipated as heat. This simple example applies to any device. In addition,

if the system is closed, the system provides the electricity, this electricity is consumed and given back to the system in the form of heat.

In conclusion, with the assumption of negligible energy sent out by internal devices, the electrical production from solar panels comes down to an internal dissipation. For a one-node approach, the only difference between direct heat flux is that, due to the battery, the dissipation can be distributed over time while the direct heat flux is imposed by illuminated/eclipse phases. This is only true if we do not consider the potential part of the energy sent out by the electrical device (q_{ext}) which is a realistic assumption in most cases.

$$q_{in,OFF} = \alpha \frac{G_s + G_a + G_e}{A_{out}} \qquad q_{in,ON} = \alpha_{th} \frac{G_s + G_a}{A_{out}} + \alpha \frac{G_e}{A_{out}} + q_{int}$$

With $G_{in} = G_s + G_a + G_e$, the incoming heat flux (solar, albedo and Earth IR), q_{int}, the internal dissipation, $q_{in,OFF}$ and $q_{in,ON}$, the absorbed fluxes in case of non- and operational solar panels.

Figure 1.29 shows this difference by displaying the heat fluxes over time for the sphere covered by solar panels. The left part corresponds to the situation of non-operational solar panels (which implies the non-operation of the internal device): the Earth IR, albedo and solar fluxes stack up to $q_{in,OFF}$ (black line). The right part corresponds to the situation of operational solar panels ($q_{in,ON}$): the same fluxes heat up the sphere, however a part of the albedo and solar fluxes is turned into electricity. This electricity is assumed to be constantly consumed by the electrical device, hence a constant heat dissipation (blue).

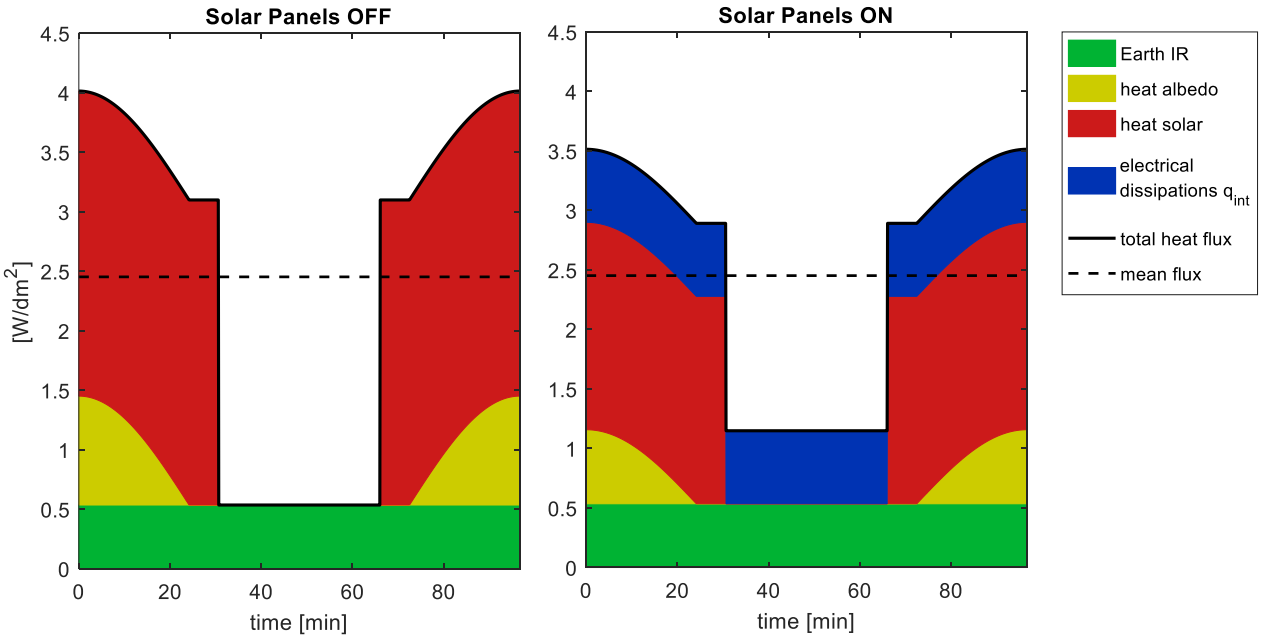


Figure 1.28- Solar panels influence on absorbed heat flux

In this figure are plotted the absorbed heat flux per unit area, q, it generalizes the idea for any size of the sphere. To have an idea of the order of magnitude of the power producible by an object in Earth orbit covered with solar panels, the maximal power given by a sphere, which occurs for an orbit without eclipses, is[5]

$$P_{sphere,\max} = \frac{1}{4} F_{sp}\, \eta\, E_s = 0.82 \left[\frac{W}{dm^2}\right]$$

[5] For simplicity sake, this power does not consider the albedo flux.

The mean value of this power over the orbital period is q_{int} and is displayed in blue in Figure 1.29 (for $\beta = 0°$). The maximal mean value occurs for $\beta > \beta_{\max}$ at what point it is equal to $P_{sphere,\max}$.

The actual maximal power per unit area producible by any object in those conditions is the power produced by a large plate with one face pointing the Sun. With a cross-section to area ratio approaching $1/2$, $P_{\max} = 2\, P_{sphere,\max}$.

As said, the mean heat received by the sphere (dashed black line on Figure 1.29) is the same for both cases, the heat is just distributed differently over time. The energy conservation is respected, in the second case, the solar radiations, before transforming into heat, have been used to make the device work. It is simply a better use of solar energy before it ends up being transformed into heat.

1.8 One-Node Analysis Parameters Discussion

In this section, we will discuss the influence of some of the parameters on the thermal behavior of the sphere. It helps us grasp the importance of each parameter.

1.8.1 LTAN and Scale Effect

A legitimate question is to ask what the influence of the LTAN of an SSO on the thermal behavior of our sphere is. While this consideration is interesting to discuss, we must keep in mind that parameters such as LTAN or scale depend on the mission objectives and are not adjustable for thermal requirements.

The main influence of the LTAN is the eclipse duration, from a maximum of one third of the time for LTAN 12:00 to a minimum of no eclipse for LTAN between 4:40 and 7:20. As the eclipse duration decreases, the mean temperature increases, this effect is plotted on Figure 1.30.

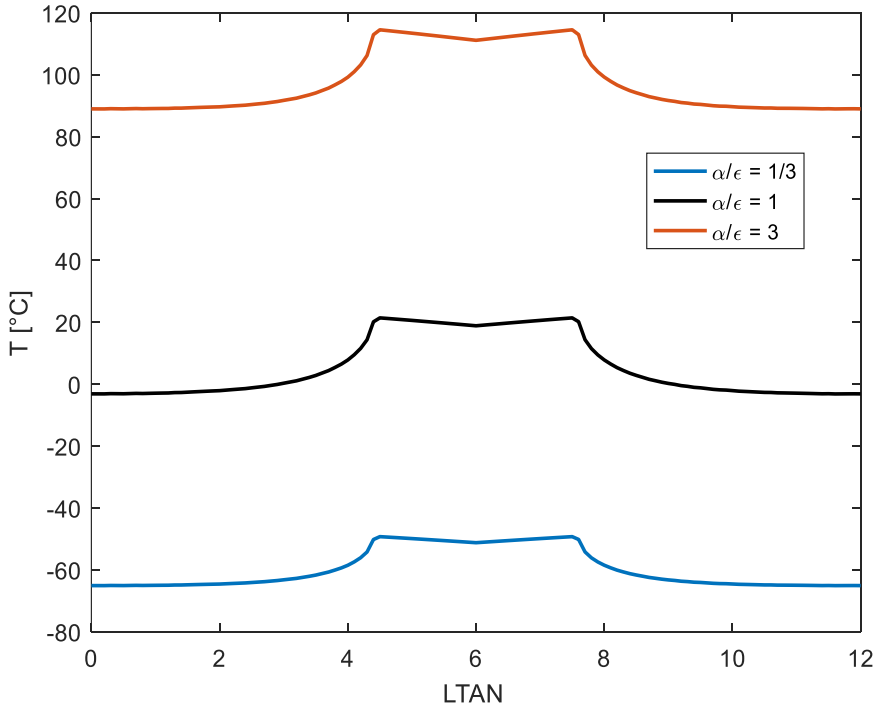


Figure 1.29 - LTAN impact on the mean temperature

The slight decrease of mean temperature for LTAN from 4:40 to 6:00 is due to the decrease of albedo effect for the same effect from the Sun and Earth IR. As it has been presented in section 1.7, the ratio α/ϵ is also of great influence concerning the mean temperature. It is why the mean temperature has been plotted for three different ratios, in order to see the relative impact of the LTAN with respect to the optical ratio impact.

From Figure 1.30 it is clear that the main parameter for the mean temperature is the ratio α/ϵ, the LTAN effect is small compared to that. The main influence of the LTAN on the mean temperature is the presence or not of an eclipse. Indeed, the mean temperature is about the same for LTAN with an eclipse ($|\beta| < |\beta_{\max}|$), and also similar for LTAN without an eclipse.

Another point to consider is that these curves are slightly modified with the dimensions of the sphere. Let us plot the mean temperature of unit optical ratio (black line on Figure 1.30) for different scale factors in Figure 1.31.

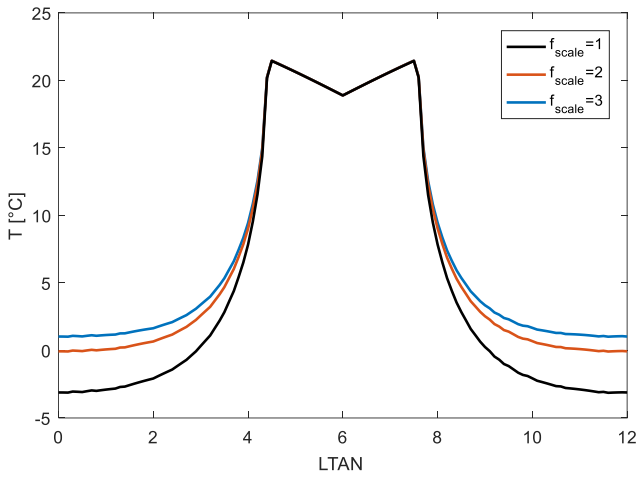


Figure 1.30 - Scale factor effect on mean temperature

As it can be seen, the impact of the scale is minimal.

But what does the scale affect?

To answer this question, we will use the balance equation,

$$\frac{\mathrm{d}T}{\mathrm{dt}} = \frac{Q_{in} - Q_{out}}{m\,c} = \frac{A}{m\,c}\,(q_{in} - q_{out})$$

With A the external area of the sphere of mass m made of material with specific heat c.

We define the scale factor as being the factor that multiplies the sphere radius. For a reference sphere with radius r, mass m and specific heat c, the scale factor f will act as follow,

$$r' = f\,r \qquad A' = \pi r^2 f^2 \qquad V' = \frac{4}{3}\pi r^3 f^3 \qquad m' \propto V' \rightarrow m' = m\,f^3 \qquad c' = c$$

The area increases to the square of the scale factor, while the mass, being proportional to the volume, increases to the cube of this factor.

The above equation becomes,

$$\frac{\mathrm{d}T'}{\mathrm{dt}} = \frac{A'}{m'\,c}\,(q_{in} - q_{out}) = \frac{1}{f}\frac{A}{m\,c}\,(q_{in} - q_{out})$$

The impact of the scale factor is inversely proportional to the variation of the temperature through time. In other words, the scale factor is directly proportional to the thermal inertia. It means that the greater f is, the less the temperature will fluctuate.

This effect is shown in Figure 1.32, where is plotted the temperature evolution of the sphere with different scale factors for a $\beta = 0°$.

As for the mean temperature, it increases with the scale factor as observed in Figure 1.31. The reason is that during the illuminated time, the temperature almost reaches its equilibrium while it does not during the eclipse, therefore small thermal inertia will decrease the temperature more during the entire eclipse, the longer the eclipse the greater the effect. It is why on Figure 1.31 the scale factor has a greater effect for LTAN with longer eclipse time. When there is no eclipse, the equilibrium temperature is reached, the thermal inertia has no influence anymore therefore neither has the scale factor.

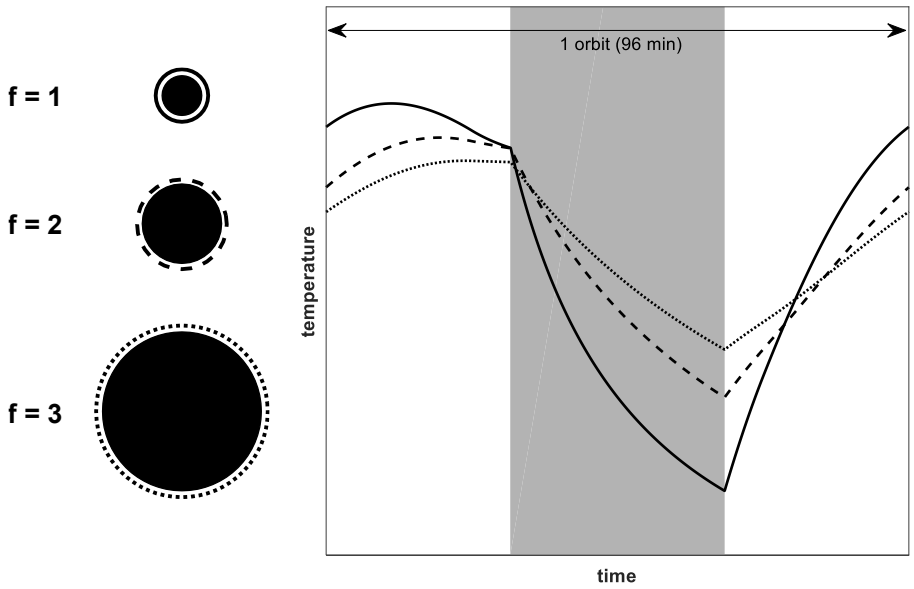


Figure 1.31 - Scale effect on the temperature: thermal inertia impact

The main aspect to remember about the scale effect is that the larger the scale factor, the greater the relative thermal inertia is.

1.8.2 Equilibrium Temperature during Daytime and Eclipse

For this section, let us use again the three spheres of section 1.5, i.e. one made of water, one of aluminum and one of gold. They all have the same mass and therefore different dimensions. In addition, they are now free of coating, and thereby have different optical properties.

As presented in section 1.1, the equilibrium temperature of an object in space is determined by a power balance between the incoming flux (from the Sun and the Earth[6]) and the outgoing flux (from its own emission),

$$Q_{in} = Q_{out} \quad \Rightarrow \quad T_{eq} = \left(\frac{\alpha}{\epsilon}\frac{A_{in}}{A_{out}}\frac{E_{in}}{\sigma}\right)^{\frac{1}{4}}$$

With E_{in} the incoming flux and α and ϵ the absorptivity and emissivity of the object of external area A_{out} and front area A_{in}. This latter area is referred to as the projected area of the object and depends on its shape. For example, the projected area of a sphere is its cross-section, it gives $\frac{A_{in}}{A_{out}} = \frac{1}{4}$, for a plate perpendicular to the solar rays, the projected area is one side of the plate, it gives $\frac{A_{in}}{A_{out}} = \frac{1}{2}$.

Let us now determine the equilibrium temperatures of our three spheres during the daytime but also during the eclipse (Figure 1.33). The case of the plate is also compared as it has a different shape.

[6] For simplicity sake, the albedo flux is not considered.

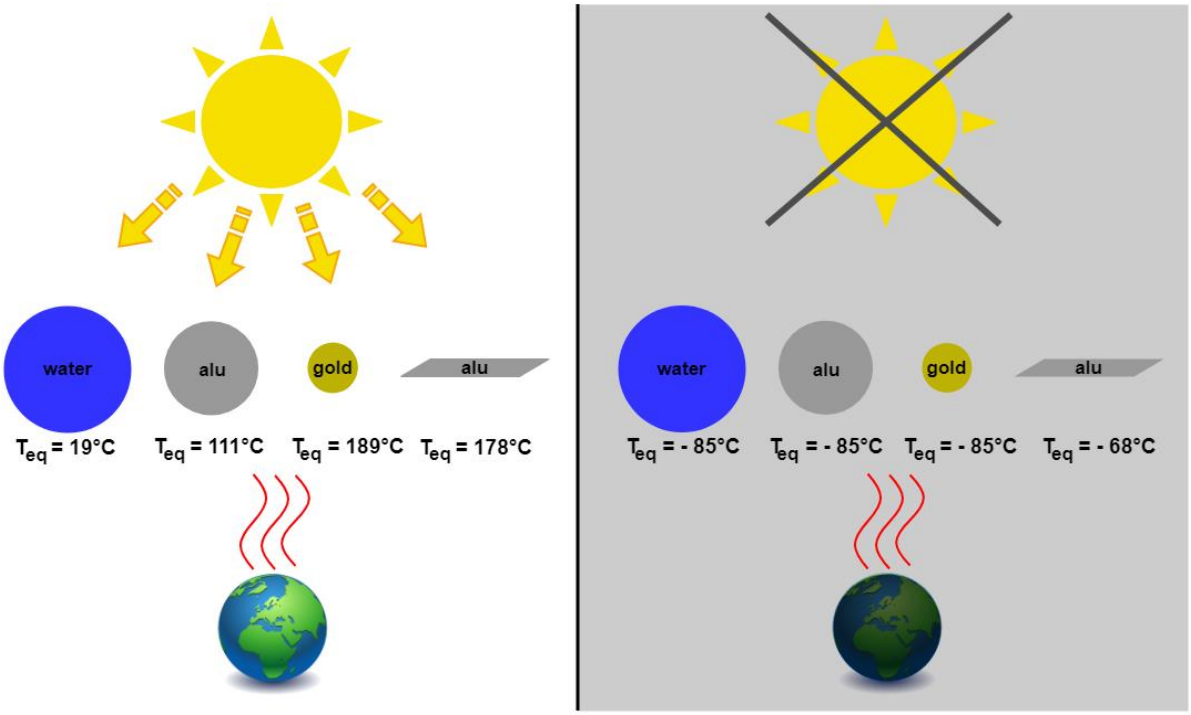


Figure 1.32 - Equilibrium temperature for different objects during daytime and eclipse

The following observations can be made:

- During the daytime, for the three spheres, only the ratio α/ϵ differentiates them from each other. Respectively, they have a α/ϵ ratio of 0.9/0.9, 0.15/0.05 and 0.25/0.04. It explains why their respective equilibrium temperature is increasing. Having a smaller A_{in}/A_{out}, the plate's equilibrium temperature is higher than the sphere made of the same material.
- During the eclipse, all spheres have the same equilibrium temperature. It is quite counter-intuitive since they have many differences. In fact, it comes from the previously mentioned fact: at far-infrared wavelengths, absorptivity and emissivity are similar, $\alpha_{IR} = \epsilon \longrightarrow \alpha_{IR}/\epsilon = 1$. Because, during eclipses, the only incoming flux is the Earth IR, the optical properties do not matter.

$$T_{eq,ecl} = \left(\frac{\alpha_{IR}}{\epsilon}\frac{A_{in}}{A_{out}}\frac{E_{in}}{\sigma}\right)^{\frac{1}{4}} = \left(\frac{A_{in}}{A_{out}}\frac{E_e}{\sigma}\right)^{\frac{1}{4}}$$

While A_{in}/A_{out} solely depends on the shape of the object, E_e also depends on the altitude of its orbit[7]. These two parameters constitute the only parameters that influence the equilibrium temperature during eclipses. Whatever its size, its mass, its coating or the material it is made of, an object will tend towards the same temperature during eclipses.

It is seen, for example, that for a plate which has a higher area ratio, the equilibrium temperature is higher.

This result is very interesting but must be put into perspective. While the actual dimensions and optical properties of the object will not affect the temperature it tends to, they will affect the rate to reach it. As seen in section 1.8.1 and 1.7, if the dimensions or the optical properties increase, so does the thermal inertia. With a higher thermal inertia, the equilibrium temperature is more slowly reached. In addition, the eclipse period being short, the equilibrium temperature is often never reached, the rate is thus essential.

[7] The altitude influence is limited in the considered altitude range. The change between 470 km and 650 km brings at most 4°C of difference.

1.8.3 Optical Properties Considering Solar Panels

In section 1.7, our sphere was only covered with solar panels, a more realistic situation is to have a mix of solar panels and another material as the coating. The optical properties of the solar panels are set, but those of the remaining area can be chosen, in this section, we look at the influence of such a choice.

The overall absorptivity and emissivity are, in that case, defined with the ratio of each material,

$$\alpha_{tot,OFF} = \alpha_{sp} r_{sp} + \alpha_2 (1 - r_{sp}) \qquad \alpha_{tot,ON} = \alpha_{sp,th} r_{sp} + \alpha_2 (1 - r_{sp})$$
$$\epsilon_{tot} = \epsilon_{sp} r_{sp} + \epsilon_2 (1 - r_{sp})$$

With r_{sp}, the ratio of solar panels area to total area, α_{sp} and α_2 the absorptivity of the panels and the second coating (same indexes for emissivity), $\alpha_{tot,OFF}$, the total absorptivity seen by the IR flux from Earth (wavelength radiation outside the visible range and not convertible into electricity by the panels) or in case of non-operational solar panels, $\alpha_{tot,ON}$, the total absorptivity seen by the solar and albedo fluxes in case of operational solar panels, and ϵ_{tot}, the total emissivity of the sphere.

The sphere temperature is plotted for different coatings in Figure 1.34. On the left, the first coating is a coating with black body properties (black line), the second is a coating made entirely of solar panels (yellow line), the last one is a coating made of aluminum (gray line). The optical properties are respectively [5] : α/ϵ = 1/1, 0.75/0.75, 0.15/0.05. For the second case, with solar panels, the electricity produced is dissipated as heat throughout the orbit, as analyzed in section 1.7. The right part of Figure 1.34 presents the sphere with a coating made of a mix of solar panels and aluminum, this mix is assumed to be homogenous over the external surface. The temperatures correspond to a ratio of solar panels area to total area, r_{sp}, ranging from 0 (gray line, only aluminum coating) to 1 (yellow line, only solar panels), with constant increments of 0.05.

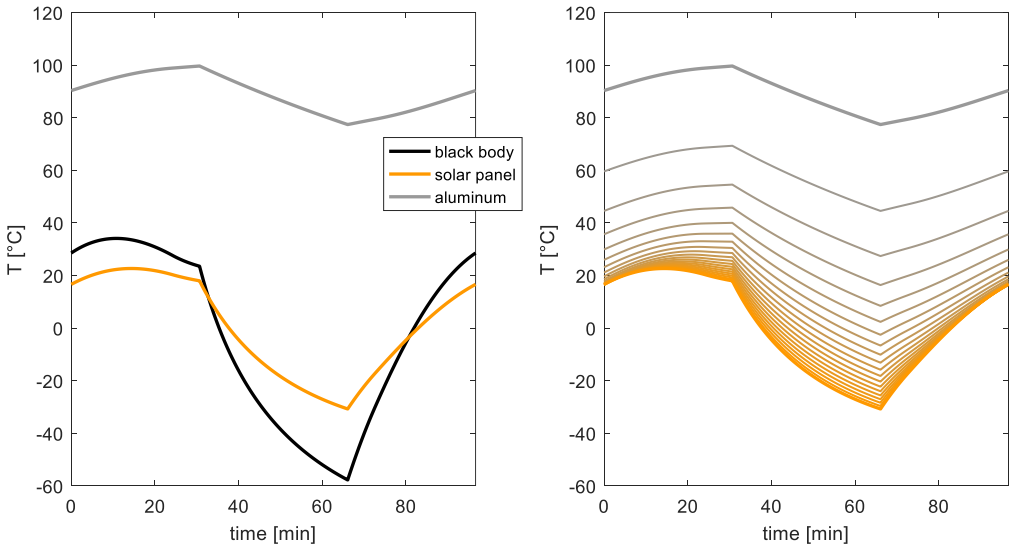


Figure 1.33 - Sphere temperature with different coatings

The following observations can be made:

- On the left of Figure 1.34, the mean temperature of the two first coatings is similar while it is way larger with the aluminum coating. It is due to the absorptivity/emissivity ratio, indeed, the third coating has a ratio three times larger than the others.
- The temperature with the black coating fluctuates more than the two others, it is due to its larger absorptivity and emissivity (see section 1.7).

- On the right of Figure 1.34, each increment of r_{sp} does not have a similar effect on the temperature. Indeed, the presence of aluminum only affects the temperature when r_{sp} is small. It means when there is a lot of aluminum compared to panels because its optical properties are smaller than the one of the solar panels. As the aluminum becomes more prominent, the ratio α/ϵ get larger, increasing the mean temperature, and the values of α and ϵ become smaller, which decrease temperature fluctuations.

In other terms, varying the mix constituting the coating is equivalent to vary the overall optical properties of the sphere. If we let the second material's optical properties be tunable, the overall properties will be too, to a certain extent.

We have learned from this section that solar panels have a great influence on the temperature of an object in space that needs to produce power. It is due to their optical properties of high values which cannot be tuned.

1.8.4 Altitude Variation

The altitude range considered is from 470 to 650 km. Since the beginning, we have considered an altitude of 600 km, implicitly assuming the interval to be small enough for its influence to be neglected.

What is the actual influence of the altitude variation?

Concerning the incoming fluxes intensity, while the solar flux remains the same, the Earth IR and albedo flux intensity decreases with the altitude. Indeed, the further the sphere is compared to the Earth, the less it will be reached by fluxes coming from Earth. By the view factors introduced in section 1.4, we compute a decrease of 9% between the amount of heat received by the sphere at 470 km and 650 km of altitude.

Another influence of altitude variation is on the eclipse proportion per orbit. As the altitude increases, the eclipse proportion decreases, Figure 1.8 in section 1.3 helps intuitively understand this fact. The difference in eclipse proportion for an altitude of 470 and 650km is shown in Figure 1.35 (left) as a function of the LTAN of the orbit.

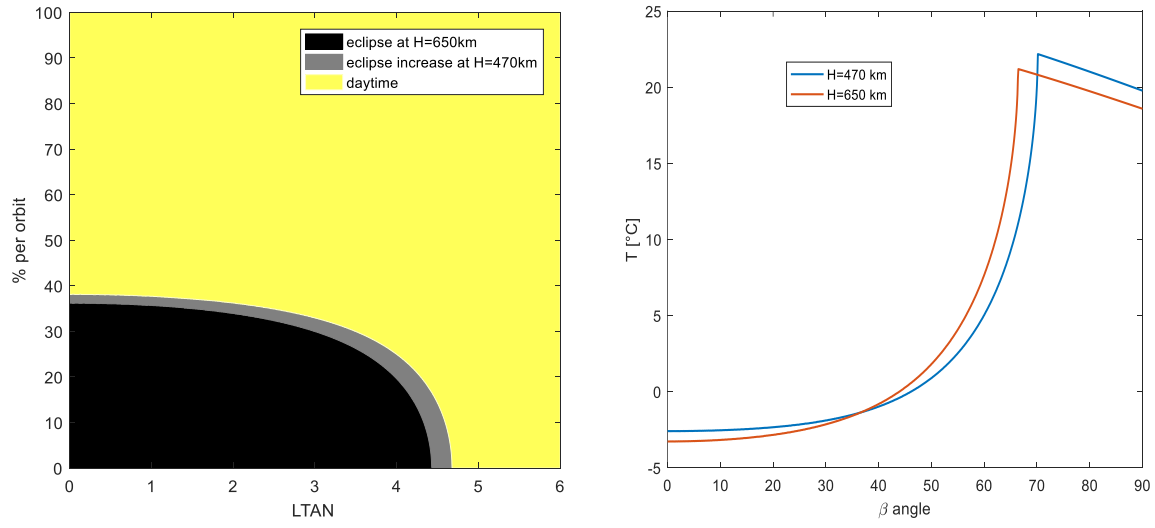


Figure 1.34 - Altitude influence (left: eclipse proportion, right: mean temperature)

Both effects of the altitude variation have an impact on the mean temperature of the sphere: on the one hand, the higher the altitude, the less heat from Earth is received, and on the other hand, the higher the altitude, the shorter the eclipse. Both have an opposite impact as the first will decrease the mean temperature and the second increase it. The mean temperature is displayed on Figure 1.35 (right), the first effect is predominant for small LTANs and the second for higher ones.

For such a small interval of altitude, this influence is only meaningful for β angles close to β_{max} when the eclipse duration approaches zero.

1.9 Comparison between Sphere and Cube

A basic CubeSat being cube-shaped, we will now analyze the impact of turning our sphere into a cube.

Shape Influence

Let us take the solar flux and place an object inside the beam, the projected area of the object, equivalent to its shadow in this case, is the equivalent area that receives the rays perpendicularly to its surface. This notion is important in our case of one-node analysis. Indeed, the external heat fluxes are expressed up to now in Watt per unit of normal area [W/m²], therefore, whatever the external shape, only its projected area will be useful to us.

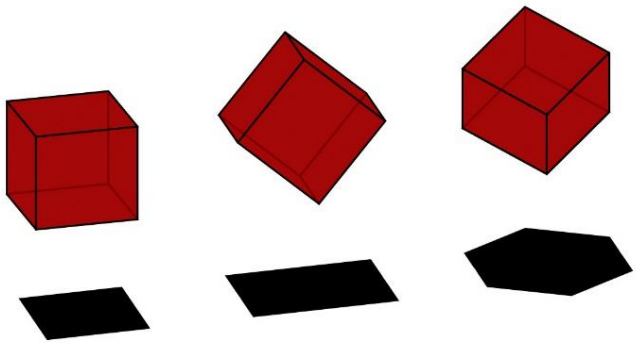


Figure 1.35 – Projected areas of a cube

The projected area of a sphere is equivalent to its cross-section, which is a disc of the same radius, that is to say πR^2, this area is constant for any external flux direction. This is not the case for a cube, this fact is shown in Figure 1.36, the projected area of the cube facing the flux is the face itself while the projected area of a cube centered on its edge or its corner is respectively a rectangle or a hexagon.

What actually matters is the ratio of the projected to total area, it corresponds to the ratio of absorbed to emitted heat flux.

This ratio, named the projected ratio r_{pr}, is unique for the sphere and equal to 1/4. For the cube, the largest projected area possible is the third case shown in Figure 1.36 where the area equals to $\sqrt{3}c^2$. The projected ratio of a cube is thus comprised in,

$$r_{pr,cube} \in \left[\frac{1}{6}; \frac{\sqrt{3}}{6}\right] = [0.167; 0.289]$$

Depending on its attitude, the projected ratio of a cube can be smaller or greater than the one of the sphere. It means that, for the same external area, a cube has the possibility to receive more or less heat from the Sun depending on its attitude. The extreme cases are the face-centered and the corner-centered attitudes (respectively on the left and right of Figure 1.36).

If we consider the cube as one thermal node, meaning that we do not differentiate each face, the thermal analysis of the cube would almost be the same of the one of a sphere of the same area. The differences are the Earth view factors, the projected ratio and the mass (considering an equivalent density). The first is intrinsic to the shape and also depends on the cube attitude, as does the second. The third implies a

diminution of mass by a factor equal to the ratio of the volume of a cube and a sphere of the same area, which is 0.72.

Randomly Spinning Cube

In this subsection, we consider a cube without attitude control, in other words, a randomly spinning cube. This cube has the same external area than the sphere analyzed up to now.

A randomly spinning cube has a mean projected area equals to $1/4$. This is actually the case for any convex polygon that randomly spins, among them, the sphere. It can be intuitively understood with the fact that we distinguish a sphere out of an extremely fast spinning cube.

The sphere and the randomly spinning cube have the same projected area for the same external area. Therefore, they share the same projected ratio, which means that they globally absorb and emit the same amount of heat.

As the previous subsection suggested, there is also a difference in the Earth view factors, which is intrinsic to the shape, and in the mass, if we consider an equivalent density.

Figure 1.37 plots the temperature evolutions of the pre-mentioned sphere (grey line) and the spinning cube (dashed black line). The temperature for the spinning cube if we consider the same mass as the sphere is also plotted (in dashed red line). The latter is almost exactly the same as the sphere, which is totally to be expected since the projected ratio and the mass are the same, the slight inequality comes from the difference between the Earth view factors. For the cube of same density, the mass reduction implies a thermal inertia reduction and therefore wider temperature fluctiations.

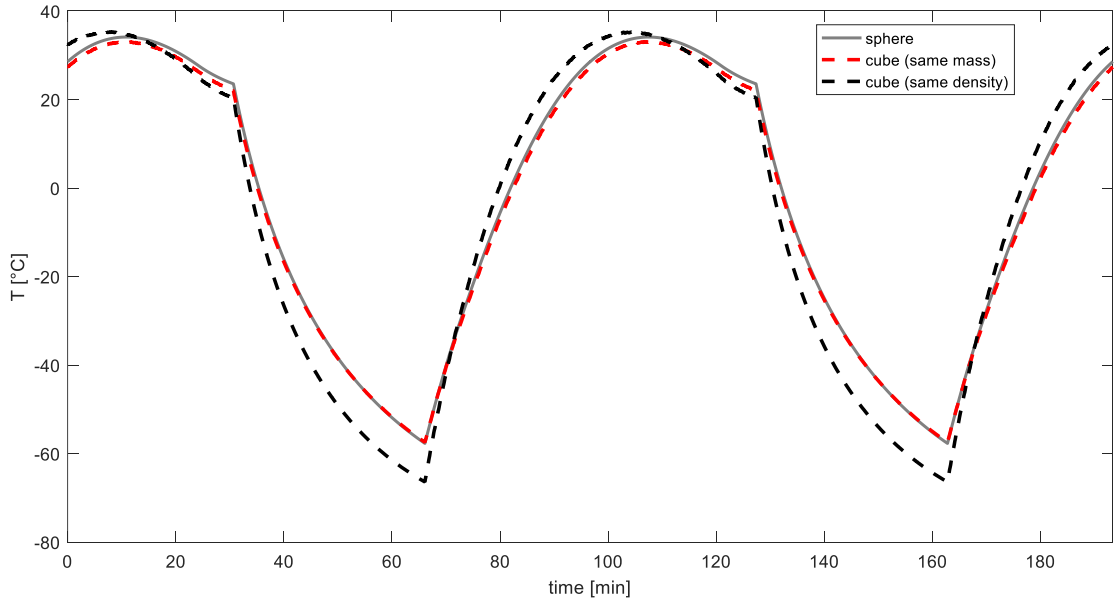


Figure 1.36 - Temperature evolution of a randomly spinning cube

The cube and the sphere are black bodies with an external area of 0.031 [m^2] and a specific heat of 900 [J/kgK]. The sphere as a mass of 0.5 [kg] and the cube one of 0.36 [kg].

This subsection showed that the entire analysis made up to now applies to a cube-shaped object orbiting around Earth.

Non-Randomly Spinning Cube

For a cube with attitude control, any attitude is possible. For example, we could imagine an optimal attitude which is for the cube to face the Sun-centered at one corner (third position of Figure 1.36) in order to have the largest projected area that always faces the Sun. This attitude is the optimal one in terms of electricity production, but another legitimate attitude is that one face always faces the Earth, this attitude gives a constant link with the Earth which can be helpful for easy communications or in case of Earth observation missions.

For the latter case, it is more interesting to consider each face separately. We have previously analyzed the incoming flux to the sphere in general, in other words, the sum of all the fluxes coming from different directions. By considering each face, the direction of the fluxes will have its importance since each face does not see the same incoming flux.

Let us consider this case, an attitude control such as one face is always oriented towards Earth, also called Earth or nadir attitude.

Each face has now a defined direction, the denomination of the different directions is,

- Nadir: direction towards the Earth. (1)
- Zenith: direction towards the Sun at subsolar point, opposite to nadir. (2)
- Velocity: direction of the movement of the cube. (3)
- Anti-velocity: opposite direction to velocity. (4)
- Pitch: direction orthogonal to zenith and velocity. (5)
- Anti-pitch: opposite direction to pitch. (6)

Figure 1.38 helps visualize the different directions that describe each face of an orbiting cube in a nadir attitude.

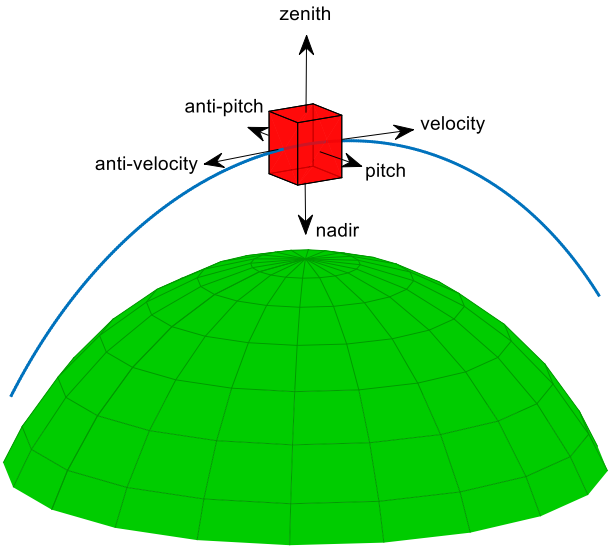


Figure 1.37 - reference directions of an orbiting cube

The numbers in parentheses are the numbers that will be used to denominate each face.

The faces of a cube being flat, the solar flux sees a face multiplied by the cosine of ρ, with ρ the angle between the face direction (Figure 1.38) and the direction of the solar ray (Sun-Earth axis),

$$G_{s,i} = \cos(\rho_i)\, E_s\, F_{ecl} \left[\frac{W}{m^2}\right]$$

The index i corresponds to the faces from 1 to 6, respectively nadir, zenith, velocity, anti-velocity, pitch, anti-pitch.

The radiation from Earth to the sphere was described by a view factor F_e, for a cube, each face is described by a view factor $F_{e,i}$. The view factor between a plate i and a large sphere is given by the following expression in function of η_i, the angle formed by the normal of the plate and the plate to the sphere center direction (right part of Figure 1.39), [5]

$$for\ |\eta_i| \leq \text{acos}\left(\frac{1}{h}\right):\ F_{e,i} = \frac{\cos(\eta_i)}{h^2}$$

$$for\ |\eta_i| > \text{acos}\left(\frac{1}{h}\right):$$

$$F_{e,i} = \frac{1}{\pi h^2}\left(\cos(\eta_i)\,\text{acos}(y) - x\sin\left(\eta_i\sqrt{1-y^2}\right)\right) + \frac{1}{\pi}\text{atan}\left(\frac{sin\left(\eta_i\sqrt{1-y^2}\right)}{x}\right)$$

With $x = \sqrt{h^2 - 1}$ and $y = -x\cot(\eta_i)$

Figure 1.39 depicts the situation (not at scale) on the right, and on the left, the view factor $F_{e,i}$ as a function of η_i. The black line corresponds to an altitude of 470 km, the red area comprises the values for an altitude from 470 to 650 km. The altitude difference in this interval does not affect much the view factor.

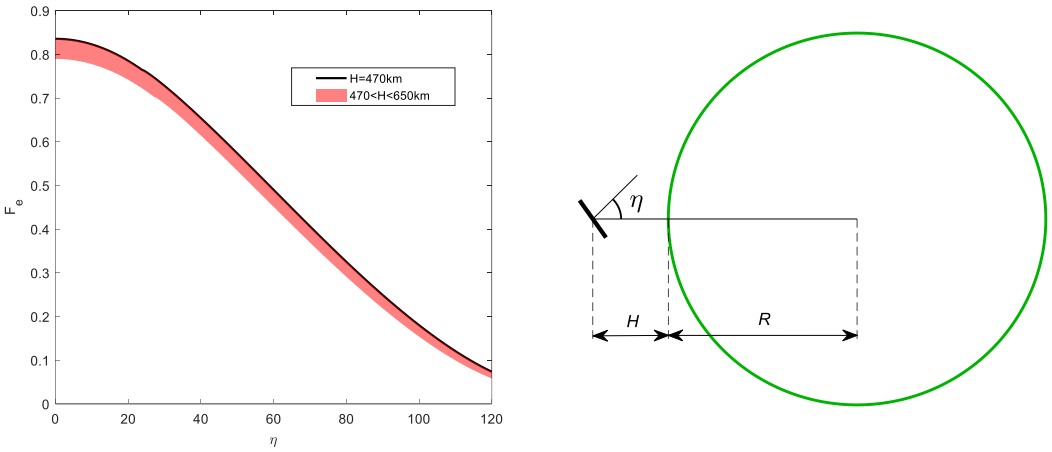


Figure 1.38 - view factor from plate to Earth

One can observe that the view factor is not null for $\eta > 90°$, indeed, the plate is so close to Earth that, for such angles, it still sees a part of it.

Let us now compare the view factors of the sphere and the cube by comparing the flux intercepted by the satellite during the eclipse:

- The sphere receives $G_e = F_e\,E_e = 1.19\,E_e\ \left[\frac{W}{m^2}\right]$ (see section 1.4.1), this value is per unit area of cross-sectional section, in order to compare the two on the same basis, we will modify it in per unit of total area since they have the same, $G'_e = 0.297\,E_e\ \left[\frac{W}{m^2}\right]$.
- The cube intercepts $G'_e = \frac{1}{6}\sum F_{e,i}\,E_e$. In the pre-mentioned attitude, the nadir face sees the Earth with $\eta = 0°$, and the 4 perpendicular faces see it with $\eta = 90°$. It gives $G'_e = \frac{1}{6}(0.835 + 4 * 0.25)E_e = 0.305\,E_e\ \left[\frac{W}{m^2}\right]$.

The two satellites, cubic and spherical, for such an attitude, see approximately the same amount of flux coming from the Earth. This fact does not change either within this range of altitude or with the satellite properties (mass, area, etc.) as long as the two satellites have the same external area.

Figure 1.40, on the left, shows the incoming flux per unit area on each face of the cube for an SSO 12:00. On the right, the total incoming flux per unit of total area of the cube is compared to the one of the sphere that has been analyzed in the previous sections.

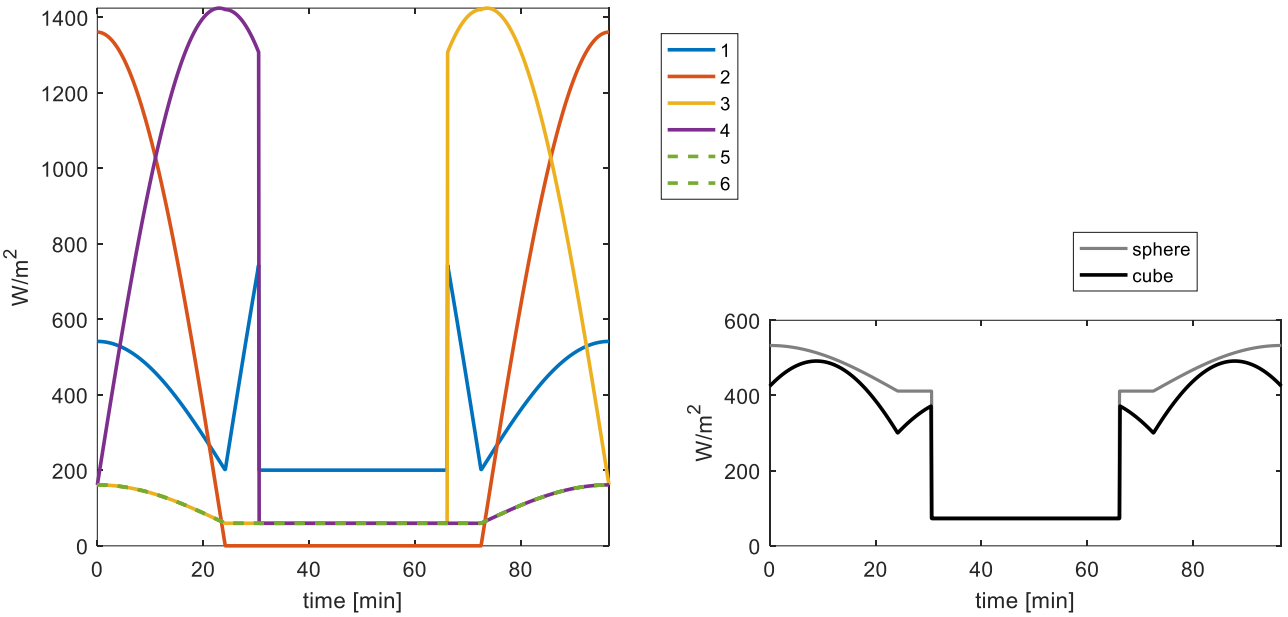


Figure 1.39 - Incoming heat flux on each face of a cube (left) and on average (right)

Let us analyze the incoming flux on each face (left part in Figure 1.40):

- Nadir face (1): At the start, the cube is at the subsolar point, the flux received is the maximum flux from Earth (albedo and IR), as the cube moves away from the sub-solar point, this flux decreases. Until it reaches the fourth of its period and the solar flux starts to see the face, only for a brief moment before entering the eclipse phase when only the Earth IR flux reaches it. The second part of the period is logically symmetric to the first.
- Zenith face (2): As it is opposed to nadir, only the solar flux can reach this face, the incoming solar flux starts at its maximum (subsolar point) and decreases until the eclipse begins at what point no flux reaches it anymore.
- Velocity and anti-velocity (3 and 4): For the velocity face, at the beginning, only the Earth fluxes reach it. The incoming flux is weaker than at the nadir face as these faces are perpendicular to Earth. The flux decreases down to a constant value (only IR, no albedo anymore), until it exits the eclipse phase, at which point it is illuminated by the Sun. The fluxes reaching the anti-velocity face are symmetric.
- Pitch and anti-pitch (5 and 6): The flux reaching both faces is the same. None of them ever sees the Sun, and they have always a perpendicular position compared to Earth, therefore they receive the same flux from Earth albedo and IR.

We must pay attention that it is a nadir SSO 12:00, it is the only case where two sides of the cube do not see the Sun (pitch and anti-pitch). In any other LTAN for a nadir SSO, only one side will never see the Sun.

As for the right part of Figure 1.40, the total incoming heat flux on the sphere is less fluctuating, because of its more regular shape, and its mean value is superior because it has a superior projected ratio than the cube in this attitude. As analyzed, the incoming heat flux during the eclipse is about the same for the

sphere and the cube. To have a meaningful comparison, a cube with the same external area as the sphere is considered.

For an SSO 12:00 ($\beta = 0°$), the inclination of the orbit has no impact, but this is not the case for greater LTANs as it has an impact on the eclipse duration and occurrence. The incoming flux for different LTANs with an inclination of 98°, as well as the effect of the inclination, are shown in Appendix C.

The temperature variation of the cube, with LTAN 12:00 and nadir attitude, is displayed on Figure 1.41. It is compared to the temperature of a sphere with the same orbit and the same external area. The cube, due to its shape, has a less smooth variation but keeps the same trend as the sphere.

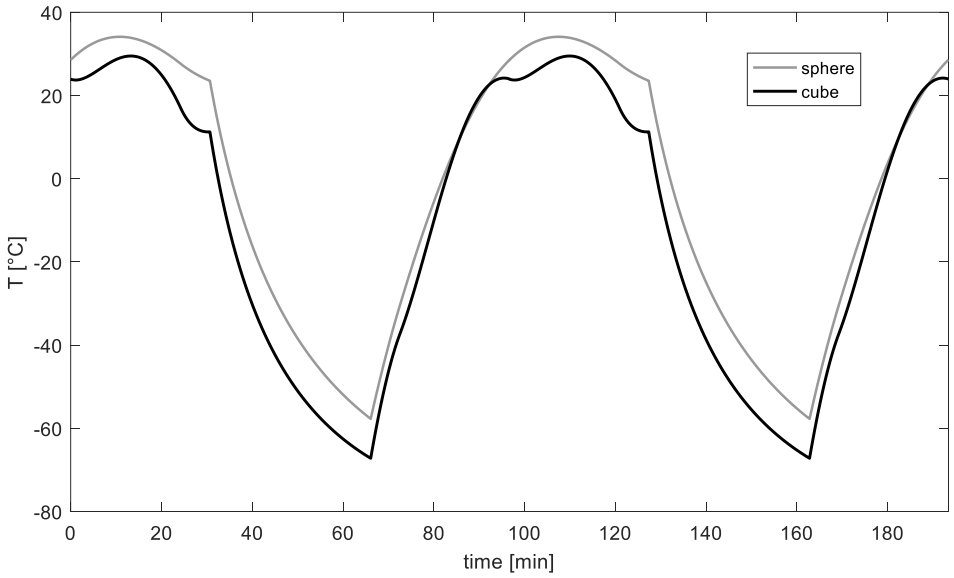


Figure 1.40 - Temperature evolution of a cube

Temperature elvolutions for different LTANs are shown in Appendix C.

This section has shown that, for a one-node analysis, a cube and a sphere share a similar thermal behavior.

1.10 Conclusion

The first chapter had for purpose to introduce the reader to the thermal behavior of an object in space with a one-node analysis. The analysis was more and more detailed throughout the chapter.

For starters, a sphere that only sees the Sun will reach a stable state at an equilibrium temperature solely depending on the optical properties of its coating. Considering the effect of the Earth, the sphere will present a periodic thermal behavior. Indeed, besides emitting heat (Earth IR) and reflecting solar rays (albedo flux), its main effect is to block the solar radiations during eclipses. The sphere cools down during eclipses and warms up when illuminated by the Sun. The presence and duration of the eclipse mainly depend on the LTAN of the orbit of the sphere. The altitude having been considered in a restricted range has a negligible impact.

By adding an internal electrical device, the sphere consumes energy that will eventually be dissipated as heat. Overall, it warms up the sphere but can also be used to regulate the temperature as it can produce heat during eclipses. The electricity consumed by internal devices usually comes from solar panels as a partial coating of the sphere. The produced power per unit area depends on the proportion of the external area covered with solar panels, as well as their locations and the attitude of the sphere. The inside of the sphere being a nearly closed system, the energy produced by solar panels is conserved and ends up being dissipated as heat. The amount of heat received by the sphere is thus the same whether the panels are operational or not. Yet, when they are operational, this heat can be distributed differently over the orbit.

Solar panels have fixed optical properties, it is thus with the remaining area that we can tune the averaged optical properties of the sphere. The main parameter is the ratio of absorptivity to emissivity which characterizes the coating, it determines the mean temperature which is higher as the ratio increases. For a given ratio, the actual values of the optical properties, absorptivity and emissivity, affect the temperature variations of the sphere. The closer to the unity they get, the higher are the temperature fluctuations. The mass and the material affect the thermal inertia of the sphere as its thermal capacity is directly related to it. The scale effect has the same impact, increasing the scale factor is equivalent to a growth of thermal capacity which means a gain of thermal inertia.

The concept of thermal inertia is essential for an object undergoing a cyclic thermal behavior because it reflects the rate at which the body tends to an equilibrium which varies between daytime and eclipse. On the other hand, it has no influence on the equilibrium temperature itself. While this temperature mainly depends on the ratio α/ϵ when exposed to the Sun, it becomes only a matter of object shape and altitude during eclipses.

Finally, the sphere is turned into a cube which is the shape of interest as it is the basic shape of a CubeSat. The major difference is a non-constant projected area which depends on the attitude of the cube. Two cases are distinguished, a randomly spinning cube (no attitude control) and a cube with attitude control. Without attitude control, the cube matches the thermal behavior of a sphere with the same external area and mass. With attitude control, it makes more sense to analyze the incoming heat fluxes on each face of the cube.

This analysis considered a cube as being one node, the temperature of the cube is taken as a whole and does not differentiate the temperature on each face. It corresponds to a cube with infinite thermal conductivity. This is evidently not the case and this chapter, as it became more and more detailed, introduces the need for a more detailed model. Such a model must correspond to a specific mission and loses in generality as it was the objective of this first chapter. Nonetheless, it is important to link those considerations with a concrete example, it will constitute the third chapter. The second chapter will present the main features of a CubeSat and its thermal requirements.

2 CubeSat Architecture and Thermal Requirements

This chapter presents the different subsystems of a typical CubeSat: technical description, thermal requirements and performances. In particular, the Thermal Control System (TCS) and its existing technologies are detailed. Beyond introducing the reader to the operation of a CubeSat and its main technical features, this chapter has for underlying objectives to establish the subsystems' operating temperature ranges, its mass breakdown and its power budget. These elements will come in handy for the last chapter.

2.1 CubeSat Subsystems

A CubeSat is divided into different subsystems. Each subsystem carries a key function for the satellite survival or for its mission objectives.

Each subsystem can be found as a commercial off-the-shelf (COTS) component. It stems from the desire for standardization and it implies that subsystems are separated from one another and usually stacked in layers of PCB. The standardization has many advantages such as cost reduction, conception time and resources reduction and use of state-of-the-art components. This philosophy contrasts with the way space engineers traditionally thought. Indeed, for conventional satellites, they used to prefer components that had proven to work in orbit, making the advancements in space technologies progress slowly.

The general configuration of a CubeSat is given in Figure 2.1 for a 2U CubeSat.

The payload is the reason for the satellite, it will fulfill the purpose of its mission, for example, a camera in an observation satellite. The Attitude Determination and Control System (ADCS) orientates the satellite in space. The On-Board Computer (OBC) is the brain of the CubeSat, it commands the other subsystems and checks

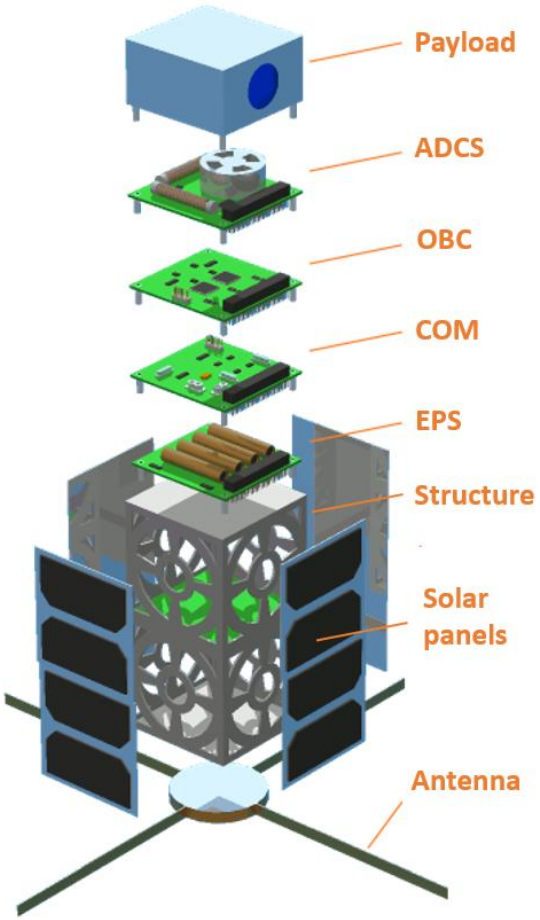


Figure 2.1 - CubeSat configuration, adapted from [118]

their operations. The communication subsystem (COM) is in charge of the communication with Earth or other satellites. The Electric Power System (EPS) manages the power generation, storage and distribution within the satellite. The structure is the skeleton of the satellite, it keeps every subsystem together.

Figure 2.2 is the block diagram of a CubeSat. It connects all subsystems with regard to power distribution and data exchange (respectively solid blue and dashed oranges arrows).

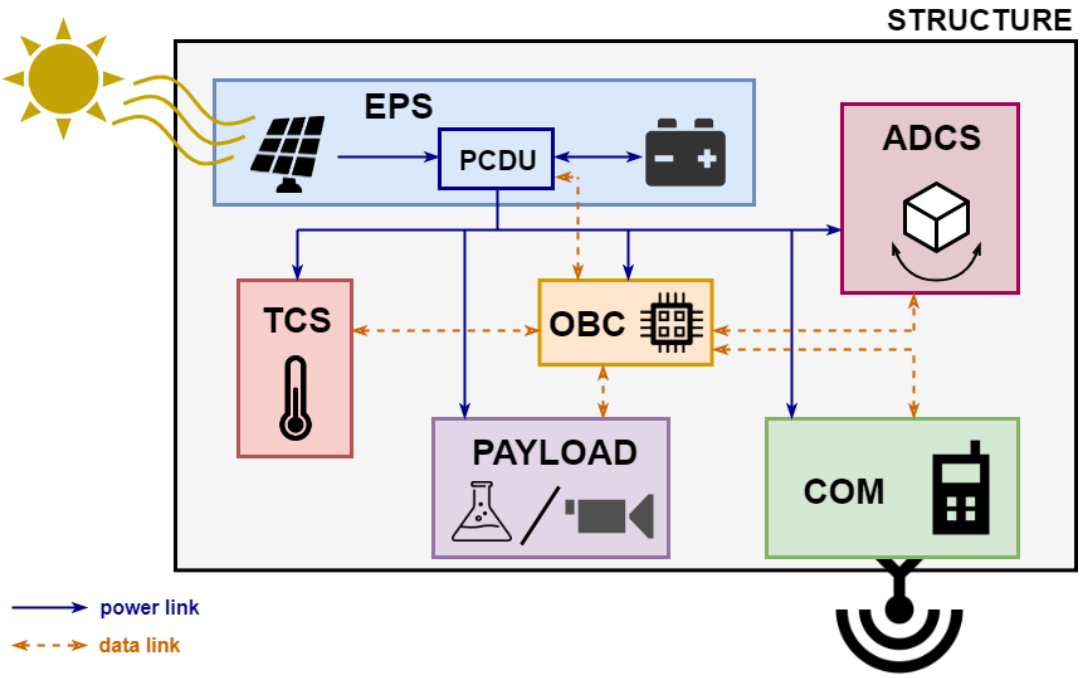


Figure 2.2 - CubeSat's subsystems block diagram

This subsection aims to present each subsystem and detail their technical contents, thermal requirements and performances. In our concern, thermal requirements mean temperature limits. Due to their COTS nature, the temperature range of a component is most likely provided by the manufacturer.

An important consideration to point out is that the temperature limits given by the manufacturer can result from 3 situations:

- The device fails, breaks or deteriorates beyond these limits.
- The device decreases in efficiency or performances, below an acceptable threshold defined by the manufacturer.
- The device has been tested up to these temperature limits and was still operating as required. More extreme temperatures have not been tested because it was not necessary or by lack of means.

The third reason implies that the temperature limits indicated by the manufacturer ensure that the device can properly work up to those limits but do not say that it does not work beyond. The manufacturer is just not able to ensure it. It also says that the limits are not always specified for physical limits, one component could work beyond the limits, as well as it could not.

The second and third reasons explain why different manufacturers usually have different temperature limits for similar components.

2.1.1 Primary Structure

The primary structure, also called frame or chassis, is the skeleton of the CubeSat, it carries all the mechanical loads. The two most important properties of the structure are strength and stiffness. From launch to orbit, the satellite is put under great forces, the material of the structure must maintain its integrity and not break or bend at any moment. The materials that comply the most with those requirements are carbon composite or metals.

Other important properties of the material are low density and good resistance to extreme temperatures. In addition, its economic viability will also be considered.

Thereby, aluminum is the most often chosen material. On its own, it is not incredibly strong but when combined into alloys with other metals, it becomes much stronger.

The most common aluminum alloys for a CubeSat's structure are 6061 and 7075 aluminum. The first is composed of 95.8 to 98.6% of aluminum, with magnesium and silicon as main alloying elements. The second is composed of 87.1 to 91.4% of aluminum, the main alloying elements being zinc, magnesium and copper. These alloys have a density of 2.7-2.8 [g/cm^3].

The primary structure usually accounts for about 10% of the total mass.

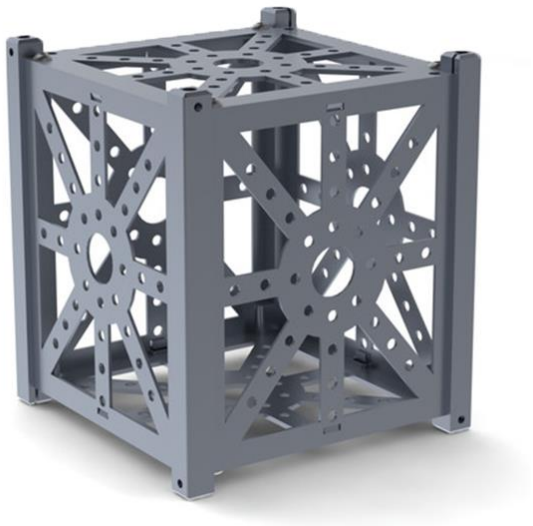


Figure 2.3 - CubeSat structure [104]

The thermal limits for the structure are not constrained by its melting point (>500°C), nor by its strength decrease point (>150-200°C) [7], but by its expansion with temperature. Indeed, over one orbital period of about 96 minutes, the alloy compresses at low temperatures (during the eclipse) and expands at high temperatures (during the daytime). It undergoes a cycle of expansion and compression which fragilizes the structure over time. Therefore, a safety thermal range is imposed on the structure by the manufacturers, which typically is -40°C to 80°C. [8]

2.1.2 Electric Power System (EPS)

The EPS represents the entire electric power system, it comprises the electric power generation via Solar Panels (SP), its storage via batteries (BAT) and its distribution and management via power electronics or Power Conditioning and Distribution Unit (PCDU).

Power Generation

The power generation is the subsystem that produces electricity for the satellite. It exists several technologies to generate power on a satellite, such as combustion cells via chemical reactions or thermoelectric cells via nuclear reactions, but the most common way to produce electricity on a CubeSat is with solar cells gathered in solar panels.

The use of solar cells for power generation comes with limitations: no generation during eclipses, degradation over time, high surface area needed, mass and cost. Solar cells, or photovoltaic cells, are made from thin semiconductor layers that produce an electric current when exposed to light thanks to the photoelectric effect. Most of the cells manufactured on Earth are single-junction cells, cells constituted by one type of material that is responsive to a specific portion of the solar radiation spectrum. Those cells are for terrestrial uses and achieve an efficiency of usually less than 20%.

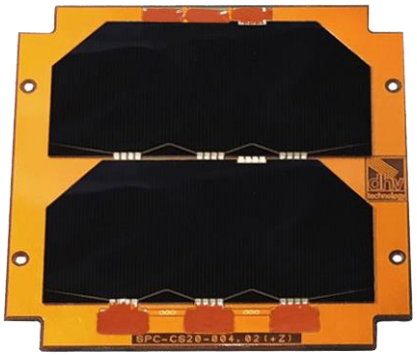


Figure 2.4 - Solar cell for CubeSat [11]

The surface area coverable by solar panels being limited, small spacecraft engineers favor multi-junction solar cells, constituted by multiple types of material which are responsive to multiple portions of the solar radiation spectrum, thereby widening the absorbed part of the spectrum.

The theoretical efficiency for an infinite-junction cell is 86.6% in concentrated sunlight [9]. However, in aerospace industry, triple-junction solar cells are commonly used, they present the most advantageous efficiency to cost ratio. Triple-junction cells efficiency ranges from 26 to 30%[8] for in orbit demonstrated technologies. The efficiency of the solar cells is defined at 25-28°C under AM0 conditions (solar spectrum outside atmosphere, E=1367 [W/m²]).

A solar panel is an assembly of solar cells connected through wires, the solar cells do not make the entire surface of the solar panel. The ratio of effective cell area to panel area is called packing factor. Solar panels are manufactured following the standard ECSS-E-ST-20-08C, it implies an average of 60cm² of effective cell area per unit-panel which corresponds to a packing factor of 0.6. For a typical efficiency of 30%, the power of a solar panel is 2.3W for 1U solar panel and weights approximatively 50g. However, solar panels can be customizable to increase the packing factor. [10] [11]

The lifetime of a solar panel is defined by the acceptable decrease of efficiency set by the manufacturer. Any material in space is hit by radiations, solar cells are fragile and particles with high energy degrade it over time. The cumulated strikes, or fluence, of 1 MeV electrons/cm² is the scale to estimate the lifetime of a cell. In LEO, a fluence of 1e14 corresponds to 10 years, after that time, the efficiency would be decreased by maximum 6%. [12] [13]

The temperature limits imposed by manufacturers vary a lot, from -120 to -55°C for the lower limit to +130 to +150°C for the upper limit [11] [14] [10]. It depends on the type of solar panels and the efficiency drop acceptability, nevertheless a fair range would be -80 to +130°C. The efficiency of a solar cell decreases with increasing temperature, this effect can be seen in Figure 2.5 where the I-V curve of a typical solar cell is drawn for different temperatures. As the temperature increases, the voltage decreases meaning a decrease of output power and therefore of efficiency. In general, a solar cell presents an efficiency diminution of 0.3-0.4 [%/°C] [13] [12] [15].

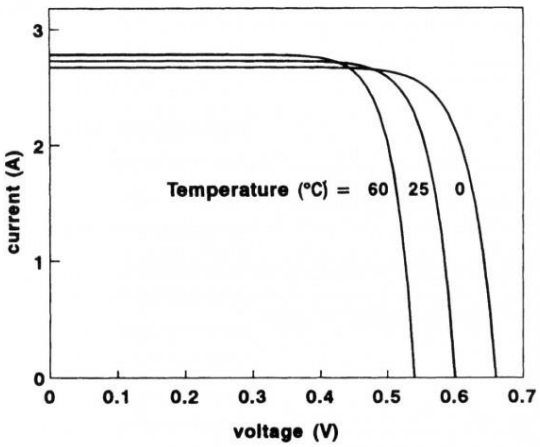


Figure 2.5 - Temperature effect on solar cell [136]

[8] The efficiency of solar cells for space and terrestrial applications is respectively based on AM0 and AM1.5 conditions, the second gives a higher value compared to the first.

Manufacturers set the upper temperature limit at the efficiency drop which they consider as critical. At 130°C, the efficiency is lowered by about 25% from the 25°C reference. Inversely, at a lower temperature, the efficiency of the cells is increased. However, at a too low temperature, typically below -80°C, solar cells become very sensitive to electrical shunts and may suffer from flat spots, an unpredictable effect that can significantly lower the efficiency [16]. This effect sets the lower temperature limit.

The usual location of the solar panels is on the sides of the CubeSat. However, if high power is needed, the satellite can be equipped with deployable panels. Deployable panels allow more surface to be covered with solar panels and a better exposition to the Sun.

Power Storage

Power storage may be required in order to supply electricity during eclipses or in case of peak loads. In modern small spacecrafts, Lithium-ion (Li-ion) and Lithium-polymer (LiPo) are the rechargeable batteries of choice. They have good rechargeability, low weight and high energy density compared to other types of batteries. Other types such as Nickel-based batteries have had space flight heritage due to their robustness but have too low energy density for small satellites.

The characteristics of Li-ion and LiPo batteries are similar, however LiPo ones show slightly better energy and power densities. Li-ion batteries have an average specific energy of 150-200 [Wh/kg]. Typically, in CubeSat applications, Li-ion cells deliver a voltage of 3.6 V with maximal charge at 2.5C and maximal discharge at over 3C [9]. The actual mass of a battery pack comes at about 70% from the batteries and 30% from the associated electronics. [17] [18] [19] [20] [21]

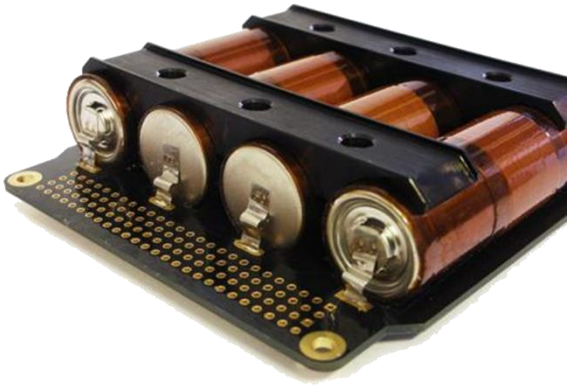


Figure 2.6 - Battery pack of a CubeSat [134]

The life span of a battery is determined by its life cycle, the number of charge/discharge cycles that it performs. The life cycle of a battery depends on several factors such as battery chemistry, operating temperature, charge and discharge rates and most importantly the Depth-of-Discharge (DoD). The DoD of a battery is the extent at which the battery discharges at each cycle. For example, a 100Wh battery that provides 20W for 30 minutes (10Wh) at each cycle of discharge, has a DoD of 10% because it provides 10% of its capacity.

The batteries charge when exposed to the Sun and discharge during eclipses. The charge/discharge cycles of the batteries are thus determined by the number of revolutions around Earth done by the satellite throughout the mission duration. A satellite in LEO will orbit around 5500 times per year.

At 100% DoD, Li-ion battery's life expectancy (65% remaining capacity) is about 500 cycles [20] [22]. However, a key property is that as the DoD decreases, the life cycle increases. For example, a typical LiPo battery's life cycle is over 5500 cycles for a 30-40% DOD with 50% remaining capacity[10] [23] [24] [25]. This limited life expectancy is usually one of the main limiting factors in the satellite mission duration. In order

[9] C-rate: proportional to 1C which equals 1-hour charge, e.g. at a 3C discharge, the battery will be discharged in 20 minutes.

[10] This is a very low remaining capacity; typical battery datasheets consider a higher value to determine the life expectancy.

to extend the mission duration, the batteries must have a larger capacity which implies, for the same power consumption, a lower DoD, and therefore a longer life cycle. The need of a low DoD for long duration missions is brought out by Figure 2.7[11]. A larger battery capacity also means larger mass and volume requirements: an optimal configuration must be studied for each mission.

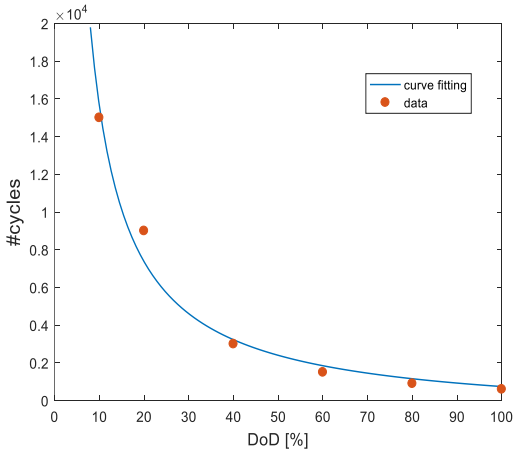


Figure 2.7 - DoD influence on life cycle, data from [26]

Batteries are like humans, they function best at room temperature and the temperature variation from these room conditions has an important impact on it. Low temperatures cause electrolytes to solidify and hence increase the internal resistance while high temperatures decrease the life cycle [23] [26]. The increase of internal resistance results in a decrease of performances, or battery capacity, e.g. at -20°C most batteries are at about 50% performance level [26]. On the other hand, the life cycle is reduced by 20 to 50% if the battery operates at 45°C [20] [26]. The temperature effect on a battery is shown in Figure 2.8: when the temperature increases, the life cycle of the battery decreases and its capacity increases. This figure presents the trend for any type of battery, the actual values depend on the battery model.

However, the charging process is more delicate than the discharging one, for Li-ion cells the acceptable temperatures are comprised between 0 and 45°C for charge and -20 to 60°C for discharge. [26] [18] [20]

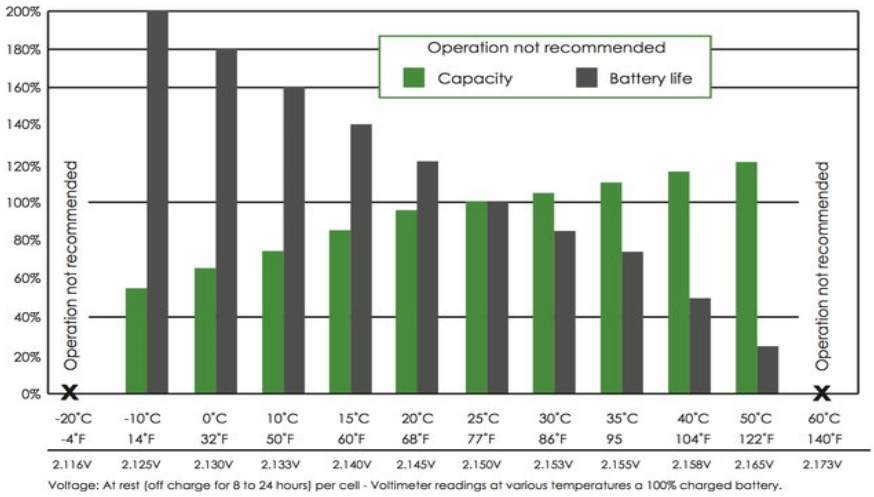


Figure 2.8 - Effect of the temperature on battery performance and life cycle [129]

The majority of small satellites are equipped with solar panels in conjunction with rechargeable batteries, also called secondary batteries, in 2009, they accounted for approximatively 85% of all small satellites [23]. The remainder, only short missions (days to few months duration), is powered by primary, or non-rechargeable, batteries.

The efficiency of a battery is defined as the ratio of output to input energy. There are two main efficiencies that must be considered in a battery cell, coulombic and voltage efficiency, the overall efficiency

[11] Considering 70% battery capacity remaining.

is the multiplication of both. Coulombic, or Faraday, efficiency considers the losses due to the participation in unwanted side reactions by the electrons. Voltage, or charge, efficiency describes the fraction of energy lost through overpotential, the potential difference due to thermodynamic irreversibility and internal resistances. For Li-ion cells, the Coulombic efficiency approaches 100% [26] [27] while the voltage efficiency at nominal charge current reaches 97% and decreases as the charge current increases [22]. The overall efficiency of a Li-ion cell is thus very high, the associated losses will result from the connections between cells in a battery pack [22] and the power electronics needed to convert the input and output voltages to required values.

Power Conditioning and Distribution Unit (PCDU)

The last part of the EPS is the power management and distribution (PCDU). It comprises power control and regulation, and power distribution. The first converts the voltage to suitable values for battery and load inputs, it mainly consists of power electronic dc-dc converters. The second controls the power distribution to the loads through complex switches interfaces.

The Battery Charge Regulators (BCRs) make the interface between solar panels outputs and the battery bus. It is constituted of a power stage and a centralized end of charge voltage controller that provides a 'constant current, constant voltage' charge regime suitable for the battery. It also usually comprises a Maximum Power Point Tracking (MPPT) which tracks the combination of voltage and current giving the maximum power output. The Power Control Units (PCUs) make the interface between the battery bus and internal load inputs. They are dc-dc converters that regulate the raw battery voltage. Telemetry and telecommand functionalities are handled by the OBC via an Inter-Integrated Circuit (I2C). The last components of the PCDU are protections, triggers which disconnect the battery or a load in case of over-current or under/over-voltage. The different parts of the PCDU mentioned are represented in Figure 2.10.



Figure 2.9 - PCDU board [126]

For small CubeSats, PCUs have typically two output voltages, 3.3 and 5V with an efficiency up to 95% while BCRs have an efficiency of maximum 90% [28] [29] [30]. Higher values are possible for high power applications.

The power busses at the input of the loads are the following: 3.3V, 5V, 'battery raw' (output of the battery, without passing through a PCU) and 'BCR out' (output of the BCR, without passing through the battery and PCUs). The typical overall efficiency from the output of the solar panels to the power busses is ~80%, 87%, and 90%, respectively for PCU outputs (3.3 and 5V), 'battery raw' and 'BCR out'.

The PCDU operational temperature range is from -40 to 85°C [31] [32] [33]. It corresponds to the industrial operating temperatures, industrial electronics are designed to operate in this reference interval. Other standard types exist such as the commercial and military electronics which have respectively smaller and larger operating temperature ranges. The cost of the electronics evidently adapts. [34]

Figure 2.10 illustrates the EPS of a satellite, with the three parts: power generation in blue, power storage in green and power management and distribution in red.

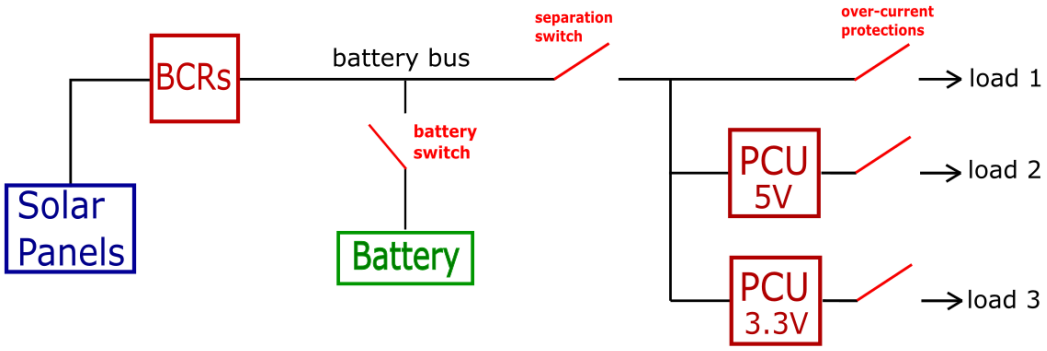


Figure 2.10 - Electric Power System (EPS)

In total, the EPS commonly accounts for up to one third of the total spacecraft mass. [19]

2.1.3 Attitude Determination and Control System (ADCS)

The ADCS[12] is the subsystem in charge of determining the attitude of the satellite first and then maneuvering it to have the desired attitude. The attitude refers to the orientation of the satellite, a change in attitude implies a rotation but no translation.

Once the CubeSat is deployed, it will naturally randomly spin around while orbiting Earth. The ADCS function is to stabilize the CubeSat and to control its attitude. For example, the ADCS of an Earth observation satellite will control the satellite's attitude so that the nadir face always faces the Earth.

The ADCS is made of sensors, collecting data for attitude determination, and actuators, performing maneuvers for attitude control. A closed feedback loop is run between sensors and actuators to ensure pointing accuracy.

Possible sensors are Earth (or horizon) and Sun sensors, star trackers, gyroscopes and magnetometers. Star trackers show high accuracy (up to few arcseconds), but require significant volume and weight, too much for 1U CubeSats for instance. Sun and Earth sensors have a low price but lack accuracy (about 1°). Finally, magnetometers need samples, thus memory storage, and gyroscopes can be compact but present very noisy measures [35]. Every sensor has its advantages and disadvantages, the mission type will determine which assets or combination of assets are the most crucial [19] [36].



Figure 2.11 - Sun sensor [124]

Common actuators are magnetorquers (or torque rods), permanent magnets, reaction wheels and thrusters [19] [36]. Permanent magnets are less precise but are the only passive actuators, one-quarter of all CubeSats use them, especially 1U CubeSats [35]. Magnetorquers are lightweight and efficient which make them ideal for CubeSats but the attitude control on 3 axes can be complicated to implement. Reaction wheels need too much energy and space to be accurate in unit-CubeSats [35], but are used in

[12] The abbreviation AOCS is also used, it refers to Attitude and Orbit Control System and comprises the localization function. In our case, when referring to ADCS, we also include the localization function.

larger ones. Three wheels are required for full control, yet, the common practice is to add a fourth one in case of the failure of one. Indeed, they are very subject to degradation by friction, it is actually the second reason, after batteries' life cycle, that limits the mission duration.



Figure 2.12 - Magnetorquer board [44]

Magnetorquers and reaction wheels can rotate the spacecraft around its center of mass but only thrusters can effectuate a translation movement to the satellite. However, except for scientific purpose [37], thrusters are rarely used in CubeSats due to their impact on the volume and mass budgets.

Usually, ADCS combines multiple sensors and actuators to increase pointing accuracy. Such COTS integrated units have a pointing capability from 0.002 to 1° [19]. However, higher accuracy also goes with larger volume and mass.

The power budget for the mentioned sensors and actuators in CubeSats is the following: Sun sensors (lots of 6) consume about 100-150mW, magnetometers less than 1mW, gyroscopes about 25-30mW, magnetorquers (3-axis) around 500-800mW. Small reaction wheels adapted for small CubeSats require, at peak power, less than 2W (3-axis) and about 0.5W on average. [38] [39] [40] [41]

The ADCS dependence with other subsystems is shown on Figure 2.13. The ADCS is connected to the OBC that manages the algorithm for position determination and control, in COTS ADCS integrated units, the unit usually comprises a motherboard that handles this function. [42] [43]

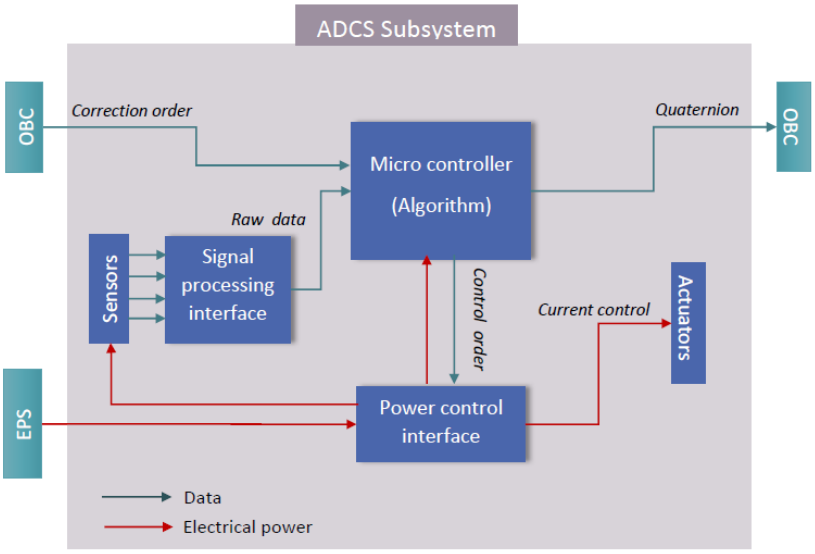


Figure 2.13 – ADCS configuration [35]

The staple temperature limits are defined by the industrial range, -40 to +85°C, which corresponds to the temperature range of the electronics. The specific temperature range depends on the temperature effect on the sensor or actuator, it usually narrows the staple temperature range. For example, a magnetorquer or a magnetometer has its upper and lower limits narrowed by 10-15°C, a reaction wheel has its upper limit lowered by 5-15°C, while a gyroscope, a fine Sun sensor or a star tracker usually does not influence the range [38] [40] [44] [45] [46] [47]. Although, for the same component, the temperature limits vary with the manufacturer [35]. Indeed, each manufacturer sets the required performances of the component, from which the required temperature is determined.

2.1.4 Communication Subsystem (COM)

The COM subsystem is in charge of sending data to and receiving data from the Ground Station (GS). The data received are transmitted and interpreted by the OBC. In the same way, it is the OBC that transfers the data to be sent.

The COM subsystem is constituted of 3 parts:

- The antenna: It is the equipment that handles data transfer from Earth to satellite or from satellite to Earth. When used for transmission (Tx), the antenna creates electromagnetic waves from electric signals given by the OBC. When used for reception (Rx), the antenna converts electromagnetic waves into electric signals transmitted to the OBC.
- The transceiver: It is the modulator/demodulator part, it converts the signal in its appropriate form, analog for data to be sent (Tx), digital for received data (Rx). The transceiver also amplifies the signal for it to have enough energy to reach the GS. A transceiver is a device that acts as a receiver and an emitter.
- Data processing: It encrypts the frame before being sent and decrypts it after being received. It is usually included in the transceiver term.

For CubeSats, the transceiver operates at radio frequencies, mature bands used are VHF and UHF (Very and Ultra High Frequency), ranging respectively from 30 to 300MHz and from 300MHz to 3GHz [19]. This frequency range suits the satellite communication for two reasons. First, too low frequencies are reflected by the atmosphere and do not reach the receiver. Second, the higher the frequency, the stronger the attenuation when passing through the atmosphere[13]. These reasons can be seen in Figure 2.14, showing the electromagnetic frequencies at which the atmosphere is not opaque.

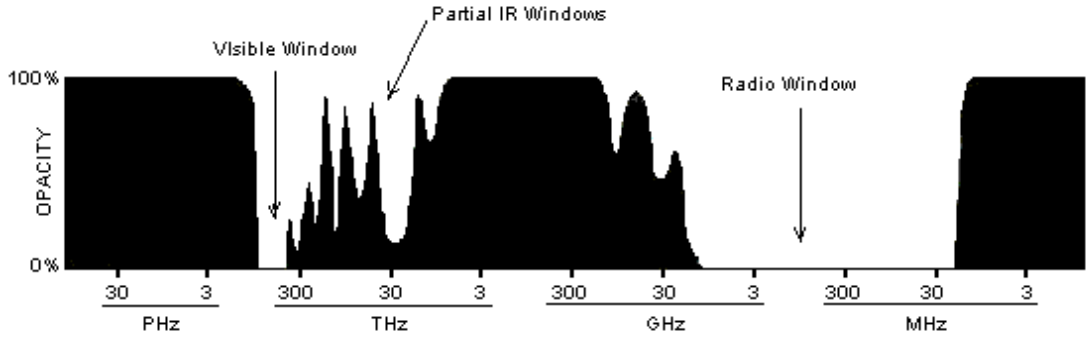


Figure 2.14 - atmospheric windows in the electromagnetic spectrum [122]

Furthermore, the frequency of the uplink (GS to satellite transmission) and of the downlink (satellite to GS transmission) must be different to avoid interferences. This is not compulsory, but it allows simultaneous uplink and downlink which can be interesting knowing that the satellite is visible for about 10 minutes at the GS. VHF band is generally chosen for the uplink with a frequency around 145MHz, UHF for the downlink with a frequency of around 400, 420 or 435MHz. As mentioned, the higher the frequency, the higher the attenuation caused by the atmosphere. The satellite, due to its weight and size, cannot afford highly sensitive receivers while the GS can. The GS is thus more qualified to receive attenuated frequency. In addition, emitting at a higher frequency means a higher data rate and a smaller antenna (a whip antenna is one-quarter of a wavelength long), which benefits to the satellite. Inversely, the ground station can emit with high power to counteract the attenuation, it is, in part, why some satellites have inverse frequencies for uplink and downlink. [1] [48] [49] [50]

[13] However, this attenuation is not encountered for inter-satellite communications, used in satellite constellations.

Typically, a whip, a dipole or a patch antenna is used in CubeSats. [19]

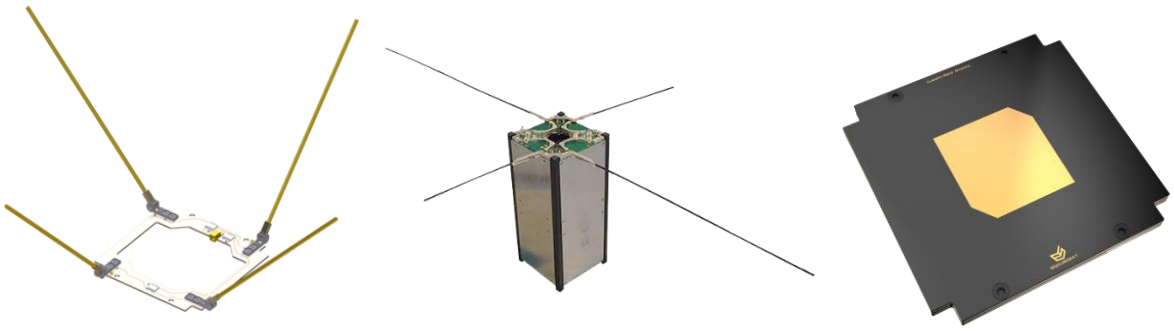


Figure 2.15 – Whip, dipole and patch antenna (from left to right) [51] [133] [132]

Recent technologies present patch antennas that reach higher frequencies, typically, in the S-band (2.2-2.5 GHz), X-band (8.2-10.5 GHz) or Ka-band (26.6 GHz) which can be used for higher data rate, e.g. high-resolution camera as payload, or for inter-satellite communications in constellations. However, because the frequency increases, these technologies also require a higher power consumption. [19] [1] [48] [49] [50]

The operating temperatures are required to be in an interval that ensures the components to properly work. For the antenna, the generally allowed interval is the industrial one, -40 to +85°C. As for the transceiver, it requires a narrower interval, a general operating temperature range is from -20 to +60°C. The corresponding mass is a few dozens of grams for the whip antenna up to 100gr for some patch antennas, and more for the transceiver. The COM subsystem needs low power to receive data (Rx mode) or during standby (IDLE mode) but is power-intensive for transmissions (Tx mode). As mentioned, the power needed for transmissions depends on the operating frequency and in Tx mode, the power consumed is approximatively 5 to 8 times higher than the radio output power. For UHF downlink in CubeSats, the transmitted power ranges between 0.5 and 2W while the transceiver consumes between 4 and 10W. For VHF downlink, the power consumption can go down to 1.7W. As for Rx mode, the power needed ranges from 0.5 and 1W. [50] [51] [52] [53] [54] [55] [56] [57]

2.1.5 On-Board Computer (OBC)

The OBC is the brain of the satellite, it is an embedded computer dedicated to command and data handling, it manages all the tasks taking place within the satellite. It has two main functions. The first is to interpret the orders from Earth, treat them and return the results. To complete this function, the OBC has a memory module for data storage and uses the COM subsystem to communicate with Earth. The second function is to monitor and maintain the proper functioning of the entire system, the OBC is the link between the subsystems.



Figure 2.16 - OBC of a CubeSat [59]

The memory module stores all kinds of data, essentially data from the payload and onboard parameters for housekeeping, e.g. temperature and power consumption in different parts of the satellite. It constitutes telemetry data that will be download to the GS during an overpass. The storage capacity of the OBC

depends on the payload function. For example, an observation satellite that needs to store high-resolution photographic data will need more storage capacity than a geolocation satellite that only stores coordinates.

In addition to its previously mentioned relationship with the COM subsystem and the payload, the OBC monitors:

- the EPS by controlling the activation of the different switches to manage the power supply and by reacting to the activation of protection modules.
- the ADCS by making use of the data from ADCS sensors and controlling its actuators to maneuver the satellite's attitude (it performs the loop feedback).
- the TCS in case of active control requiring intelligence, e.g. thermostat function.

The microcontroller, processing unit of the OBC, usually operates at 32-bits. In the past, 8- and 16-bits were mostly used in CubeSats, however, with the reduction of the 32-bits core architecture's complexity, 32-bits processors have become predominant. The power supply of the microcontroller is commonly 3.3V, as for its power consumption, it strongly depends on its performance which is specified by the mission. [36]

For small CubeSat (1-3U), typical power consumption is between 200 and 400mW for a respective OBC mass of 50-100g. [58] [59] [60]

The temperature range is basically the same as the PCDU because the OBC is essentially made of electronics. While most analyses stick to that range [36] [35], some consider that an operating OBC is more delicate and must function in a narrower range [58] [60] [59]. However, a usual OBC should be rated for the industrial operating temperature range, that is the say between -40 and 85°C [36].

2.1.6 Payload

The payload is the reason for the mission. A camera for an observation satellite (Figure 2.17), an extra telecommunication system for a telecommunication satellite, an innovative instrument for technology demonstration, an experimental setup for scientific research or any other captor for a scientific purpose. The necessary volume, mass and power for the payload will depend on the mission.



Figure 2.17 - Camera for CubeSat [63]

As presented in the introduction, the mission types can be categorized as follow: communications, educational, Earth imaging, science and technology demonstration. Earth imaging is the predominant mission for CubeSat.

It is interesting to note that the payload is not vital for the satellite, it is not necessary for its well-functioning, but the satellite would be meaningless without. Yet, the payload will influence the characteristics and performances of the other subsystems. For example, some payloads request high power which will influence the design of the EPS, others require high data rate transmission which will affect the setup of the COM subsystem.

Each different payload is described by its own operating temperatures. For instance, the operating temperature range can be quite wide for basic cameras with -25°C to +65°C [61] but is narrowed for cameras with higher performances up to a range from +10°C to +30°C [62] [63] [64]. Note that regarding the storage (non-operating device), the acceptable temperature range becomes much wider.

2.2 Temperature Requirements Summary

Table 1 summaries the temperature ranges required for the typical components of a CubeSat. The details and references for the presented values can be found in section 2.1.

Component	Minimal temperature [°C]	Maximal temperature [°C]
Structure	**-40**	**+80**
EPS Solar Panels	**-80**	**+130**
EPS Li-ion battery (charge)	**+0**	**+45**
EPS Li-ion battery (discharge)	**-20**	**+60**
EPS CPDU	**-40**	**+85**
ADCS Fine Sun Sensor	**-40**	**+85**
ADCS Star Tracker	**-40**	**+85**
ADCS Magnetometer	**-25**	**+70**
ADCS gyroscope	**-40**	**+85**
ADCS Magnetorquer	**-25**	**+70**
ADCS reaction wheel	**-40**	**+70**
COM Antenna	**-40**	**+85**
COM transceiver	**-20**	**+60**
OBC	**-40**	**+85**
Payload	**?**	**?**

Table 1 - Temperature requirements of the components

This table has been built with the will to correspond to typical temperature intervals of typical components of a CubeSat. It does not make a general truth about every subsystem but rather try to generalize their thermal requirements while their exact specifications will depend on the chosen model.

The temperatures indicate the operating limits, the non-operating range is usually wider. The common practice is to try to maintain all units within their operating temperature ranges at all times as it makes a more robust system. It also allows to turn on any unit at any time if the mission asks for it without being concerned about potential damages. In addition, some components also have a minimum switch-on temperature that can differ from the operating range, this table does not include this consideration.

2.3 Thermal Control System (TCS)

Section 2.1 demonstrated that each component must operate within a specific temperature range to avoid failure, malfunctioning or efficiency decrease. The TCS of a satellite gathers all means set up in order to maintain the components within their temperature limits, the TCS must guarantee the respect of Table 1.

The thermal control can be passive or active. Passive control does not require any power, it passively controls the heat flows, it is preferred by engineers as it is easier to implement, usually for a low cost, low weight and high reliability. Unfortunately, it may lack performances and sometimes need active means to further control the temperature. Active controls are essential in some cases but imply power consumption.

Whether it is passive or active, thermal management occurs in two environments:

- Internal environment: The interior of a fully enclosed spacecraft is usually dominated by conductive heat transfer. The internal TCS mainly consists of means to move heat from a place to another with efficiency or not (conductive or insulating materials) or dissipate heat if necessary.
- External environment: The heat exchanges with the external environment are driven purely by radiative transfer. The external TCS consists of managing the overall energy balance of the satellite by controlling the absorbed and emitted heat.

This section intends to present the most common thermal control means and highlight their implementation and performances in CubeSats.

2.3.1 Coatings

The basic passive option to regulate the absorbed and emitted heat flux is the application of a specific coating on a surface. Doing so is the easiest way to modify the optical properties of a surface, commonly referred to as solar absorptivity and IR emissivity, which determine its ability to absorb and emit heat. These properties are almost solely surface properties and are ensured by coatings. These coatings can be encountered in the form of paints, tapes, films, glass sheets or enhanced surface finishes (polishing, anodizing metals, …) and can be applied on nearly any surface.

Basic Coatings

The coating is to be chosen from a wide range of possibilities in order to match the desired overall energy balance. Figure 2.18 indicates the range of optical properties for different types of materials. A coating can be a combination of two or more materials in order to obtain the desired absorptivity and emissivity. The adjustments can be made by varying the thickness of the material, by using specific coating patterns or by implementing several layers. For example, second surface mirrors are a very common coating; they consist of a

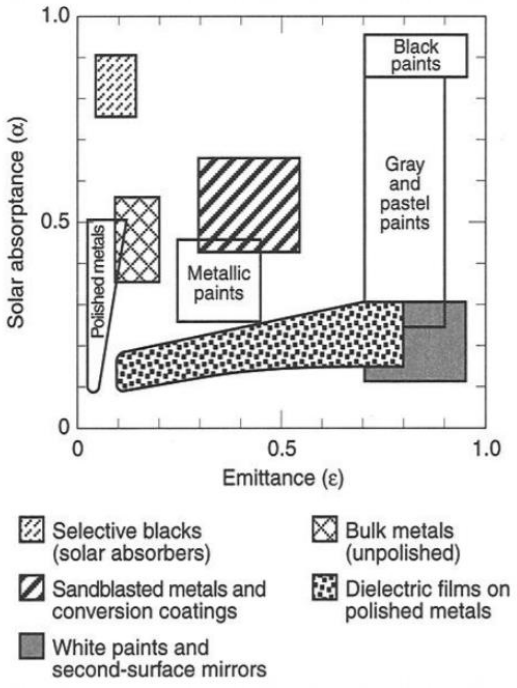


Figure 2.18 - Thermal control coatings [4]

translucent polymer film as primary surface and a metallic second surface. The first determines its emissivity which can be modified by tuning its thickness. The second determines its absorptivity since the upper layer is translucent. [65]

The use of paint is the most intuitive coating. While black paints absorb nearly any incident thermal radiation, white paints reflect the main part of them. For a similar emissivity, white paints will make a spacecraft globally colder than black paints. Another commonly used coating is tape, besides from being easily applicable and removable, it is inexpensive and has a longer lifetime than paint. [19]

Multi-Layer Insulation (MLI) Blankets

A common way for satellite insulation is the use of MLI blankets. An MLI blanket is constituted of several closely spaced layers of reflecting material, its principle is based on radiation balance: the absorbed flux by the first layer is emitted in part back to space, the other part is absorbed by the second layer. This second layer emits back a part of the flux to the first which absorbs it and partially reemits it to space, and so on. By that principle, an MLI blanket can reach low values of effective emissivity and absorptivity and serves as an excellent insulator with the more layers, the better the efficiency. An MLI blanket performance is defined by its effective emissivity or effective thermal conductivity which reflects its insulating ability. In ideal conditions, MLI's insulation efficiency cannot be matched by other coatings.



Figure 2.19 - MLI blanket [105]

The TCS of large satellites commonly consists of making the structure an insulated box and canalizes the internal dissipated heat towards radiators. MLI blankets are thus broadly used for such spacecrafts. On small satellites, on the other hand, their drawbacks commonly result in using other coatings instead. Indeed, MLI blankets drop efficiency as their size decreases, they drastically decline in performance if compressed which happens at the edges of the faces and they are fairly delicate. It makes them not suited for external surfaces of small satellites that will be deployed from a dispenser. Furthermore, the surface of the outer panels is partially covered with solar cells, leaving little room for MLI blankets. As for the use of MLI blanket on the internal surfaces, it can often be replaced by low emissivity tapes or coatings that perform as well in that context, using less volume and at a potentially lower cost. [19]

2.3.2 Radiators

In the case of an insulated satellite or a satellite with high internal heat dissipations for low external emissions, a path to evacuate the heat outside may be needed.

Coating Radiators

A classical passive thermal control is to canalize the internal heat and to conduct it towards a specific external surface with high emissivity, called radiator as its primary function is to radiate heat away. Along with high emissivity, low absorptivity is also required to enhance its efficiency. In addition, it must, as far as possible, not be oriented towards the Sun. The radiated power depends on the surface emissivity and temperature.

Optical Solar Reflectors (OSR) are used as radiators on spacecrafts, they are a type of second surface mirror. The top layer is made of quartz which is highly IR-emissive and lets the solar rays through, these rays then reflect on the metal (or mirror) layer. It results in a material with good emissivity and low absorptivity, typically 0.8 or higher and 0.08 respectively. [5] [66]

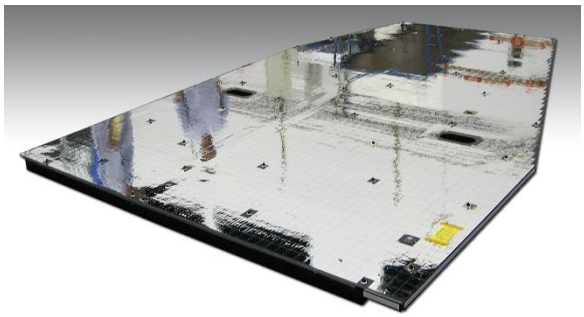


Figure 2.20 - Spacecraft radiator [19]

However, tapes are preferred over OSR for CubeSats as it is easier to implement and less fragile. As stated in [19], second-surface silvered FEP (Fluorinated Ethylene Propylene) tapes are an excellent choice for radiator coatings. Indeed, besides having the benefits of tapes, they achieve similar performances to those of OSRs. [67]

Louvers

Supposing a satellite with internal power dissipation varying widely caused by equipment duty cycles, it will need a system that can modify its heat rejection depending on the internal dissipation level. Such a system is achievable by installing a louver over a passive radiator. Louvers are deployable mechanisms that modify the accessibility to the surface below by controlling the openness of small blades. It results in a tunable average emissivity of the exterior surface. Common louvers are venetian blind types like the one shown in Figure 2.21. In general, a louver in its fully opened state rejects six times as much heat as it does in its closed state. [4]

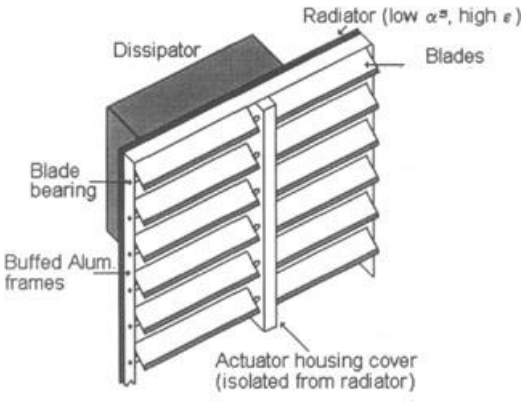


Figure 2.21 – Spacecraft louver [102]

Although this mechanism shows great efficiency on large satellites, its integration on small satellites has been challenging as it requires power and mass. However, a 6U CubeSat equipped with a louver has already flown, this miniaturized louver was operating passively as the opening of the flaps were controlled by metallic springs which expand as the temperature rises. [19]

Deployable Radiators

On large satellites, there is enough outer surface available to incorporate right-sized radiators and louvers. On CubeSats on the other hand, the available surface can lack, especially in the case of body-mounted solar panels. To make up with the lack of space, deployable radiators have been imagined. They

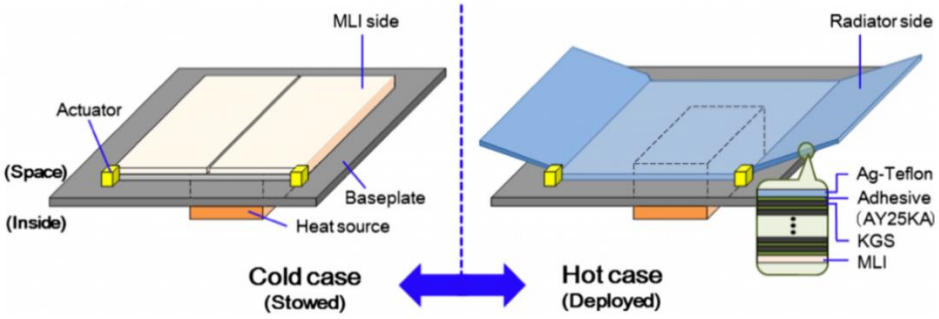


Figure 2.22 - Deployable radiator [19]

consist of a lightweight material that is either insulating in stowed mode or radiating in deployed mode (Figure 2.22). The fin is stowed or deployed by a passive actuator consisting of a shape memory alloy and a bias spring. This mechanism is at the research stage and has never proven its performances except ground tests. [19]

2.3.3 Thermal Links

The frame itself is an important thermal link between components. Indeed, it is connected to every component as it supports them and holds them together. It represents thus a considerable thermal coupling between components. However, if it not enough, e.g. a power-intensive subsystem may need to be directly linked to the radiator, several means can be implemented.

Thermal Straps

Thermal straps are the basic thermal link in small satellites, they use thermal conduction for heat transfer. Linking two components with a thermal strap allows enhancing their thermal coupling. Thermal straps are constituted of a highly thermally conductive material and by linking the different components they form the thermal network of the spacecraft which ends to the radiators.

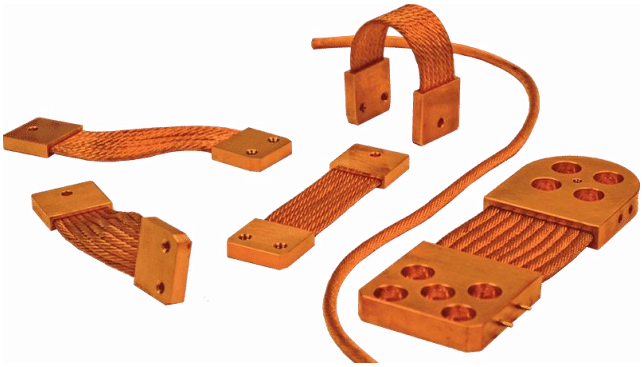


Figure 2.23 - Thermal straps [69]

They represent an adequate thermal link for CubeSats as they are lightweight, relatively flexible and can be fitted to any length for design. Traditional and usual thermal straps are made of aluminum or copper, the use of one or the other depends on the need: where mass is critical, aluminum is preferred as it has 58% of the thermal conductivity of the copper with only 30% of its mass, where volume is critical, copper is favored. These common metals go with low prices but also with limited performances, they have a thermal conductivity around 200 to 500 [W/mK] whereas more peculiar materials such as pyrolytic graphite or graphene show much higher conductivity, respectively reaching 1500 and 3500 [W/mK]. Such materials find application in cooling very sensitive equipment. [68] [69]

By consuming power, through the use of thermoelectric devices, it is possible to enhance and control the performances of the thermal straps. Flexible and Enhanced Active Thermal Straps (FEATS) are a recent technology which is said to be a reliable means of mitigating hot spots. Anyway, it is still waiting for in-orbit tests.

Fluid Loops and Heat Pipes

If solid thermal links are not enough to manage the heat conduction towards the heat sink, fluid loops can be needed. A pumped fluid loop can achieve great cooling performances between multiple locations via forced fluid convective heat transfer and are used to transfer the heat on longer distances. This active means requires power for the pump and is associated with large mass needs, it makes it uninteresting for small satellites.

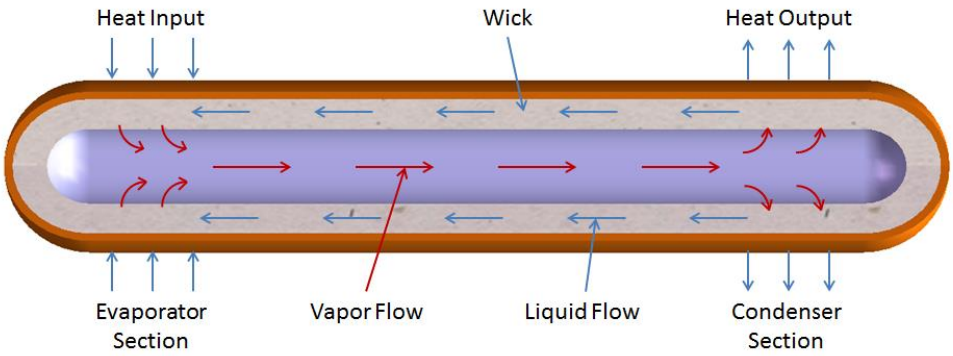


Figure 2.24 - Heat pipe schema [119]

Heat pipes are a passive variant of fluid loops. They use a closed two-phases fluid cycle, at the hot-end, the fluid evaporates and goes towards the cold-end where it condenses (Figure 2.24). During the evaporation, the fluid absorbs heat from the hot-end, and during condensation, it rejects it to the cold-end, usually a heat sink or directly a radiator. The system is passive as it uses capillarity action to ensure the liquid fluid to return to the hot end, the cycle thereby repeating.

Heat pipes are very efficient while being a passive mechanism. With an effective thermal conductivity from 10 to 100 [kW/mK], they can achieve performances up to 250 times better than copper which has a thermal conductivity of 0.4 [kW/mK]. [70]

Heat pipes have already flown in small satellites of 50-100kg, however, miniaturized heat pipes for CubeSat applications remain at the research stage. [19]

Thermal Gap Fillers

At an interface, e.g. between PCBs, a lower or higher thermal coupling may be needed. For that purpose, fillers are placed to fill the empty space. They can consist of a thermally conductive material, allowing the heat to flow more easily at the interface, e.g. aluminum spacers placed around threaded rods linking two PCBs. At the contrary, they can consist of low conductive material and, by blocking the view, they prevent from radiative heat exchanges. Their thermal conductivity can reach less than 1 [W/mK]. [71]

Fillers are also used for the mechanical coupling of two components, nevertheless, the specific material can still be chosen to enhance or reduce their thermal coupling.

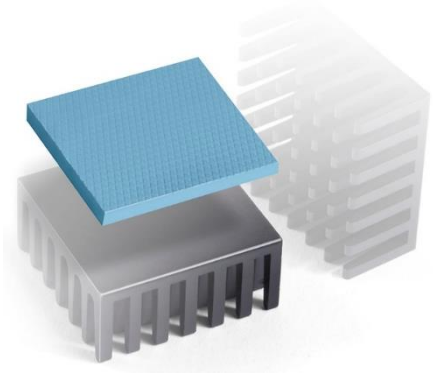


Figure 2.25 - Thermal gap fillers [130]

2.3.4 Sunshield

A sunshield, or sunshade, is a deployable passive mechanism that is oriented towards the Sun, it shields against the solar heat flux to prevent it from hitting the spacecraft and thereby reducing its insolation and thus its heating. It consists of layers of metal-coated sheets that reflect the heating rays.

Sunshields are common on large spacecrafts, and recently it has been implemented in a CubeSat application, the CryoCube-1, 3U CubeSat intended to be launched in 2019 (Figure 2.26). The satellite is developed by NASA Kennedy Space Center (KSP) to perform cryogenic fluid management experiments. Its sunshields are placed towards the Sun (along with deployable solar panels) and towards the Earth to block both solar and IR radiations. This arrangement enables the payload to reach cryogenic temperatures. [72]

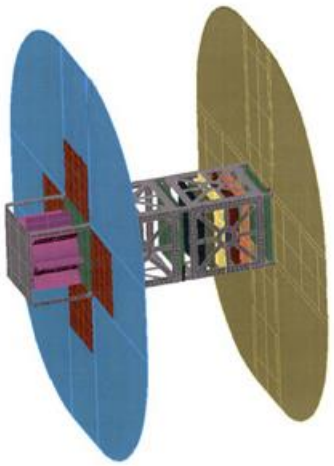


Figure 2.26 - CryoCube-1 [72]

2.3.5 Heat Storage

Thermal storage units include a vessel filled with a phase-changing material. Such material offers the possibility to store thermal energy as latent heat of fusion or sublimation. It allows this unit to store and restore thermal energy, giving the ability to prevent peak temperatures and stabilize the temperature fluctuations. However, such a device seriously impacts the mass budget as the heat storage capacity is directly proportional to its mass. It makes it not yet conceivable for CubeSats.

2.3.6 Heaters and Cryocoolers

Heaters

Heaters are the typical active thermal control; they consist of electrical resistance and dissipate heat when current passes through due to the Joule effect. They are placed in different locations in the satellite to ensure that the temperature of sensitive components does not go too low. They are commonly used in CubeSat, typically to maintain battery or payload temperature during cold periods of the orbit and are controlled by a thermostat via temperature sensors.

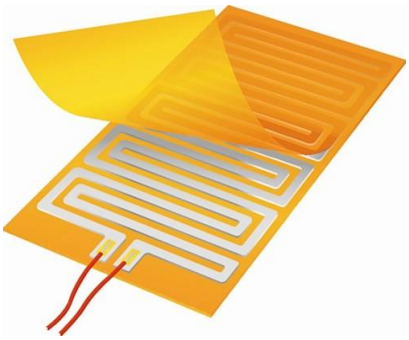


Figure 2.27 - Heater [125]

Cryocoolers

Active coolers, or cryocoolers, are devices that transport heat up a temperature gradient to achieve lower temperatures at the cold end, such devices require electrical input power. The Peltier effect coolers are the most common cryocoolers as they are the lightest (Figure 2.28). They can reach temperatures down to 170K but have low efficiency and thus require a lot of power which, paradoxically, imply high heat dissipations. Such coolers are used to cool down specific parts of the satellite, they are not used in cryogenic applications. Other cryocooler types, mostly using closed thermodynamic cycles such as Stirling or Joule-Thompson devices, can attain very low temperatures but go with other disadvantages such as vibration, complexity, power consumption or are still at the research stage. [73]

As for passive ways to reduce the temperature, besides radiators, stored cryogens are able to reach extremely low temperature, typically around 4K. They consist of a vessel containing a cryogen such as liquid helium or solid neon, the cryogen absorbs heat by boiling or sublimation. This passive solution implies a substantial increase in launch mass and has a lifetime limited to the stored cryogen. [73]

There have been recent improvements in mini cryocoolers for small satellites, although none have ever flown yet. The first CubeSat mission performing cryogenic management tests will be CryoCube-1, planned for 2019, its cryogenic temperatures are intended to be reached thanks to stored liquid oxygen and sunshields (Figure 2.26). [19] [72]

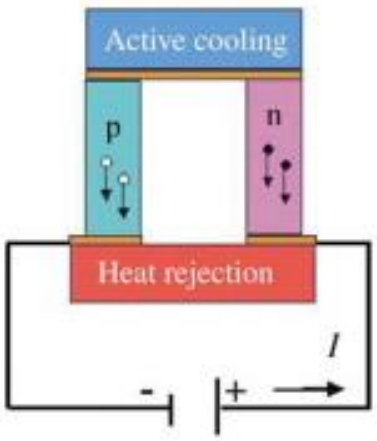


Figure 2.28 - Peltier effect [103]

2.3.7 TCS Approach for CubeSat

The principle of a CubeSat is to limit as much as possible its mass and power. The TCS of CubeSat will thus privilege passive and lightweight equipment.

Another consideration in active thermal control is that it is easier to warm up than cool down. Indeed, heaters dissipate energy that warms up the targeted component while active coolers cool down the targeted unit but require energy to do so which means heat dissipations, the opposed effect than the wanted one.

Classic TCSs in CubeSats avoid active cooling and implement a passive TCS that prevents from reaching high-temperature limits. If this passive TCS implies low-temperature limits to be crossed, heaters must be added to remedy it.

A typical TCS of CubeSats consists of

- **External coatings**: The external coating determines the general energy balance of the CubeSat. Part of the external area is usually covered with solar panels which have high values for optical properties [74]. Body mounted solar panels usually cover more than half of the satellite, the remaining area should be covered by low emissive material. It reduces the total emissivity and thereby reduces the highest and lowest temperature experienced throughout an orbit (see section 1.7). The absorptivity of the coating covering the remaining area determines the mean temperature of the CubeSat.
- **Internal coatings**: The inner part of the bus is usually painted in black as it favors thermal coupling with internal components. Internal components are not coated except for sensitive components which are better to be thermally isolated in order to keep their heat during cold cases.
- **Radiators**: Passive radiators in the form of highly emissive and little absorptive coatings are usually used when one or several non-Sun oriented faces of the CubeSat are available.
- **Thermal links**: Passive thermal straps, made of aluminum or copper, and thermal gap fillers are used to thermally couple components together, as well as to the structure and the radiators. Thermal links are sometimes not needed as the structure already gives a thermally conductive path between PCBs and side panels.
- **Heaters**: Heaters are commonly used in CubeSats, they warm up sensitive components, typically batteries or some payloads, during cold phases, e.g. eclipses. They consist of a support, e.g. polymer (such as Kapton) or silicone rubber, and a dissipative material, e.g. silver or copper.

2.4 CubeSat Configuration

CubeSat configurations are plenty, there are as many configurations as existing missions: size, mounting, presence of deployable panels and/or camera, arrangement of solar panels, patch or whip antenna, etc. So many parameters that influence the overall layout. Figure 2.29 displays the configurations of some existing CubeSats. The figure does not list all CubeSat configuration types, its sole purpose is to give visual content to the reader and help him get an idea of what CubeSats can look like.

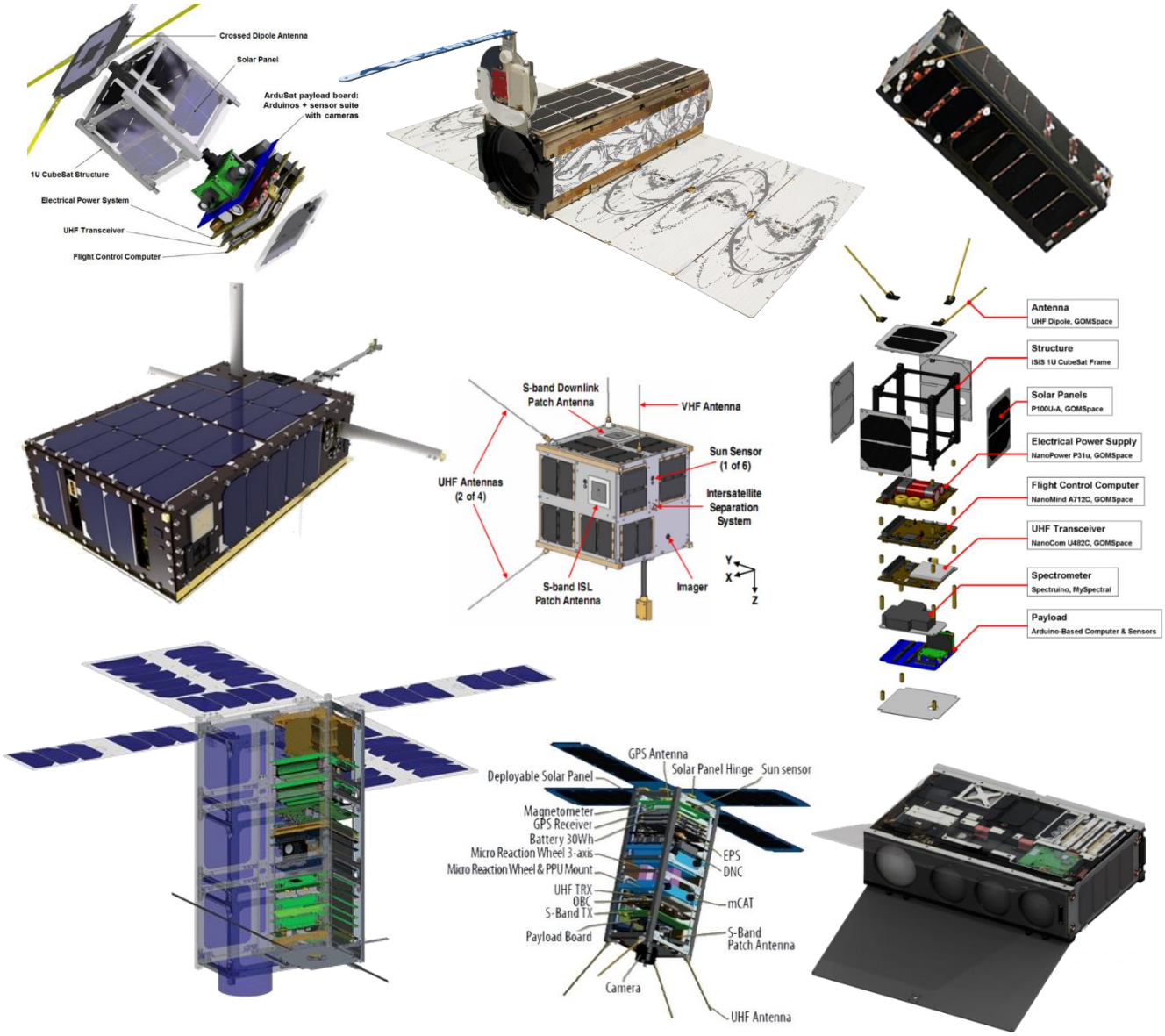


Figure 2.29 - Some CubeSat configurations, from left to right, top to bottom [107, 110, 117, 115, 37, 131, 128, 94, 82]

2.5 Power Budget

The power budget of a CubeSat is an extremely important part of its design, it gathers the consumption of all components of the CubeSat. From it, it will be decided the number of solar panels, their disposition and the need or not to implement deployable panels, as well as the capacity of the batteries.

For the thermal analysis, it is as important because it reflects the internal dissipations of the satellite.

It is very difficult and seemingly irrelevant to establish a typical CubeSat power budget. Indeed, the power budget is strongly affected by the payload of the mission and each mission presents its own payload. For example, an observation mission will require to send much more data than a technology demonstration mission as images are heavier than operating data. The power design of the COM subsystem will be affected, and their power budgets will not be similar.

In addition, missions can have multiple operating modes. Typically, a 'payload mode' during which the payload is active, a 'communication mode' during which data is sent to the GS, and an 'idle mode' (or standby mode) during which only critical subsystems are running, allowing the batteries to recharge. To achieve overall energy balance, one must determine the right duty cycle of each operating modes. For each mode, the power budget displays the average consumption over one orbit. The power budget gathers the expected power consumption of all components for each operating mode during expected mission conditions and usually considers safety margins.

The best way to have a representative idea of the power budget of a CubeSat is to analyze the most typical CubeSat mission: currently, CubeSats are essentially used for Earth Observation (EO) missions.

Whether it is for scientific, military or commercial purpose, an EO satellite has for mission the imagery of the Earth. The payload is a camera and is active during the daytime. During the eclipse, the camera is inactive, and the COM subsystem is operating, for a short period of time, for telemetry and commands. The satellite is in IDLE mode when none of these subsystems is required. There are three consumption modes: Imaging, Communication and IDLE.

Section 2.1 has already introduced the power level of each subsystem, the following paragraphs will discuss their power consumption for an EO mission and its different operating modes.

The presented power budget is based on a 6U structure as it is currently the most representative design for the EO CubeSat type. Indeed, a 1U CubeSat is not technically able to support such missions due to the lens size of the camera that ensures the imagery quality. 3U CubeSats are still small for commercial applications and must be over-optimized to meet the requirements[14] and 12U are uncommon. Furthermore, as it can be seen in Figure 2.30, the trend is for an increase in the size of CubeSats, with the 6U becoming the predominant size in the coming years.

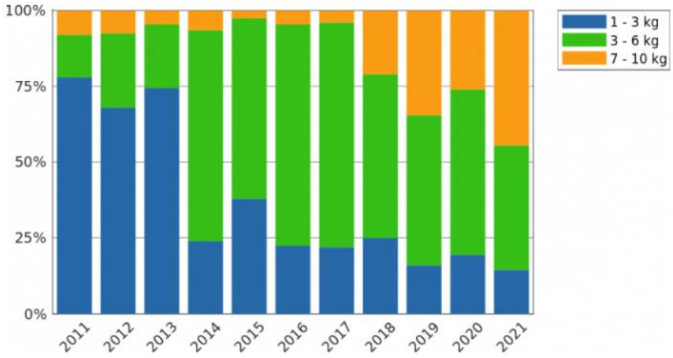


Figure 2.30 - CubeSat size trend [106]

The rest of the chapter will therefore be focused on a 6U size design.

[14] However, they are in fact the leader size in EO at the moment, it is due to the fact that the company Planet is the leader in EO constellations, and they chose an over-optimized design of 3U CubeSats. They are the only notable exception.

Subsystem Power Consumptions

Empty space is a torque-free environment, movements would theoretically need no power. Unfortunately, space is never completely empty and torques act on the satellite, i.e. magnetic, gravity gradient, atmospheric drag and radiation pressure torques. The first three are caused by the Earth, the last by the Sun. However, for a small satellite in LEO, the magnetic torque is the predominant torque and is large enough to occult the others. The magnetic torque is caused by the interaction between the magnetic field of Earth and the Residual Magnetic Dipole (RMD) of the satellite, i.e. the magnetic moment resulting from the magnetism of all the components. This torque must be counterweighted by the ADCS. The RMD of CubeSat is typically around $0.1Am^2$ for a 6U CubeSat [75] [76]. Typical CubeSat magnetorquers have a magnetic moment of $0.2Am^2$ at 5V for a power of 200mW, which indicates a needed power from the ADCS actuators of 100mW to counteract the magnetic torque [40] [44] [77]. With the losses, the sensors consumption and the need for adjustments making, i.e. feedback loop, the total ADCS power requirement for IDLE mode is estimated at 300mW.

During imaging, the ADCS needs are higher to ensure better pointing accuracy. For 6U CubeSats, a consumption from 1 to 4W is representative, it depends on the accuracy requirements and the inertia of the payload. For such a size of CubeSat, star trackers and reaction wheels are usually required, along with magnetorquers, magnetometers, gyros and/or Earth/Sun sensors [78] [79] [80] [81]. This power includes the power for the algorithm and data handling. During communication mode, ADCS asks for higher power as well, but not for such high pointing accuracy, the power required is estimated at 1 to 3W.

The power dissipation of the EPS corresponds to the efficiency of the subsystem and is thus related to the generated and consumed power. As stated in section 2.1.2, the power generated goes through converters (BCRs) with a 90% efficiency and the power consumed comes from other converters (PCU) rated at 95% of efficiency, in between there is a passage or not through the batteries characterized by almost zero losses. The consumption of the EPS is thus directly calculated from the power production and its consumption by the loads. However, the efficiency is also affected by other factors, e.g. the temperature, and a safety margin will be applied to the efficiencies to account for performances declines.

The losses associated with the EPS depends on the acuteness of the model. For a general analysis, a constant value depending on the operating mode of the satellite is enough. For each mode, we assume,

- IDLE mode: 10% of loads consumption and 7.5% of the average production, as this mode occurs during daytime and eclipse.
- Imaging mode: 10% of the consumption loads and 15% of the average production.
- Communication mode: 10% of loads consumption. It occurs during the eclipse, there is thus no production.

These proportions consider a safety margin (addition of 5%, i.e. 10% for consumption and 15% for production).

The OBC must be active at all times to respond to any situation that may occur, to effectuate the mode switches, and to monitor all subsystems at any time. The OBC corresponds here to command and data handling of the housekeeping. Its consumption is considered as constant with a value of 400mW.

For such CubeSats, the COM subsystem is usually divided into two modules. The first is a VHF/UHF or UFH/UFH command uplink/housekeeping downlink module which is linked to the housekeeping OBC. It is a transceiver that communicates with the GS, the data to be exchanged are not heavy and can be transmitted at low data rate, hence the low frequencies. This module needs approximatively 0.5W for

reception (Rx) and 4W for transmission (Tx). The second module is used to transmit the payload data, much heavier. It uses thus a higher frequency, it is typically an S-, X- or Ka-band transmitter. However, for a basic camera, with little data to send, the use of only the first module is feasible. For that case, a Tx power of 10W at UHF can be enough to transmit housekeeping and payload data. For the case of heavier data, e.g. high-resolution images, the second module alone typically requires 10W for S-bands, or 13W for Ka-bands. [52] [51] [82] [50]

The COM Tx is inactive during most of the orbit period, only when it is visible by a GS, it performs reception and transmission of the data. As for the COM Rx, it is always operating in case of urgent uplink command.

For an EO mission, the payload is active during the daytime, the COM subsystem must thus be active during the eclipse for distribution of the consumed power. The CubeSat is visible by the GS during a small time, about 10 minutes, during which the communication mode is switch on.

Payload Power Consumption

For the observation type, in strict terms, power is only needed to supply the camera optics, i.e. the actuator. However, an extra OBC specific to the payload, with as main function the storage and the processing of the data, is generally included in the payload pack. It is thus also included in its associated power consumption. In addition, some sensitive payloads may require active TCS components, e.g. heaters or Peltier elements, to maintain their temperature in the required range. This power consumption is also usually included as part of the payload consumption. Other consumptions, e.g. from the EPS or ADCS, are related to the payload but are not included in the payload power budget.

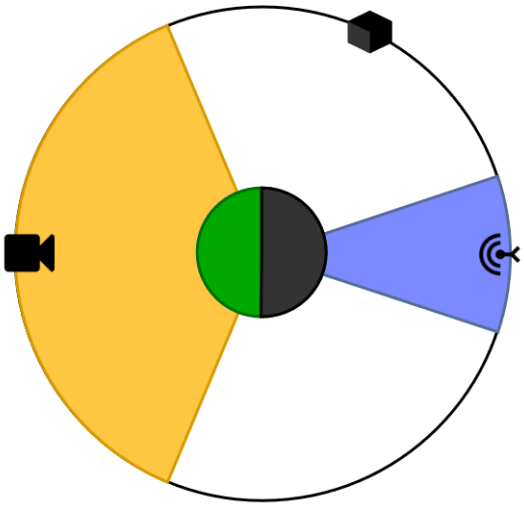


Figure 2.31 - Modes distribution over the orbit

In general, EO satellites focus on the imagery of the emerged lands. We will assume a constant acquisition of images outside of the polar circles during the daytime. It is to say between $\pm 66°$ or 37% of the orbit period.

In between payload and communication modes, the IDLE mode is activated. During which, the power consumption is at its minimum. The repartition of the operating modes is shown in Figure 2.31, respectively, the yellow, the blue and the white areas correspond to the imaging, communication and IDLE modes.

For a basic camera, a total power of 5W is estimated while the power required by a high-resolution imagery system (several cameras can be used simultaneously) is assumed up to 18W [63] [64] [83] [62].

Power Budget Table

Let us differentiate the case of a basic EO payload, e.g. basic camera, and of a complex one, e.g. high-resolution imagery system. The intervals considered in Table 2 correspond to those cases, they do not intend to set absolute boundaries but rather to propose a realistic range for the power budget of EO 6U CubeSats.

	Idle		**Imaging**		**Communication**	
Components	**[W]**	[%]	**[W]**	[%]	**[W]**	[%]
EPS	**0.6 – 1.1**	33 – 48	**1.6 – 4.7**	19 – 17	**1.2 – 2.1**	9 – 9
OBC hk[15]	**0.4**	22 – 17	**0.4**	5 – 1	**0.4**	3 – 2
COM – RX **– TX hk** **– TX pl**	**0.5** **0** **0**	28 – 22	**0.5** **0** **0**	6 – 2	**0.5** **4** **6 - 13**	4 – 2 30 – 17 46 – 57
ADCS	**0.3**	17 – 13	**1 - 4**	11 – 15	**1 – 3**	8 – 13
Payload	**0**		**5 - 18**	59 – 65	**0**	
Subtotal	**1.8 – 2.3**		**8.5 – 27.6**		**13.1 – 23**	
Duty cycle	**0.53**		**0.37**		**0.10**	
Total	**0.95 – 1.22**		**3.15 – 10.21**		**1.31 – 2.3**	
	5.4 – 13.7 [W]					

Table 2 - Power budget for EO missions

The two cases, of low and high power payload (respectively blue and red line), are shown in Figure 2.32[16]. This figure, related to Figure 2.31, presents the power level required for each operating modes as a function of time.

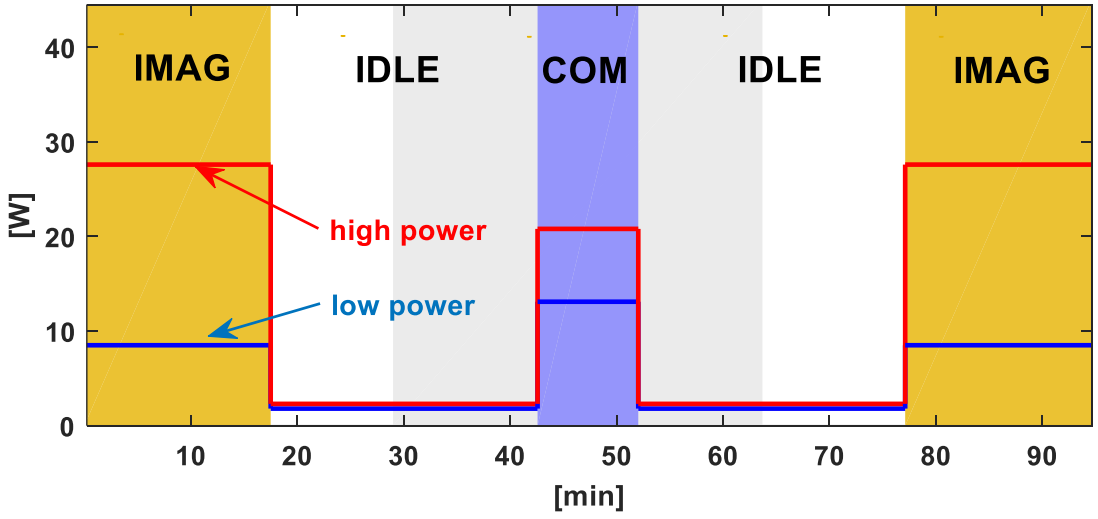


Figure 2.32 - Power level depending on the operating mode

[15] hk stands for housekeeping, pl for payload.

[16] The gray area represents the eclipse for an SSO 10:30 at 500km.

It can be seen in Table 2 that, even though the power values sometimes significantly differ between the low and the high-power levels, the percentage levels are more consistent. On Figure 2.33, the power is broken down between the different subsystems for the average consumption throughout one orbit. The main power-intensive module is the payload which nearly accounts for half of the power consumption of the spacecraft. The COM consumption is significant and attests that, even if it transmits data only for a few minutes during the orbit period, it has an important part in the power budget. As for the EPS consumption, it corresponds to its efficiency, with a safety margin, presented in section 2.1.2.

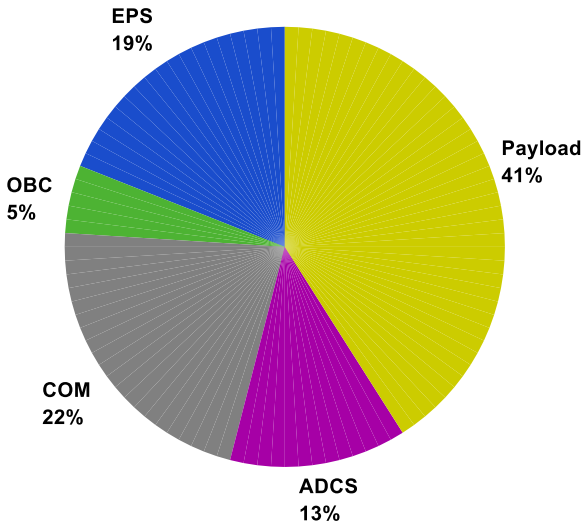


Figure 2.33 – Typical average power breakdown for EO missions

Production and Storage Requirements

The primary purpose of establishing the power budget is to determine the need of electricity production and the batteries capacity.

The average production over one orbit must correspond to the average consumption over one orbit with a safety margin. A 10% margin is generally a minimum. The amount of electricity production needed will influence the configuration of the CubeSat. Indeed, it determines if deployable solar panels are required or if only body-mounted ones are sufficient. For the highest power requirements, rotating deployable panels along with body-mounted ones can be implemented. In our case, a production of more than 6 – 15 W is needed for respectively a low and a high-power payload in an EO 6U CubeSat. As it will be detailed in the next chapter, such power is achievable by body-mounted solar panels for the low-power payload case and needs deployable panels for the high-power payload.

Along with the mission duration, the total consumption during the eclipse is usually the parameter that determines the batteries capacity. The first is the main element that sets the acceptable DoD of the batteries (see section 2.1.2), the second sets the equivalence of this DoD in Watt-Hours.

A fair value for the acceptable DoD is 15-20%, a value which allows a typical few years of mission duration. However, it is customary to install more batteries in case of failure of one of them, the DoD considered thereby drops to about 10%. The cumulated needed power during eclipse is 3.2 – 4.8 [Wh], energy corresponding to 10% of the batteries' capacity. Their capacity is thus rated at 32 – 48 [Wh]. This consideration assumes that the batteries are fully charged at the beginning of the eclipse, which is not always the case.

In this analysis, only the average power is considered. It is justifiable by the batteries' capacity and their high discharge ability. Indeed, a simple calculation will testify for it. The worst-case concerning the power demand is during the communication mode which is power-intensive and happens during the eclipse. The power requirement is up to 23W for 10 minutes. To cope with that demand, the 48Wh battery has to provide the power at a rate of 0.5C. Such a discharge rate is well under the threshold of more than 3C (see section 2.1.2). This is a basic calculation which justifies our average power approach and fits this general analysis, it does not make it a general truth. Electrical issues are extremely more complex and occupy a prominent place in the design of a satellite.

2.6 Mass Budget

The mass budget is capital to establish for the mission in itself but also for the thermal analysis. Indeed, the thermal capacity of a component is proportional to its mass, and it determines the thermal inertia of the component. As the orbit duration is short, the heat fluxes fluctuate rapidly, the thermal inertia of the components will strongly affect the reached temperatures.

Like the power budget, the mass budget is very difficult to establish as it depends on the mission and the total mass of the spacecraft. It is why a mass breakdown is more relevant to provide in a general approach as it loses the size dependence.

However, the mass budget is less strongly mission dependent than the power budget and it is possible to build a range for the mass breakdown, valid for almost any CubeSat mission. Table 3 gives a general overview of this mass breakdown.

This table is based on the elements advanced in section 2.1, as well as on the comparison of different existing CubeSats. [84] [85] [86] [87] [88] [89] [90]

Component	Mass breakdown
Structure	15 – 30%
Solar panels	10 – 20%
EPS - Batteries	2 – 8%
PCDU	3 – 10%
OBC	2 – 5%
COM	2 – 15%
ADCS	3 – 25%
Payload	15 – 50%

Table 3 - Mass breakdown overview

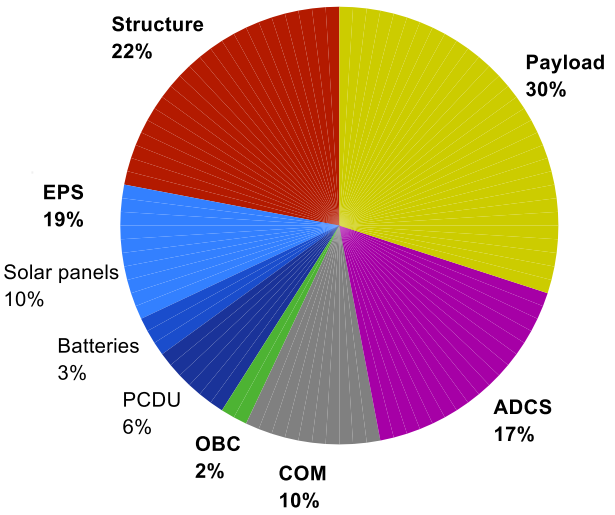


Figure 2.34 - Typical mass breakdown for EO missions

To understand the ranges in Table 3, it is important to keep in mind the following different influences on the mass breakdown:

- The size: A 1U CubeSat has its main volume occupied by basic subsystems and less proportional volume can be dedicated to the payload. In addition, the structure of a small CubeSat has a bigger importance in the mass budget than the one of a larger CubeSat, since the volume increases faster than the surface.
- The ADCS nature: For small CubeSats, the ADCS can be managed by passive means, i.e. simple permanent magnets, which takes a smaller part of the total mass than more sophisticated ADCSs.
- The payload mass: A more intuitive reason for the disparity of the mass breakdown is the effect of the payload mass as it shapes the other mass proportions. A heavy payload will leave little room for the relative mass proportion of other subsystems.

- The presence of deployable panels: Deployable panels that carry solar cells will impact the mass of the structure. However, deployable systems mean high power production and, usually, high ADCS accuracy and high data rate COM subsystem. There is thus a mass increase in EPS, ACDS, COM subsystem and payload accompanying the mass increase of the structure. It results in an overall higher mass which can be assumed as having the same mass breakdown.

The estimated mass of the mentioned mission type, i.e. a 6U EO CubeSat, is broken down in Figure 2.34. It represents an estimation for a typical EO mission; therefore, some adjustments are to be made to match specific missions.

3 Study Case

The analysis of the first chapter introduced the space thermal environment and its implications on a satellite, the impact of its shape, size, covering and internal dissipations. The second chapter introduced the real CubeSat's architecture, its different subsystems and in particular its means to comply with the thermal requirements.

This chapter has for purpose the introduction to a study case. This is the grouping of the two first chapters in the actual thermal analysis of a CubeSat. The chapter follows the trend of the whole work and aims to be as general as possible with a CubeSat model as realistic and representative as possible.

The study case proposes two variants of a 6U EO mission: a low-power and a high-power mission. These two missions were introduced in the last chapter, section 2.5. The first mission is equipped with a low-power payload, e.g. a basic camera, the second with a high-power payload, e.g. a high-resolution camera. The low-power case needs low power production and a body-mounted configuration is sufficient. The high-power case, inversely, requires deployable solar panels to provide enough energy. Each configuration has its own advantages: the one with deployable solar panels produces more power, the one with body-mounted solar panels presents a lower overall cost.

As understanding and intuition are the guidelines throughout the work, there is room for relevant simplifications. In that optic, the analysis will be carried out with basic programming, i.e. MATLAB, instead of any more accurate software packages, e.g. ESATAN or THERMICA. This approach is adopted to avoid the "magic" aspect of software, in which you enter some parameters and receive results without understanding the inter-process. In a simplified analysis, it is possible to guide the reader towards the results and relevant analyses.

For starters, the CubeSat model is presented along with its relevant features. The resolution method is then detailed and the assumed simplifications are discussed. Finally, the results are analyzed and the respect of the components' thermal requirements is evaluated.

3.1 Study Case Model Architecture

In this section, the studied CubeSat and its thermal-wise relevant characteristics are presented. Two cases will be analyzed, the low-power EO type and the high-power EO type, these cases were already introduced in the last chapter. The internal layout of the CubeSat is the same for in both cases but the external layouts present differences.

Table 4 summarizes the main characteristics of the CubeSat missions.

Mission	Power level	Size	Mass	LTAN	Altitude	Inclination	Orbital period
EO	**Low-power**	**6U**	**8 kg**	**10:30**	**500 km**	**97.5°**	**94.5 min**
	High-power		**10 kg**				

Table 4 - Mission characteristics

As mentioned in section 2.4, CubeSat configurations are numerous and a typical configuration does not stand out, however the exact configuration does not really matter for our basic thermal analysis. A schematic view of the chosen configuration for our model is given in Figure 3.1, the configuration is similar to the bottom left CubeSat in Figure 2.29.

Figure 3.1 is a sectional view between the velocity and anti-velocity faces[17], these are 6U faces (each black cube is 1U). Nadir/zenith and pitch/anti-pitch are respectively 2U and 3U faces. Each subsystem is represented by a unique colored block, only the EPS are divided into the solar panels, the battery pack and the PCDU-1/2. The PCDU has 2 units, the first, above the COM subsystem, contains the PCUs, the second, below the batteries, comprises the charger modules. The payload block includes the camera system and its own OBC, this computer unit differs from the OBC block (in orange) which monitors the housekeeping operations. The COM subsystem is linked to the patch antenna which is localized on the nadir face.

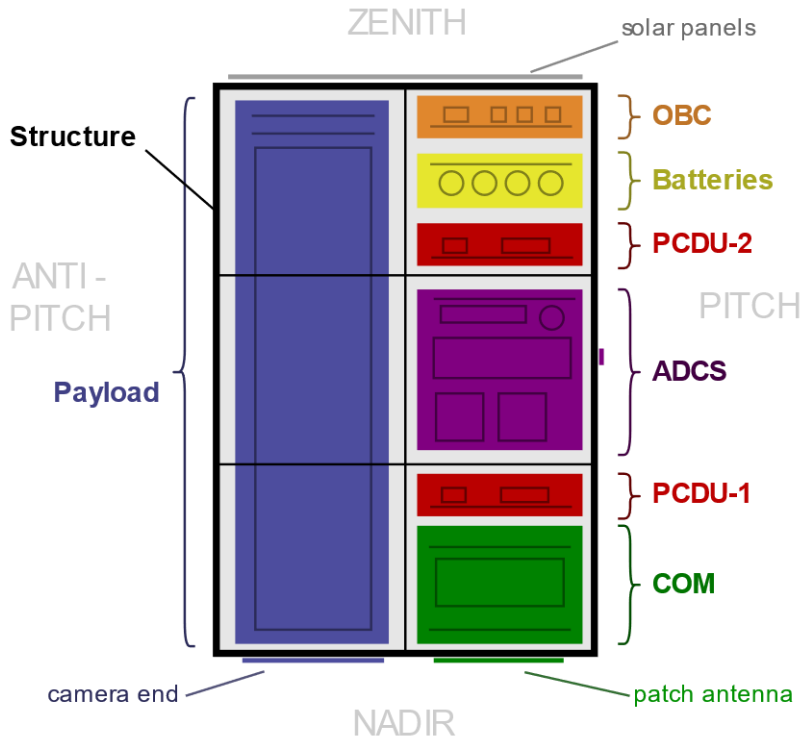


Figure 3.1 - CubeSat configuration schematic view

[17] See section 0 for faces nomenclature.

The typical power budget and mass budget of a 6U EO CubeSat have been established in sections 2.5 and 2.6, the same budgets are considered in this study case. The power budget of the low and high-power types corresponds respectively to the lower and upper bound budget of Table 2. As for the mass budget, both types have the same mass breakdown (Figure 2.34) for a total mass of 8 and 10 kg, respectively for the low and high-power type. The exact composition of each subsystem does not matter for our thermal analysis as long as the consumed power and the associated thermal capacities are given. These are provided in Table 2 and Table 8.

The two cases considered have the same internal layout (Figure 3.1), their external layouts are,

- For the low-power type: Solar panels are placed on 3 faces: velocity, zenith and anti-velocity. There is no deployable panel. (left side of Figure 3.2)
- For the high-power type: Solar panels are placed on the zenith face, as well as on the deployable panels. There are 4 deployable panels, one pair of 3Us and one pair of 6Us. (right side of Figure 3.2)

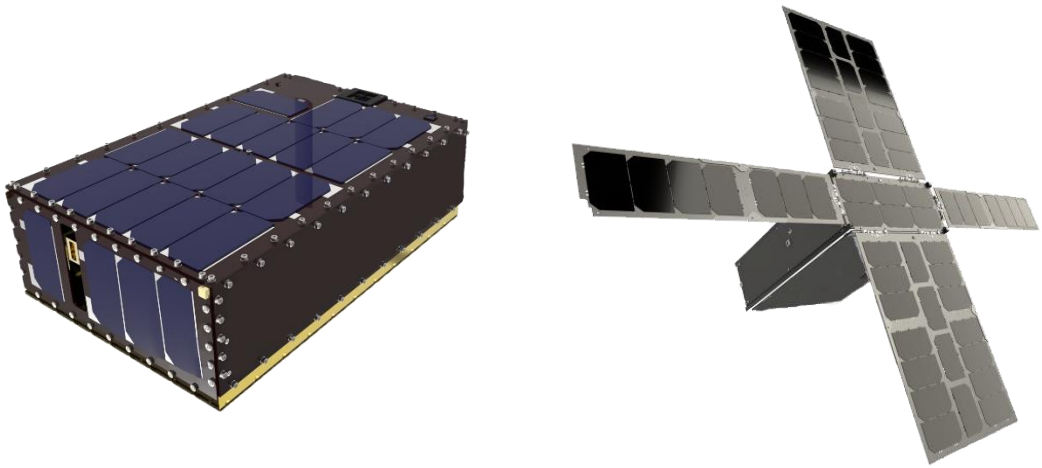


Figure 3.2 - External layout of the low-power (left) and high-power (right) cases

The battery pack of the satellite is made of Li-ion cells, a total of 32Wh and 48Wh, respectively for the low and high-power type. (see section 2.5)

As for a typical CubeSat, the components, formed by PCBs, are stacked on each other. PCBs are made of thin layers of copper inside a substrate of FR4. The FR4, for Flame-Resistant 4, is an epoxy polymer reinforced with fiberglass, it presents the following advantages: low cost, electrical insulator, lightweight, water- and fire-resistant. These assets make the FR4 the most common material for PCB's substrate. Its specific heat is 950 [J/kgK] [91], being the main component of PCBs, it constitutes its associated specific heat.

Four threaded rods hold the PCBs together, they are made of the same material as the primary structure, 6061 aluminum. [92] [93] [94]

As for the dimensions, the PCBs follow the PC/104 specifications which are an embedded computer standard [95]. This standard is classic for PCBs and is only a guideline. More peculiar configurations, such as heavy PCBs, for example, including reaction wheels, won't follow all the PC/104 specifications.

Thermal fillers and spacers are placed between PCBs except for the PCBs which are adjacent to the batteries.

The solar panels have a 30% efficiency, they are characterized by a 0.6 packing factor (solar cell area to total area ratio) when body-mounted and a 0.7 packing factor when mounted on deployable panels. The body-mounted solar panels' base material is the same as the PCBs, FR4, which is covered with a Kapton coating. The deployable solar panels' base material is titanium which is also covered by Kapton. [96]

Table 5 displays the optical properties for the components in contact with the space environment.

Component	α	ϵ	Comment
Solar cell	**0.75 (0.85)**	**0.75 (0.85)**	In parentheses values correspond to EOL values [5]. As a reminder, α is decreased of 0.3 (η_{cell}) when the cells are operational.
Solar panel base material (body)	**0.72**	**0.64**	Second surface mirror Kapton 1 mil with FR4 substrate [4] [97]
Solar panel base material (deployed)	**0.55**	**0.72**	Second surface mirror Kapton 2 mil with titanium substrate [4] [97]
Base side panel[18] (low-power)	**0.1**	**0.04**	Aluminum tape [4]
Base side panel (high-power)	**0.65**	**0.52**	Second surface mirror FEP 1 mil with Inconel substrate [97]
Nadir face	**0.25**	**0.25**	Constituted of 2/3 aluminum side panel (~0.15/0.05) and 1/3 patch antenna (~0.4/0.7). [98] [4]
Radiator (high-power)	**0.08**	**0.81**	Second surface mirror Teflon 5 mil with Silver substrate [4]
Payload optics	**1**	**1**	Considered as a black body (thermally coupled with Earth for imagery quality)
Deployable panels back (nadir side)	**1**	**1**	Black paint

Table 5 - Optical properties of the components

Second surface mirrors are composed of a substrate covered by a translucent coating, usually a polymer such as polyimide (Kapton) or fluorinated ethylene (FEP or Teflon). Their absorptivity is assumed to be mainly due to the substrate while their emissivity depends on the coating nature and its thickness, expressed in mils (1 mil = 25.4 µm).

[18] Panel non-covered with solar panels.

The structure and the side panels are made of 6061 aluminum which is the most common material for CubeSat's base material as it is lightweight (2.7 [g/cm^3]), mechanically robust and has a high specific heat (960 [J/kgK]) for better thermal inertia.

Table 6 displays the thermal capacity associated to each component.

Component	$c_p \left[\frac{J}{kgK}\right]$	**Mass breakdown [%]**	**Thermal capacity** $\left[\frac{J}{K}\right]$	**Material**
Structure	**960**	**11**	**740 – 1055**	6061 aluminum [4]
Side panels		**11**	**740 – 1055**	
Solar panels	**600**	**10**	**420 – 600**	Germanium (solar cells substrate) + FR4 (base material)
Batteries	**1100**	**3**	**230 – 330**	Li-ion batteries [99]
COM	**850**	**10**	**595 – 850**	Mix of FR4 (PCBs), aluminum (modules) and copper (electronics).
OBC		**2**	**120 – 170**	
PCDU		**6**	**355 – 510**	
ADCS		**17**	**1010 – 1445**	
Payload	**1000**	**30**	**2100 – 3000**	Mix of aluminum (mirrors), polymer (frame) and FR4 (PCBs)

Table 6 - Thermal capacities of the CubeSat's components

The thermal capacities range from the value for low-power type to the one for high-power type. As mentioned, the total masses are respectively 8 and 10kg. The mass breakdown is considered the same for both cases and was presented in section 2.6 by Figure 2.34.

3.2 Thermal Nodal Model Theory

A thermal nodal model has several features:

- It is a model: a simplified version of reality that helps us approximate the desired behavior.
- It is nodal: the studied system is decomposed into nodes. Each node is considered as being characterized by a single temperature, an isothermal node. The more nodes, the more accurate the model.
- It is a system: each node is linked to the others through means of exchanging energy. In our case, thermal conductances and capacities are these means.

The thermal nodal model is based on the electrical nodal model:

- Temperatures **T** correspond to voltages.
- Heat fluxes **Q** correspond to currents.
- Thermal resistances **R**, conductances **G** and capacities **C** correspond to electrical resistances, conductances and capacities.

The general equation, applicable to each node, is:

$$C\frac{\mathrm{d}T}{\mathrm{d}t} = Q_{in} - Q_{out} + Q_{int}$$

With C, the thermal capacity and $Q_{in,out,int}$, respectively the incoming and emitted heat fluxes and the internal dissipations.

This equation was introduced in section 1.5 and was applied to the satellite as a whole. This is the one-node model, only characterized by the temperature T_S, represented by the top of Figure 3.3.

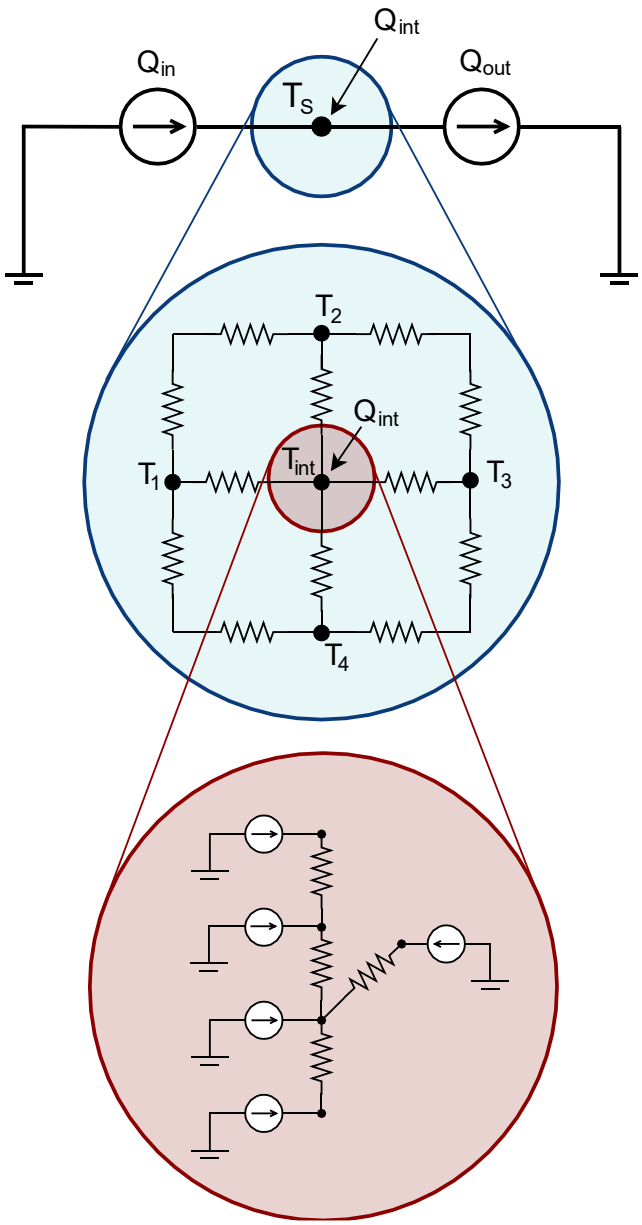


Figure 3.3 - Thermal nodal model schematic

Figure 3.3 represents the thermal model of the satellite: from a simplistic form to a more detailed one. The upper part considers the entire satellite as one thermal node subject to a global incoming heat flux and emitting a global outgoing heat flux. This is the configuration considered in chapter 1. The middle part is a zoom that divides the satellite into 6 faces (only 4 represented on the diagram) and an internal component dissipating Q_{int}. Each of the faces is one thermal node (1 to 4) linked by a thermal resistance to the others and to the internal node. The lower part is a zoom that details the internal thermal links. Each node corresponds to a part of the satellite (ADCS components, batteries, etc.) and is coupled with a heat flux source which considers its own heat dissipation.

Each node has a thermal capacity that is going to the mass (it is implied on the diagram for clearness sake), this capacity reflects the thermal inertia of the node: it does not instantly heat up or cool down. The capacity acts as a low-pass filter which results in smoothing their temperature evolution. Its value depends on the mass and specific heat of the node, $C = mc\ \left[\frac{J}{K}\right]$.

As the heat fluxes are not constant but vary through time, the system does not reach a steady state. To compute this nodal system, it is of use to discretize time in small Δt's and compute the temperature at each node for each time step. The following equation is the thermal balance at node i between time $t = t_n$ and time $t = t_{n+1} = t_n + \Delta t$.

$$C_i \frac{T_{i,n+1} - T_{i,n}}{\Delta t} = Q_{i,n} = Q_{in,i,n} - Q_{out,i,n} + Q_{int,i,n}$$

With $T_{i,n}$ and $T_{i,n+1}$, the temperature of node i at time t_n and t_{n+1}, $Q_{in,i,n}$ the incoming heat flux at node i at time t_n, $Q_{out,i,n}$, its outgoing heat flux and $Q_{int,i,n}$ its internal dissipation.

For internal nodes,

$$Q_{i,n} = Q_{cond,i,n} + Q_{rad,i,n} + Q_{int,i,n}$$

Except for the internal dissipations, the incoming and leaving heat fluxes are conducted or radiated heat from or to other nodes.

For external nodes,

$$Q_{i,n} = Q_{s,i,n} + Q_{a,i,n} + Q_{e,i,n} + Q_{cond,i,n} + Q_{rad,i,n} + Q_{int,i,n} - Q_{out,i,n}$$

It respectively corresponds to the solar, the albedo, the Earth IR, the conductive, the radiated, the dissipated and the emitted heat flux. Radiated and emitted fluxes are both radiative heat transfers, the nomenclature designates radiated for radiative transfer from or to the interior of the satellite and emitted for radiative emission towards space.

The incoming heat fluxes Q_s, Q_a, Q_e have been introduced and detailed in section 1.4, as well as for the emitted heat flux Q_{out} which is equal to,

$$Q_{out,i} = A_i \epsilon_i \sigma \, T_i^4$$

With T_i the temperature of node i of area A_i and emissivity ϵ_i, and σ, the Stefan-Boltzmann constant.

The conductive flux at node i is the sum of all arriving and leaving fluxes by conduction to or from node i, the same applies for the radiative flux,

$$Q_{cond,i} = \sum_j Q_{cond,i,j} = \sum_j G_{i,j} \left(T_j - T_i\right)$$

$$Q_{rad,i} = \sum_j Q_{rad,i,j} = \sum_j A_i \epsilon_{ij} \sigma \left(T_j^4 - T_i^4\right)$$

With $G_{i,j}$ the thermal conductance between node i and node j, and ϵ_{ij}, the effective emissivity between node i and node j.

The contribution of the conduction and the radiation are discussed in section 3.3.

The thermal nodal model applied to our study case is presented in section 3.4.

3.3 Internal Heat Transfers: Radiation versus Conduction

There are many heat transfers inside the satellite, either conductive or radiative. This section aims to compare their relative importance.

Let us take the basic case of 2 PCBs facing each other. We simplify the case by considering each PCB as an isothermal smooth plate, the two PCBs are linked by 4 threaded rods. They are thermally coupled by conduction and radiation. Figure 3.4 draws the situation.

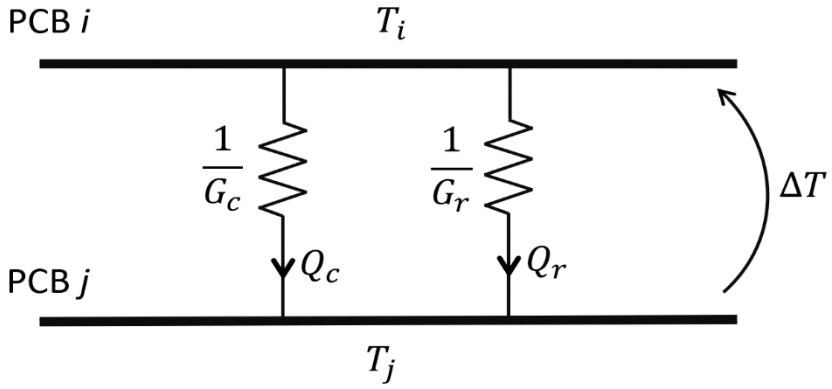


Figure 3.4 - Thermal coupling of 2 PCBs facing each other

G_c and G_r are thermal conductances representing respectively the conductive and radiative link between the PCBs. A thermal conductance is expressed in [W/K] and corresponds to the amount of heat, in watts, transferred by degree difference between the two nodes that it connects. The greater the thermal conductance, the more the nodes are thermally coupled.

Conductive Link

The heat transfer by conduction occurs through solid matter, the traversed material is characterized by a thermal conductivity k. The conductive heat flux from a node i to a node j is,

$$Q_c = G_c\,\Delta T \quad \text{with} \quad G_c = \frac{k\,S}{L}\left[\frac{W}{K}\right]$$

With $\Delta T = T_j - T_i$, the temperature gradient between node i and j, L, the length of the material connecting the nodes and S its cross-section.

In our case, the four threaded rods holding the PCBs together are the conductive material between the PCBs. They are made of 6061 aluminum of thermal conductivity, $k_{Alu} = 167\ \left[\frac{W}{mK}\right]$, with a radius, $r = 0.16\ [cm]$[19] and a length d.

Radiative Link

The heat transfer by radiation occurs between surfaces characterized by an emissivity ϵ[20]. The radiative heat flux from a surface i to a surface j is,

$$Q_r = A_i \epsilon_{ij} \sigma\,(T_j^4 - T_i^4)$$

[19] The radius is conformed to the PC/104 specifications that standardize the PCB dimensions.

[20] At relatively low temperature, emissivity and absorptivity are equal, $\alpha = \epsilon$.

With σ, the Stefan-Boltzmann constant, A_i, the area of surface i, ϵ_{ij}, the effective emissivity between the surfaces. From the fluxes balance, ϵ_{ij} can be expressed as,

$$\epsilon_{ij} = \frac{F_{ij}\epsilon_i\epsilon_j}{F_{ij}(\epsilon_i + \epsilon_j) + \epsilon_i\epsilon_j(1 - 2F_{ij})} \approx \frac{\epsilon_i\epsilon_j}{\epsilon_i + \epsilon_j - \epsilon_i\epsilon_j}$$

Where ϵ_i and ϵ_j are the emissivities of the surface i and j, and F_{ij} is the view factor between them. The approximation corresponds to the case of close enough surfaces compared to their area, which is the case.

When ΔT is small, typically less than 100K, which is the case as the PCBs in a CubeSat are thermally well coupled, the following linearization can be made,

$$T_i^4 - T_j^4 \approx 4T_m^3\,\Delta T \qquad \text{with} \qquad T_m = \frac{T_i + T_j}{2}\ (\approx T_i)$$

This linearization is very accurate: for a ΔT of 50°C at $T_m = 50$°C, which is high for two adjacent components, there is a difference of only 0.6%.

The radiative heat flux can thus be approximated as,

$$Q_r \approx G_r\,\Delta T \qquad \text{with} \qquad G_r = 4A_i\epsilon_{ij}\sigma T_m^3 \quad \left[\frac{W}{K}\right]$$

G_r is the radiative thermal conductance and T_m the mean temperature of node i and node j.

In our case, the PCBs face each other and thus a radiative link is made. The PCB's emissivity corresponds to the one of their substrates which are made of FR4, $\epsilon_i = \epsilon_j = \epsilon_{FR4} = 0.89$ [4] and $\epsilon_{ij} = 0.8$. Their side lengths 90x96 mm, are set by the PC/104 norm, give an area $A_i = 88.4\ [cm^2]$.

Comparison between Conductive and Radiative Conductances

A thermal conductance is to be correlated as an electrical conductance: the higher its value, the higher the current passes through for the same voltage. The analogy reflects that, for the same temperature difference, the higher the thermal conductance, the more heat is going through.

In our case, for a realistic distance between the PCBs[21], $d = 1.5\ [cm]$, and a mean temperature between the PCBs, $T_m = 25\ [°C] = 298\ [K]$, the thermal conductances are,

$$G_c = 0.36\ \left[\frac{W}{K}\right] \qquad G_r = 0.04\ \left[\frac{W}{K}\right]$$

G_c is large enough compared to G_r to approximate that the thermal coupling is negligently affected by the radiative heat transfer.

Figure 3.5 ensures that this hypothesis is still correct if the temperature or the distance varies[22]. The ratio stays below 0.15 for any realistic length at 25°C and any realistic temperature at 1.5 cm of distance.

[21] This is the distance implied by the PC/104 specifications.

[22] The view factor has been considered in these graphs.

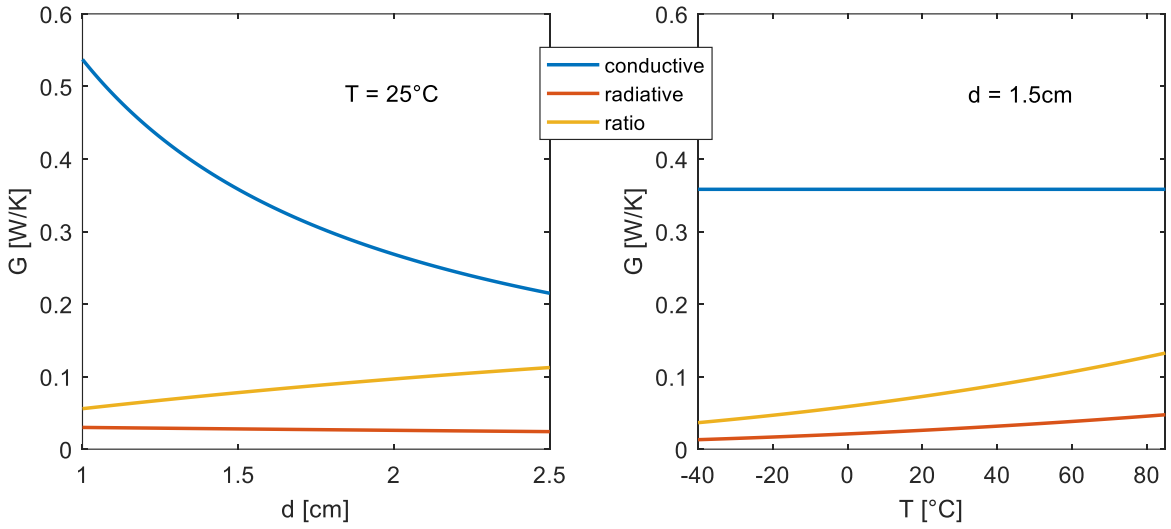


Figure 3.5 - Conductive and radiative thermal conductances as a function of the distance and the temperature

It is important to note that this situation is as simplistic as possible. Indeed, the assumption of a PCB as an isothermal plate and the assumption of a perfect transfer of its heat towards the thermal links greatly simplify the problem. On the other hand, this approach also favors the radiative transfer.

Indeed, the gap between two stacked PCBs is usually filled by connectors and fillers which enhance the thermal conduction (Figure 3.6). The PC/104 specifications include a conductive link between two stacked PCBs (Figure 3.6). This black box encapsulates 104 phosphor bronze pins of 0.36mm² linking the PCBs, their thermal conductivity is 85 [W/mK]. In addition, each of the threaded rods is enveloped by a spacer made in the same material as the structure and the rods, 6061 aluminum, with a thickness of 0.5mm.

$$G_{rods} = 0.36\left[\frac{W}{K}\right], \qquad G_{spac} = 0.21\left[\frac{W}{K}\right], \qquad G_{pins} = 0.26\left[\frac{W}{K}\right]$$

$$\Rightarrow \quad G_{PCB} = 0.83\left[\frac{W}{K}\right]$$

With G_{PCB} the cumulated conductance between two PCBs. The cumulated conductance ends up being more than the double of the conductance through the rods only.

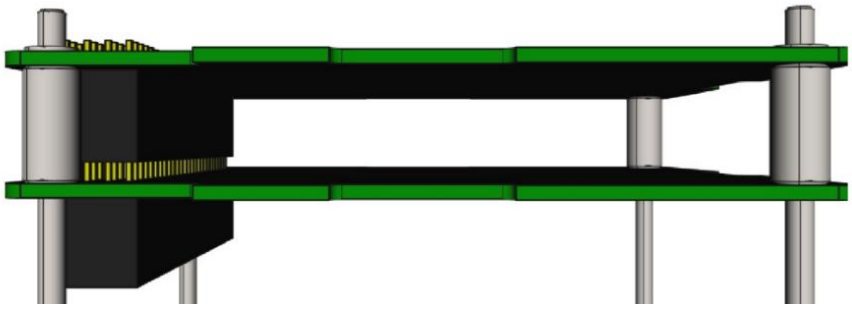


Figure 3.6 – PCB's typical stacking, modified from [98]

Side Panels and Payload Heat Exchange

The thermal coupling between the payload and the external side panels is also important to analyze. Indeed, both components have a wide area facing each other (Figure 3.7) and are not directly linked by conduction (except for face anti-pitch for high-power case). It is the coupling for which the radiative and conductive heat transfers have the closest relative importance.

Figure 3.7 illustrates the thermal links between the payload (blue cylinder) and the velocity face (green plate), the radiative links are represented by red inductances and the conductive links by resistances (orange for structure/panel, yellow for payload/structure).

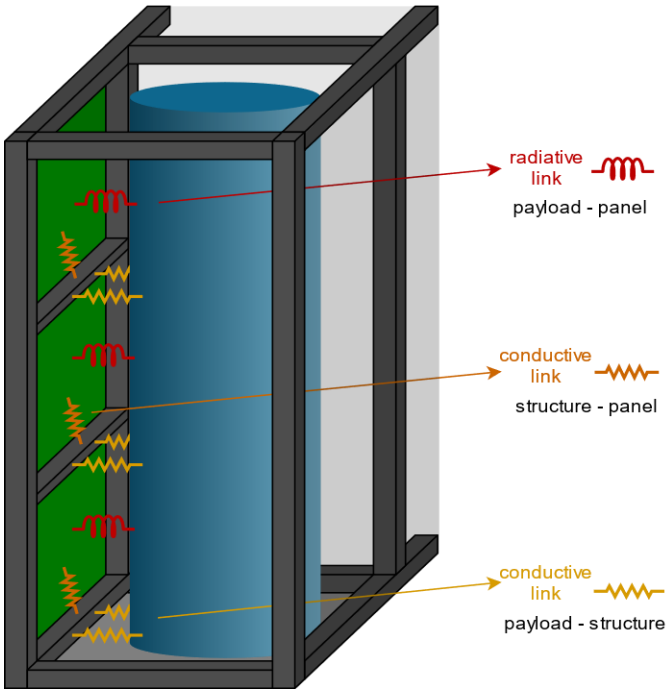


Figure 3.7 - Payload and side panel thermal interactions

Let us estimate the thermal conductances:

- For the radiative link, the payload and the side panels are facing each other and thus exchange radiations. The view factor between the payload and one panel is estimated at 1/5, and the surface of the payload is estimated at 0.06 [m²] (cylinder of 4cm radius and 25cm height). The payload and the inner side of the panels are firstly assimilated to black bodies, their effective emissivity is, $\epsilon_{ij} = F_{ij} = 0.2$. The maximal mean temperature between the two is around 40°C (see section 3.5.2). The resultant radiative conductance $G_{r,pl}$ is,

$$G_{r,pl} = 0.07 \left[\frac{W}{K}\right]$$

- For the conductive link, the two components are indirectly connected through the structure. The conductances are 0.3 and 3 [W/K], respectively for the conductive link payload/structure and structure/panel (see section 3.4). However, it is not possible to compute a resultant conductive conductance since the structure has its own varying temperature. Therefore, when it is higher or lower than both temperatures, there is no conductive heat exchange between the payload and the side panel.

We assume that the radiative conductance must be considerably inferior than the conductive conductance between the payload and the structure. This assumption is set to ensure an inferior radiative exchange between the payload and the side panel even if their temperature gradient is high and the temperature gradient between the payload and the structure is low.

In the mentioned values, the conductive link is only 4 times larger than the radiative one which does not constitute a considerable difference.

The chosen solution is to apply a low emissive coating on the payload surface so that the radiative heat exchange with its surroundings is lowered. For larger applications, an MLI blanket would have been chosen for such a function. For smaller applications such as CubeSats, a tape is sufficient. A tape made with aluminum backing ($\epsilon = 0.03$ [4]), is applied on the payload, the effective emissivity becomes, $\epsilon'_{ij} = 0.026$, and the radiative conductance,

$$G'_{r,pl} = 0.01 \left[\frac{W}{K}\right]$$

The radiative link is now negligible compared to the conductive link. In addition, the radiative link between the payload and the side panels is somewhat compensated by the temperature gradient between the side panels, e.g. the panel facing the Sun is hotter than the payload which is hotter than the panel facing the deep space, the radiative flux passes partially through the payload.

The application of the tape is a general beneficial asset for the payload because it must be isolated to the maximum in order to be kept from temperature fluctuations.

Zenith Side Panel and OBC Heat Exchange

Another location to check is the interface between the OBC and the zenith side panel. On the one hand, the OBC is the last PCB of the stack and thus has a big view of the zenith side panel. On the other hand, the OBC and the panel are not directly linked together and the OBC is poorly linked to the structure (0.2 [W/K], see section 3.4). The radiative link is 0.05 [W/K], it corresponds the link between two PCBs with an effective emissivity, $\epsilon_{ij} \approx 1$, which is due to the unity emissivity of the black painted wall. This difference is too small to be negligible, therefore, in order to keep a simple model without internal radiative links, we will assume a constant radiative link and assimilate it to a conductive conductance $G_{c,OBC}$,

$$G_{c,OBC} = 0.05 \left[\frac{W}{K}\right]$$

It is a fair assumption as the temperature of the OBC is quite constant throughout the orbit (see section 3.5.2). Turning this radiative link into a conductive link is equivalent to considering a modest thermal strap between the OBC and the zenith panel.

On the other stack side, for the case of heat exchange between the COM subsystem and the nadir side panel, the situation is not the same. Indeed, as it will be seen in section 3.4, there is a thermal strap of 1 [W/K] between the COM subsystem and the radiator (face 6) and as the side panels are also well coupled with the structure, the radiative link is thereby neglected.

This section has demonstrated the non-necessity to integrate the internal radiative links into the thermal model.

3.4 Study Case Thermal Model

For our study case, we consider 14 thermal nodes:

- 6 nodes for the faces: the face term includes the side panel, the solar panels (in case), the surface coating and the patch antenna (in case). As mentioned in section 1.9, the faces correspond to the nodes: 1 for nadir, 2 for zenith, 3 for velocity, 4 for anti-velocity, 5 for pitch and 6 for anti-pitch. In further graphs, the faces will be referred by their nodal number.
- 7 nodes for the subsystems: each of these nodes is represented by a box in Figure 3.1.
- 1 node for the structure.
- The deployable panels, in case of high-power type, are considered as thermally conductively decoupled from the satellite and therefore do not form a node but are studied in a one-node system on its own. They are referred to as DP for Deployable Panels.

node num.	1	2	3	4	5	6	7
	Nadir	Zenith	Velocity	Anti-velocity	Pitch	Anti-pitch (RAD[23])	Payload (PL)
node num.	8	9	10	11	12	13	14
	COM	PCDU-1	ADCS	PCDU-2	Batteries (BAT)	OBC	Structure (STR)

Table 7 – Nodes denomination

This model is very simplistic in order to remain consistent with the objectives. The assumptions are thus strong, for example, the structure in itself is considered as sufficiently thermally coupled to have a single temperature. This assumption is not true but fit in a basic model and allow us to make our model somewhat flexible concerning the exact internal layout.

As said in section 3.2, there is several features that connect the nodes together in a system:

- Their thermal capacity C, given in Table 6.
- The incoming heat fluxes Q_{in} which are absorbed by the 6 faces (node 1 to 6) and the payload through the camera optics (node 7). The fluxes that reach the faces G_{in} were introduced in chapter 1 and applied on cube shape in section 1.9. The absorbed fluxes $Q_{in,i}(= \alpha_i A_i G_{in,i})$ are shown in Figure 3.8, the absorptivity of the components is given in Table 5. The figure shows on the left the incoming fluxes for the low-power case, in the center for the main structure of the high-power case and on the right for the deployable panels of the high-power case. For the high-power main structure, the fluxes are altered by the presence of deployable panels.
- The emitted fluxes Q_{out} which depends on the area and the emissivity of the external surfaces, given in Table 5.
- The internal dissipations Q_{int}, given in Table 2 for the cases of low and high-power. As mentioned, the power budget is established for the three operating modes: Imaging, IDLE and communication. The satellite switches the operating mode during the orbit as shown in Figure 2.31 and Figure 2.32.
- The internal conductive links between nodes Q_{cond} which depend on the thermal conductances G by the relationship $Q_{cond} = G\ \Delta T$. The conductances between each pair of components are detailed in Table 8 which is presented in this section.

[23] In case of high-power type, the anti-pitch face is highly emissive and assimilated to a radiator.

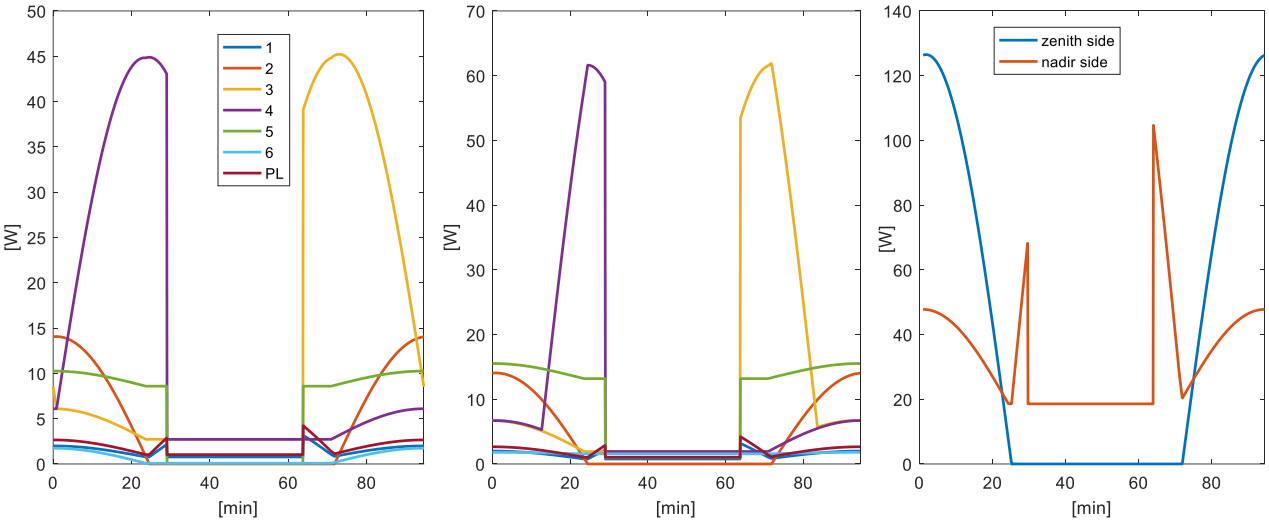


Figure 3.9 - Incoming heat fluxes, from left to right: low-power case, high-power case main structure, high-power case deployable panels

The general thermal network is illustrated in Figure 3.9, the 14 nodes are connected together by thermal conductance. The incoming, outgoing and dissipation heat fluxes are shown respectively by Q_{in}, Q_{out} and q. These fluxes are balanced during a thermally stable entire orbit.

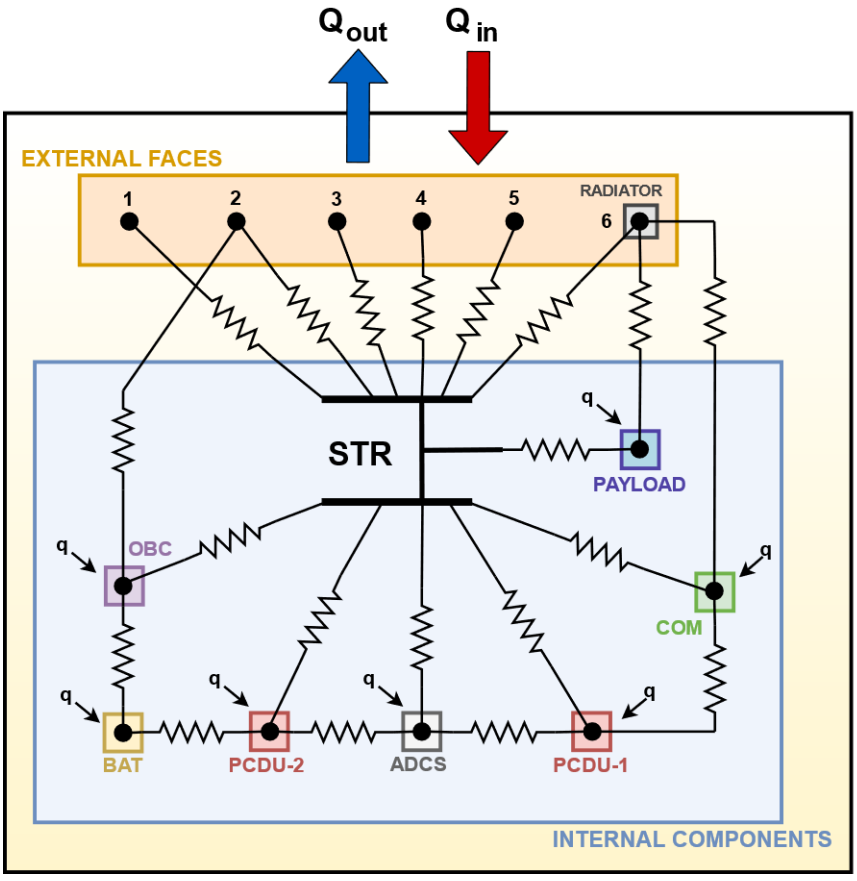


Figure 3.8 - Thermal nodal network

The thermal conductances are displayed in Table 8. The values considered are as realistic as possible and reflect the typical following considerations for a CubeSat:

- The faces are thermally well coupled with the structure in order to increase their thermal inertia and prevent extreme temperatures. It also lowers the temperature gradient between them.
- The internal components are in general well coupled together and quite isolated from the structure. This design allows the temperature to be homogeneous inside the satellite and therefore to damp any dissipation peak from a subsystem. By being isolated, it also allows preventing from flux fluctuations, specific to the surroundings.
- The payload is, in particular, isolated to the maximum. It is coated by a low emissive tape to limit the radiative exchanges and is only connected to the structure by a poor conductive link. A thermal strap connecting it to the face 6, acting as a radiator, is added for the high-power case, helping to conduct away the high dissipation specific to that case.
- The COM subsystem is a high dissipative module during operation (communication mode) for a limited mass. To prevent overheating, it is connected to the face 6 by a thermal strap.

Link		**Conductance** $\left[\frac{W}{K}\right]$	**Comment**
COM	**PCDU-1**	**0.83**	Assimilated to the conductive link between 2 PCBS with thermal fillers in between (see section 3.3)
PCDU-1	**ADCS**		
ADCS	**PCDU-2**		
PCDU-2	**BAT**	**0.36**	Assimilated to the conductive link between 2 PCBS without thermal fillers (see section 3.3)
BAT	**OBC**		
COM	**STR**	**0.15**	Assimilated to the conductance from 4 threaded rods to the structure at a 2.5cm distance and considering the contact resistance between the rod ends and the ribs of the structure.
PCDU-1			
PCDU-2			
OBC			
ADCS	**STR**	**0.3**	Twice the value of the previous link as it is considered to be attached to the structure in two places.
Payload			
Payload	**6**	**0 (2)**	Copper thermal strap (square shape strap, 5cm long, 1.1 or 1.5 cm wide). The values in parentheses correspond to the high-power case. There is no thermal strap at the payload for the low-power case.
COM	**6**	**1 (1)**	
OBC	**2**	**0.05**	Assimilated to their radiative link as detailed at the end of section 3.3.
Face 1	**STR**	**1**	The conductance between the side panels (faces) and the structure is considered to be 0.5 [W/K] per unit (1U surface).
Face 2		**1**	
Face 3		**3**	
Face 4		**3**	
Face 5		**1.5**	
Face 6		**1.5**	

Table 8 - Thermal conductances of the components

3.5 Simulation Results

This section gathers all the results and analyses drawn from the presented model.

3.5.1 Energetic Analysis

Electric Balance

The electric production and consumption for both cases are shown in Figure 3.10 (the graphs are not at the same scale, by a factor of 3). The State-of-Charge (SoC) of the battery appears is red in percentages of its full capacity, the minimum is reached at the end of the eclipse at a value of 90%, which concurs with the minimal DoD of 10% mentioned in section 2.5. It shows,

- For the low-power case: an average production of 8.2 W for an average consumption of 5.4 W. The production is higher when the satellite passes over the poles because the larger faces with solar panels are pointing towards the zenith orientation.
- For the high-power case: an average production of 16.6 W for an average consumption of 13.7 W. The production is concentrated near the zenith as only the zenith-oriented panels are covered with solar panels.

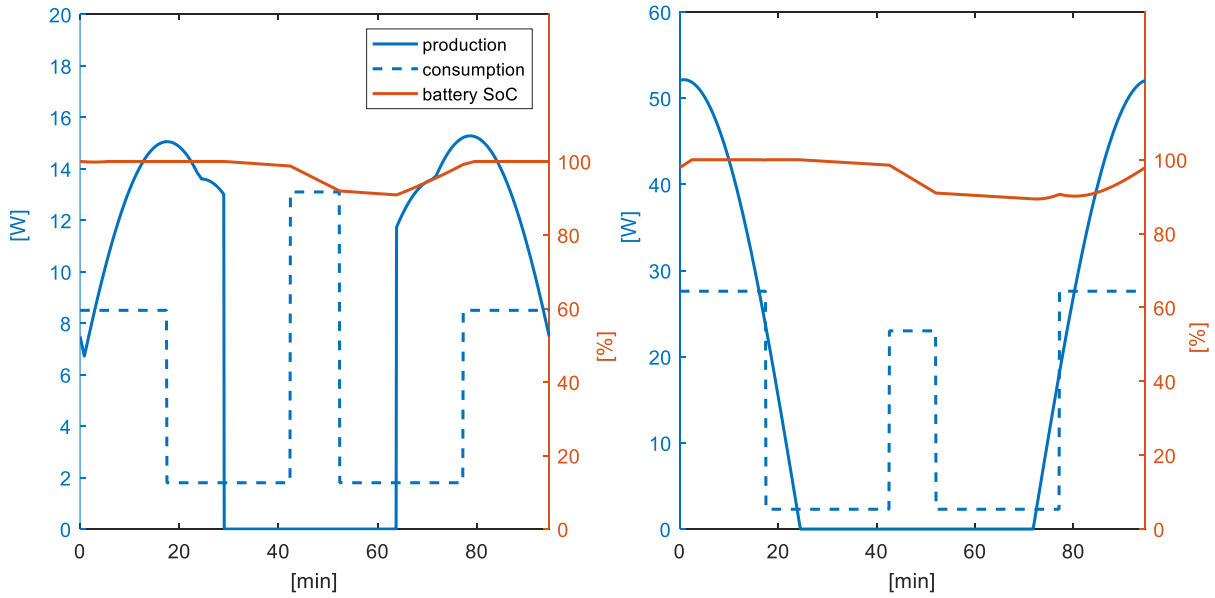


Figure 3.10 - Electric production, consumption and storage. Low-power (left) and high-power case (right)

Figure 3.10 is an electric balance: the power produced is either directly used or stored in the batteries, and, in case of greater consumption than production, the electricity is drawn from the batteries. When the batteries are full and the consumption is below the production, there is overproduction. This overproduction is designed as a safety margin and is turned into heat in case of expected power conditions (not shown on the graph).

Power Balance

It can be interesting to have an idea of the total energetic balance of the system. Figure 3.11 proposes an overview of the energy flows of the system as a Sankey diagram for the low-power case. The incoming energy flows in the form of radiations are shown on the left: solar flux, Earth IR and albedo flux. The energy is either reflected or absorbed by the external surfaces, it can be absorbed as heat or turned into electricity by solar cells. A part of the electricity is directly used. Another is indirectly used by passing through the batteries. The last part of electricity is turned into heat when there is overproduction. The term 'Elec Use' includes all subsystem power consumption. In the end, most of the electricity remains in the system and ends up as heat dissipation. Only a small part of it leaves the system in the form of RF waves via the COM subsystem for downlink communication. The absorbed heat in the satellite is then finally emitted back to space in the form of IR radiations.

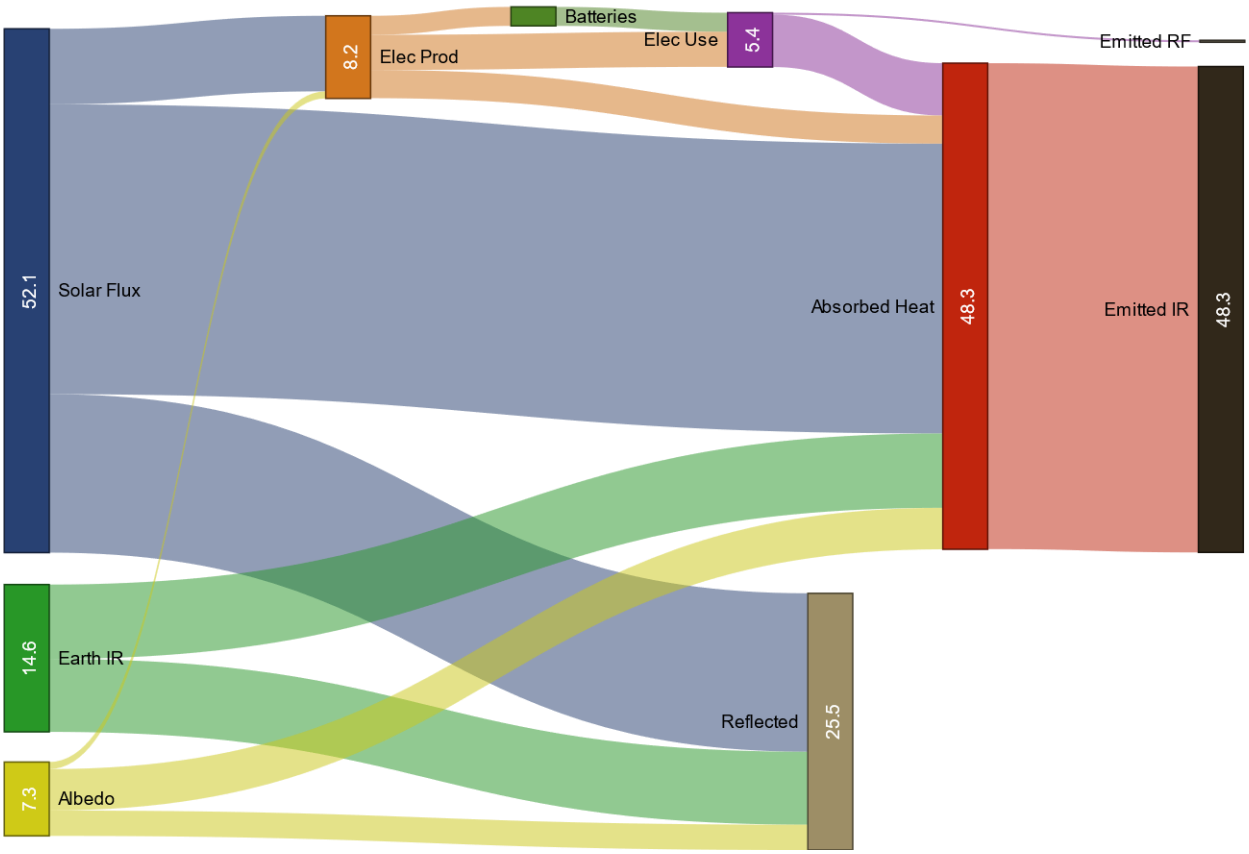


Figure 3.11 – Mean power balance (in [W]) - Sankey diagram

This power balance puts in perspective the amount of incoming energy turned into electricity (about 10% for both low and high-power cases) and the amount of energy passing through the batteries (about 35% of used electricity). It also points out that whatever the energetic modification inside the system, the input and output energy are simply radiation.

3.5.2 Temperature Analysis

The primary purpose of the thermal nodal model is to compute the temperature at each node at any time. This section displays the different temperatures and analyzes their profiles.

Temperature Evolution: Low-Power Case

All the temperatures during a stable orbit are plotted in Figure 3.12. The temperature of the external faces (node 1 to 6) and the structure (STR) are shown in the top graph, and the temperature of the internal components in the bottom graph.

The general overview corresponds with the expectations:

- The temperatures tend to decrease during the eclipse and to increase during the daytime.
- The faces' temperatures are consistent with the incoming fluxes: a decrease during the eclipse, an increase at the beginning and the end of the daytime and a plateau at the subsolar position due to the reduction of the effective area that sees the Sun.
- The structure, with its relatively high thermal inertia, acts as a temperature moderator by damping the fluctuations.
- The temperatures of the internal components range in a narrower interval due to their fair thermal isolation, in particular for the payload.
- The COM subsystem shows a temperature peak during the communication mode. This power boost is damped by the face 6 due to their thermal strap link.

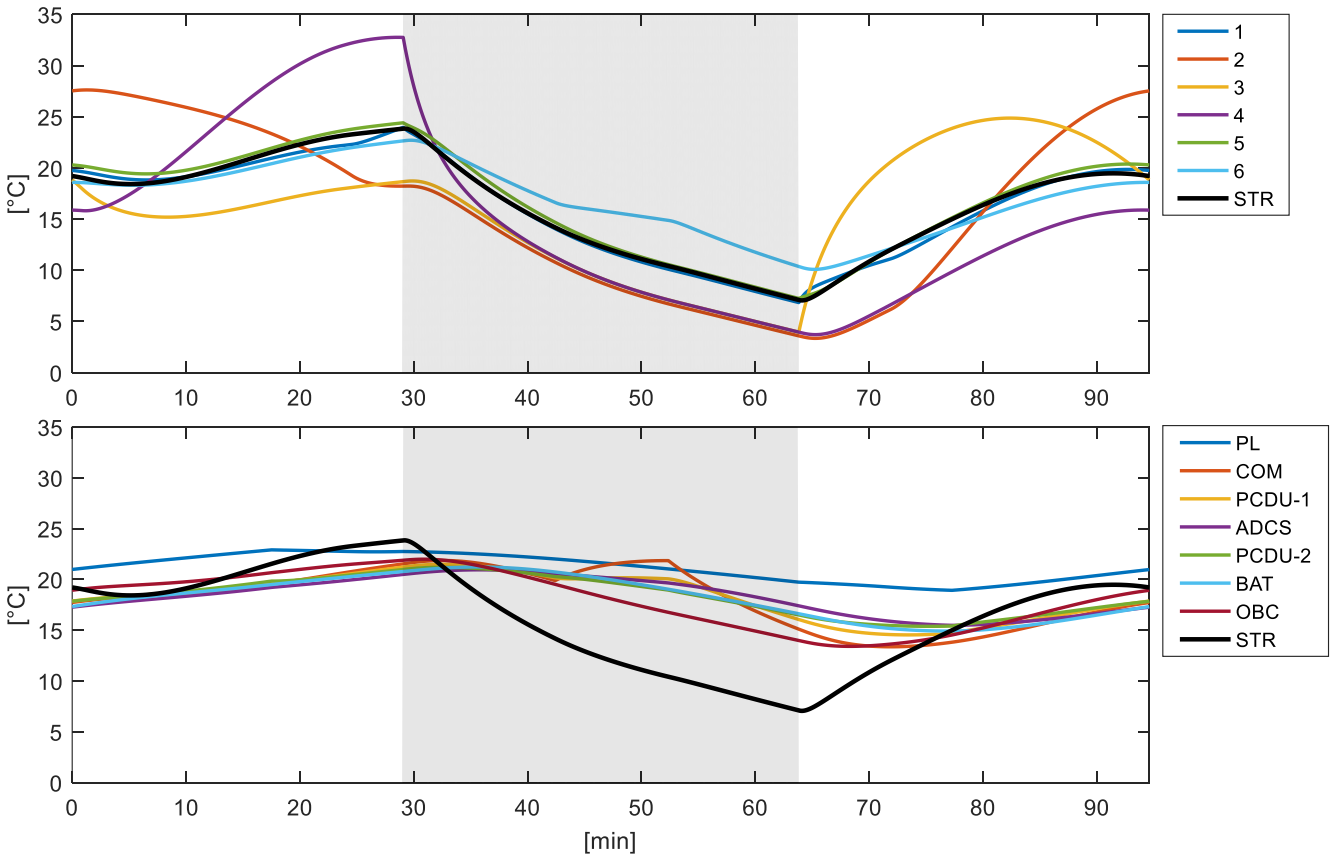


Figure 3.12 - Temperature evolution, low-power case

Temperature Evolution: High-Power Case

All the temperatures during one stable orbit are plotted in Figure 3.13. The temperature of the external faces (node 1 to 6) and the structure (STR) are shown in the top graph, the temperature of the internal components in the middle graph, and the temperature of the deployable panels in the bottom graph.

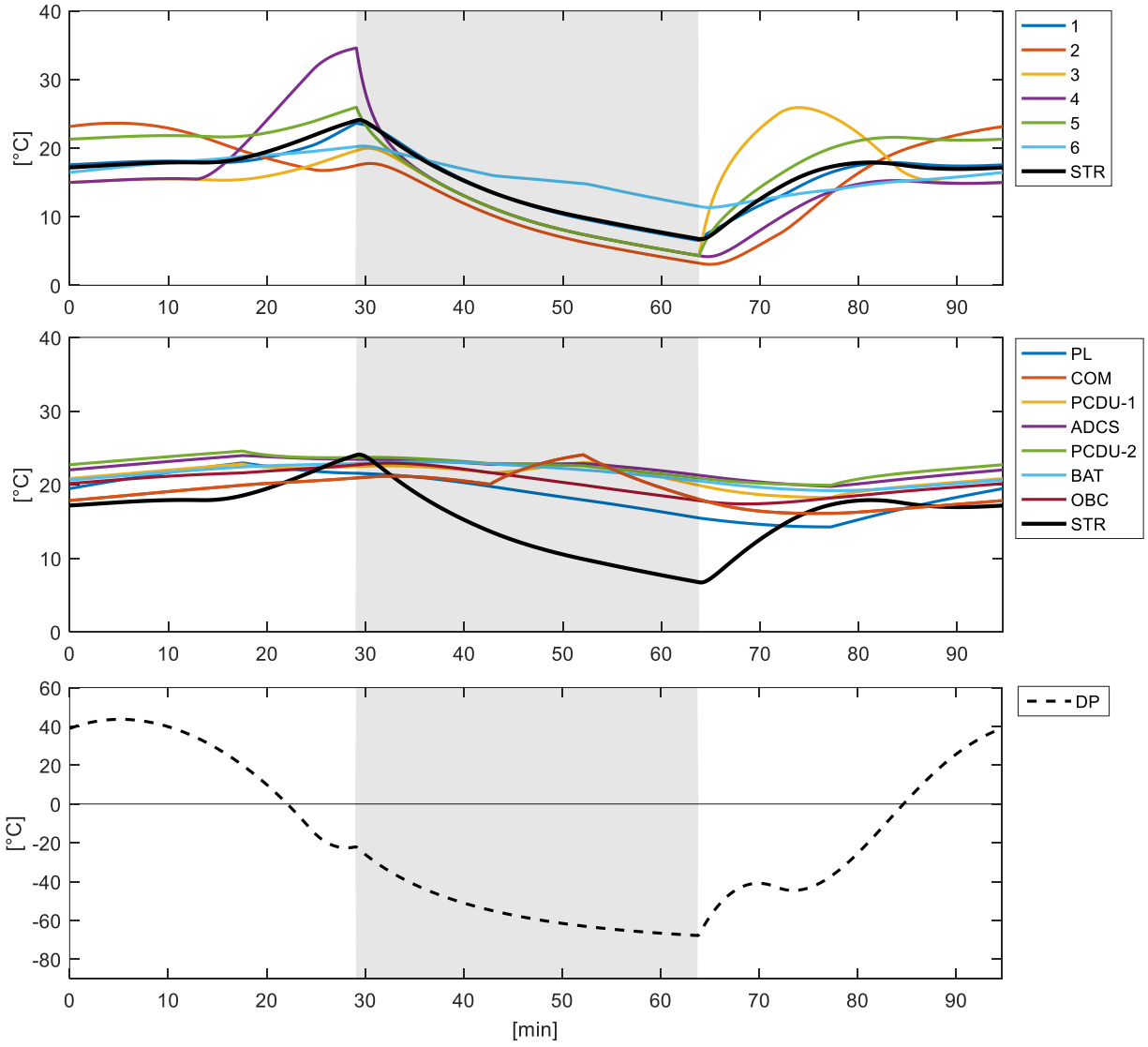


Figure 3.13 - Temperature evolution, high-power case

The trends followed by the temperatures are similar to the low-power case, nevertheless, some noteworthy differences are:

- Higher average and peak temperatures, due to the highly absorptive coating of the base panels of the high-power case. The most impacted components are the faces 3 and 4 during pole overflights when the face sees the full solar flux.
- The presence of the deployable panels which present great temperature fluctuations and reach extreme temperatures, from -68°C to 43°C. It is due to their large two-sided panels which have low thermal inertia. Indeed, the deployable panels absorb a relatively considerable amount of heat near subsolar point, they emit twice as much as other panels since their backsides are in contact

to the space environment, and their thermal inertia is too low to act as a low-pass filter. Yet, we must keep in mind that this analysis considers the panels as having no conductive coupling with the main structure.

- The plateau at subsolar position is wider. It is due to the deployable panels that partially block the other faces from the solar flux.

3.5.3 Temperature Requirements

In this section, the temperature requirements of the components of the satellite are discussed. It represents the whole point of the thermal analysis: whether the subsystems are able to stay within their allowed temperature range, and the methods taken to mitigate the effect in case of need.

Hot and Cold Cases

To compute the extreme temperatures reached by each component of the satellite, space engineers imagine the extreme situations in which the satellite could end up: the hot case and the cold case. The hot case is the case for which all the elements are set to result in the hotter situation possible for the satellite. It involves the maximum solar flux, reached during winter solstice due to the eccentricity of the Earth orbit, the maximum Earth IR and albedo fluxes, dependent on the ground and atmospheric conditions, and coatings at their End-Of-Life (EOL), which implies higher optical properties values for some components. The cold case, on the contrary, involves minimum incoming fluxes and coatings at their Beginning-Of-Life (BOL). The cold case also considers two different cases: the operational and the non-operational cold cases. The operational case refers to the case when the CubeSat is still carrying out its mission and the payload is operating. The non-operational case refers to the coldest survival situation, in our case, we consider that the satellite is forced to remain in IDLE mode for several hours. For example, it may be due to an OBC bug that takes hours to be fixed from Earth.

Table 9 lists the different features of the cold and hot cases. The operating mode differentiates the non-operational cold case (IDLE) from the operational cold case (Normal).

	Cold case		**Hot case**
Solar flux	1322 [W/m²]		1414 [W/m²]
Albedo flux	0.23		0.32
Earth IR	218 [W/m²]		260 [W/m²]
β drift	+4°		-4°
Operating mode	Non-operational (IDLE)	Operational (Normal)	Operational (Normal)
State of life	BOL		EOL

Table 9 - Hot and cold cases features

The numeric values come from [4] which also specifies that the albedo and the Earth IR fluxes are correlated and have a combined minimum and maximum which also depends on the β angle of the orbit. The values given for Earth IR correspond to the flux measured at the top of the atmosphere, 30km above ground. The β drift results of the approximation of constant β for SSOs while in reality, the β angle drifts

between +4° and -4° throughout the orbit due to the tilt of Earth [92]. A larger β is a β closer to 360° (or 0°) which means a longer eclipse so colder temperatures, and inversely.

Temperature Requirements: Low-Power Case

The purpose of this analysis is to ensure that the different components remain within their recommended temperature range. The thermal requirements have been established in Table 1, they are compared to the simulated extreme temperatures reached during hot and cold cases. In the case of an EO CubeSat, the payload is a camera which has a typical operating range of +10°C to +30°C, its survival range is quite wider, from -20°C to +50°C [63] [64]. The operating temperature range is recommended for the quality of the images. Indeed, on the one hand, the noise affecting the images, called dark current, rises exponentially with the temperature. On the other hand, low temperatures affect the performance of the rear screens of the camera which can exhibit color shifts, loss in clarity, flickering or blackouts.

Figure 3.14 shows the simulated temperature ranges reached by each component for the hot case (in red), the non-operational cold case (in blue) and the operational cold case (in green). These temperatures are compared with the allowed temperature ranges in grey. There is an extension of the grey bar for the batteries and the payload, it includes: the discharging range for the batteries (wider than the charging one) and the survival range for the payload. These extensions of the allowed temperature ranges apply for the non-operational cold case during which the batteries are not charging, and the payload is not operating.

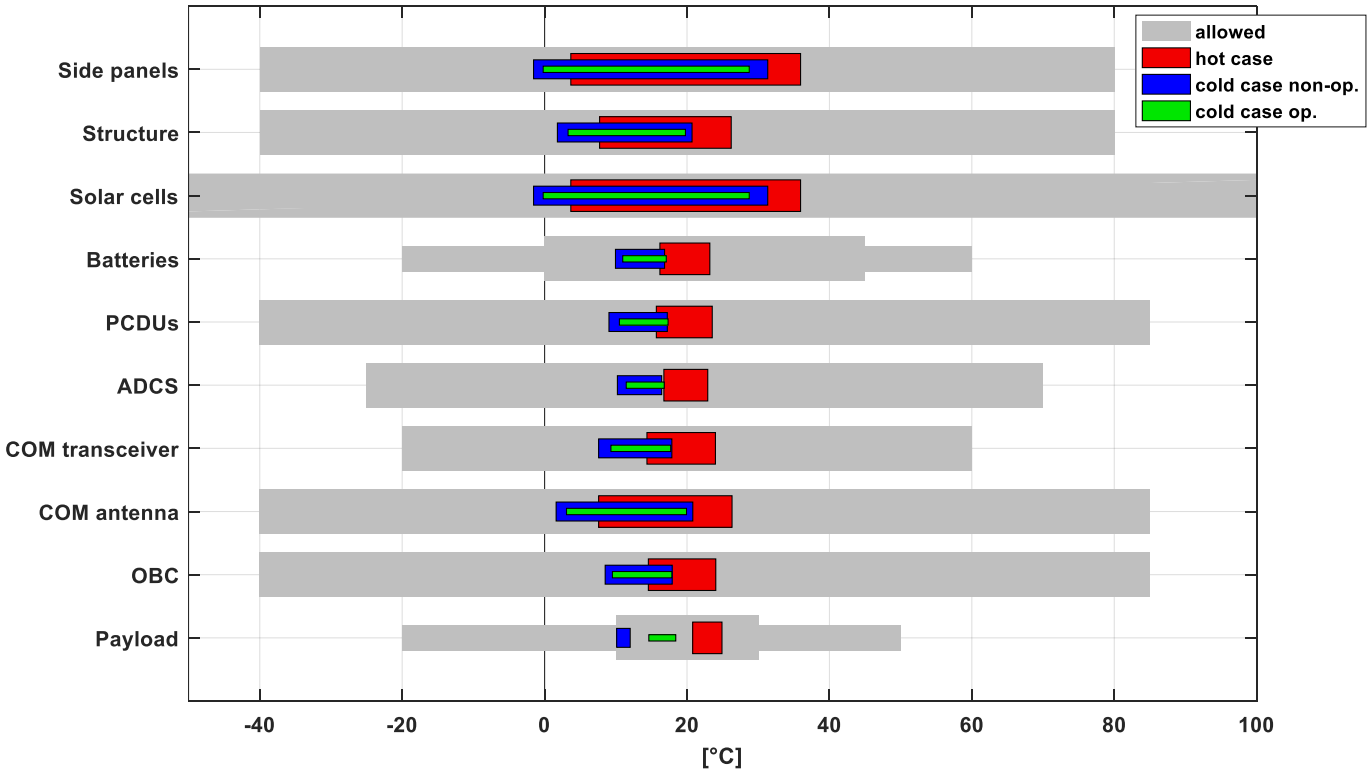


Figure 3.14 - Temperature range compared to requirements, low-power case

First of all, the simulations conclude to the satisfaction of the thermal requirements for each component in any situation for the low-power EO mission type. The thermal analysis is then completed.

Secondly, some more specific observations can be made:

- The payload, being isolated to the maximum, shows a narrower temperature range, which is good for the image quality of the camera.
- The temperature ranges for the different cases are rather close. For the operational cold and hot case, a small shift is to be expected since the incoming fluxes are relatively close. However, for the non-operational cold case, one could think that the temperatures should significantly decrease due to the lower internal dissipations. Yet, it is not the case because the incoming fluxes are still the same as the operational cold case. Indeed, the part of the solar flux that was turned into electricity (and then dissipated) is now directly turned into heat. This extra heat impacts the faces while the internal dissipation impacts the internal components: it explains why, compared to the operational cold case, the non-operational case shows a wider range for the side panels and the solar cells and a colder range for the internal components.
- The allowed range for the side panels is set by default as the same as the structure. It could be wider since there are less structural constraints.

Low-Power Case: Individual Temperatures

The two most sensitive components of the satellite are the payload and the batteries. Their temperature evolution throughout the orbit for the different cases is presented in Figure 3.15. They both show a constant behavior through the cycle. It theoretically ensures their temperatures to be in the recommended range at any time. For reminders, the payload is not operating during the non-operational cold case, therefore, a temperature of 10°C is inside its allowable temperature range.

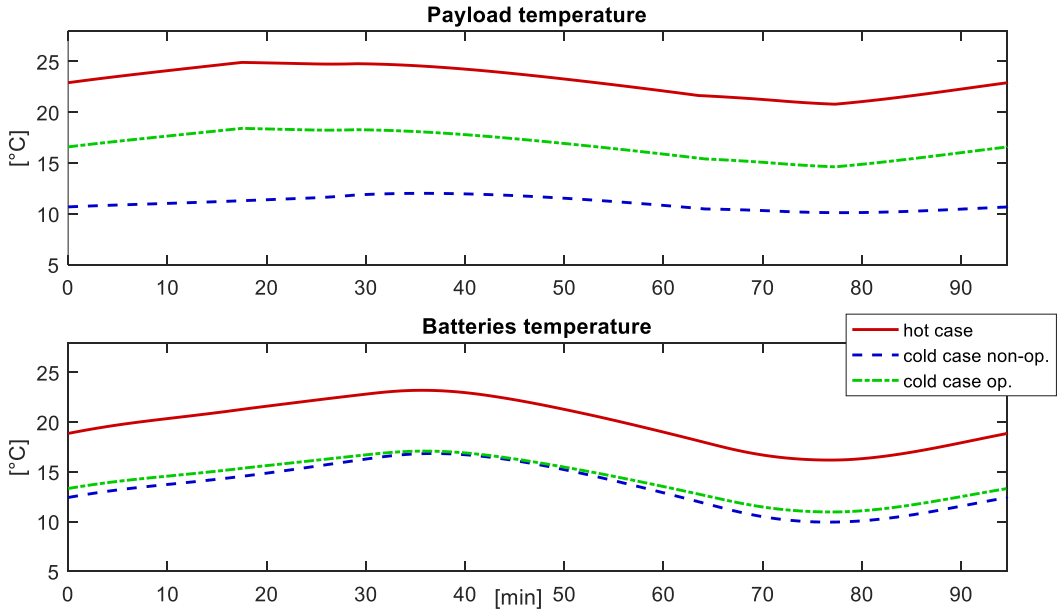


Figure 3.15 - Payload and batteries temperatures

While the operation mode during the cold case does not really affect the batteries, it is not the same for the payload that displays a lower temperature for the non-operational case. It is explained by the fact that the payload is strongly isolated from the rest: the external heat has difficulty to reach it and if it does not receive heat from its own dissipation, its overall temperature will decrease. It also explains why its temperature is almost constant in that case. The operational hot and cold case affect them in the same way: a simple shift of a few degrees.

Temperature Requirements: High-Power Case

Figure 3.16 gathers the required and simulated temperature for all components for the high-power case.

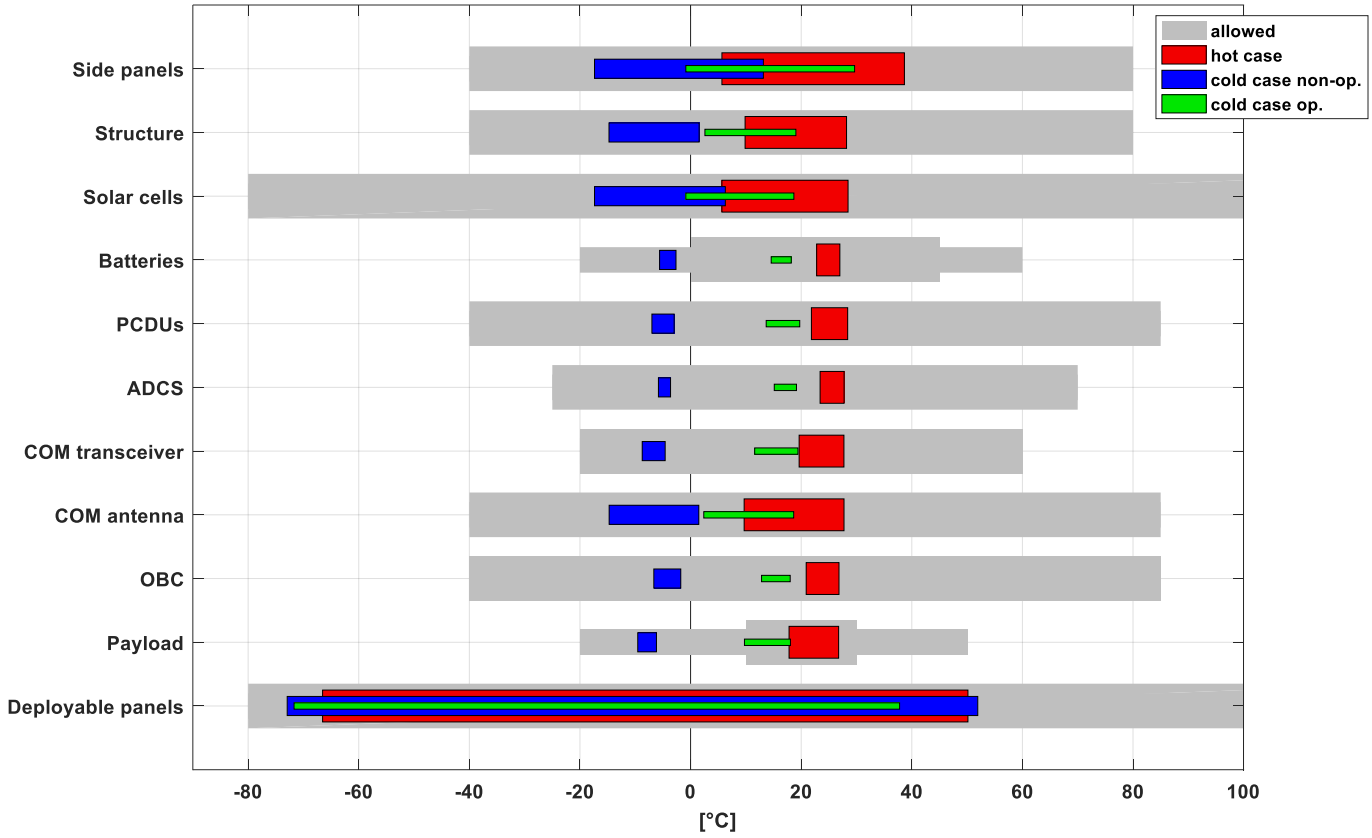


Figure 3.16 - Temperature ranges compared to requirements, high-power case

The temperature ranges for the high-power case is interesting due to its differences with the low-power case and the presence of deployable panels for which some comments are to be made:

- As already observed in Figure 3.16, the deployable panels experience extremes temperatures. Their temperature range does not reach the limits but approaches the lower one.
- The allowed temperature range corresponds to the one of the solar panels. It does not consider the thermal requirement of the structural link with the main bus which should be tested under harsh conditions.
- If judged necessary, a solution to remediate to this wide range is the addition of thermal straps to enhance the thermal conduction between the deployable and the side panels. The temperature would be smoothed as the temperature range of the main bus is narrower.
- However, two points are to be taken into account: first, the lower bound temperature is not physically fixed and varies a lot with the manufacturer (see section 2.1.2), second, this analysis considers that the deployable panels are conductively uncoupled with the main bus.
- One can observe that higher temperatures are reached during the non-operational cold case than during the hot case. It is perfectly understandable with the consideration made earlier: for a non-operational case, instead of being turned into electricity and further dissipated, the energy is directly turned into heat on the panels themselves. Therefore, the amount of heat dissipated on the panels is greater and exceeds the incoming fluxes differences between hot and cold cases.

The last point explains the fact that in this case, inversely from the low-power case, the non-operational cold case is in fact significantly colder than the other cases. Indeed, in the low-power case, there is one thermal system, the main bus, and the energy is constant for both non-operational and operational cases. For the high-power case, there are two thermal systems, the main bus and the deployable panels. They are not directly thermally coupled but exchange electricity which carries potential heat. Therefore, in the operational case, the energy of the electricity is dissipated in the main bus, while, in the non-operational case, it is dissipated in the deployable panels system.

Finally, the payload reaches its lower limit during the operational cold case. Knowing that this analysis is simplified and that the real temperatures are likely to slightly differ, one may want to ensure that this temperature limit is not crossed. It can be done by the implementation of electrical heaters, active TCS means regulated by a thermostat and preventing the payload from reaching too low temperatures. This solution has already been suggested in section 1.6.

High-Power Case: Active TCS Implementation

The latter point concluded in a possible active TCS addition by implementing electrical heaters located at the payload. We propose to implement heaters coupled to a thermostat. The thermostat has for directives to activate the heaters when the payload temperature is too low and to prevent it from going under a critical temperature. In Figure 3.17, the payload and the batteries temperatures are plotted in the case of operational cold case, the critical temperature is set at 12.5°C and the temperatures with the action of the heaters are plotted in solid lines while the temperatures with no heaters are plotted in dashed lines for reference. The power required by the heaters to meet the thermostat's thermal directives is indicated in yellow.

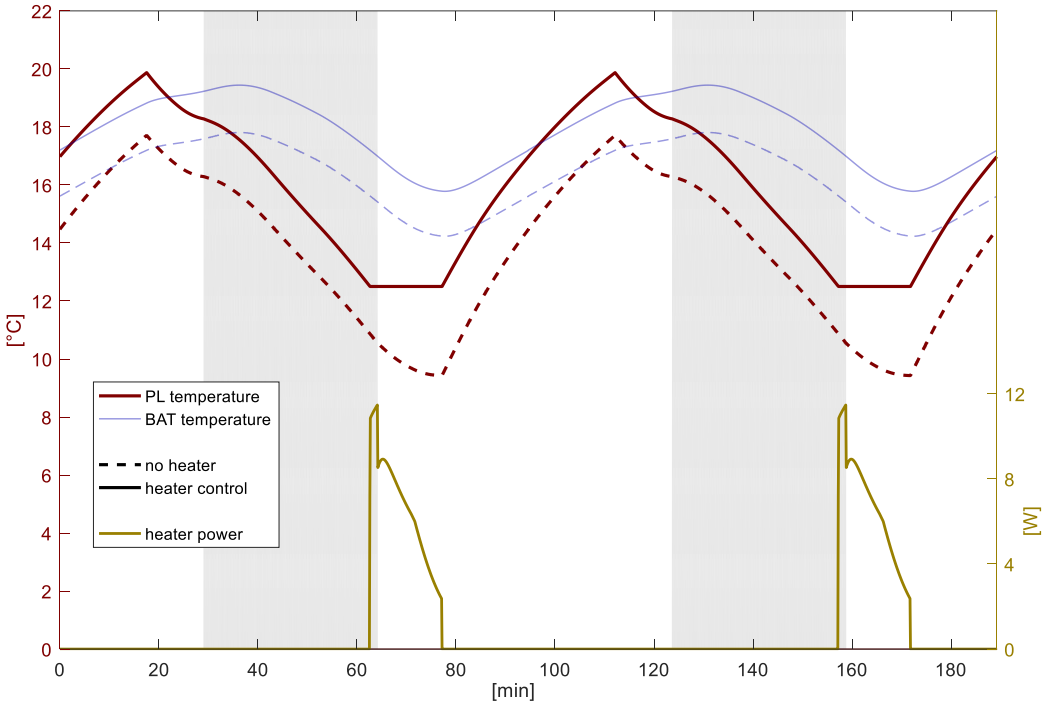


Figure 3.17 - Electrical heaters impact on temperature and power consumption

As seen in Figure 3.17, the implementation of heaters is successful and allows to comply with the new thermal requirements not to exceed the critical temperature imposed by the thermostat. It is logically accompanied by an increase in the mean temperature of the payload. The batteries temperature is plotted in the same figure for two reasons. First, the batteries are also a highly sensitive component. Second, the payload being only connected to the external assembly (structure and faces), the batteries are representative of the other subsystems. It is concluded that the heaters also have a benefic effect on the other subsystems as they increase the mean temperature during cold cases. The temperature increase is slight and happens during a cold case, there is thus no impacts on maximum allowed temperatures.

For the mentioned case, the implementation of heaters requires a maximum of 12W and a total of 1.6Wh per orbit (or an average of 1W). This power is deliverable by the system due to the extra production mentioned in section 3.5.1, updating the produced to consumed power ratio to 16.6/14.7 W. It mostly happens during the non-production period (see Figure 3.10) resulting in a 1.4Wh requirement from the batteries. It reduces its DoD to 12.5%, which is totally acceptable. This updated situation is illustrated in Figure 3.18.

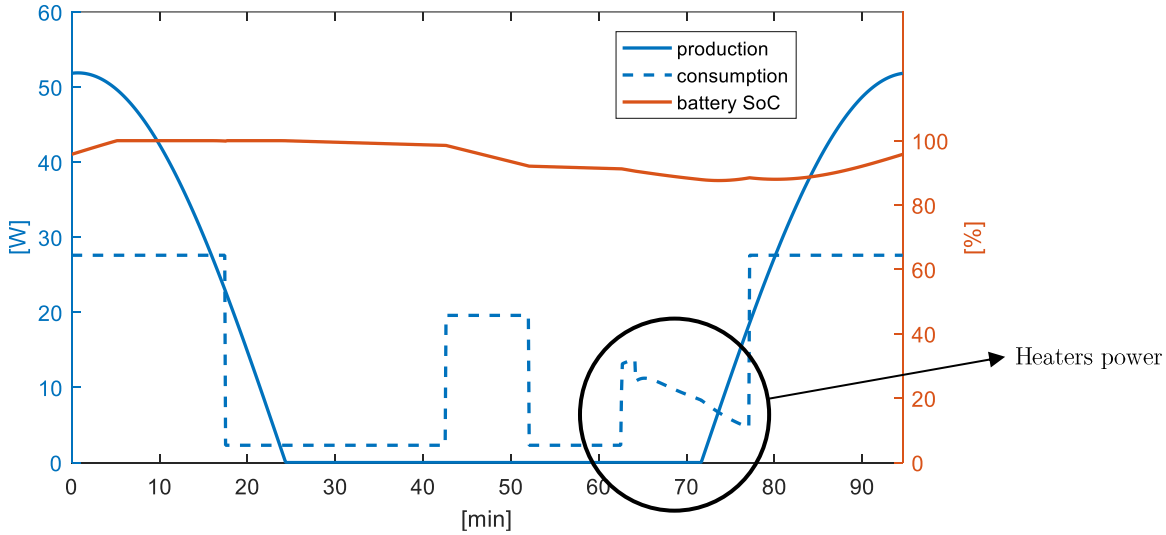


Figure 3.18 - Updated electric balance in case of heaters implementation (high-power case)

One may want to keep a better produced to consumed power ratio for safety reasons. In that case, the implementation of solar panels on the velocity face would remediate to that matter. The specific location is set as it brings solar power when the heaters need to be activated, thereby preserving the batteries.

This analysis is very theoretical and aims to provide an application of an active TCS and to be visually intuitive. In a more realistic way, the thermostat would have different directives that lead to a smoother thermal control, e.g. already powering the heaters before the critical temperature is reached. This method allows limiting the installed power of the heaters for similar results, which is a better optimization for CubeSats. This consideration is shown in Appendix D for simplistic dissipation windows from the heaters, it presents an installed power divided by 4 for similar results.

3.5.4 Heat Flows Analysis

The heat flows analysis will focus on the COM subsystem as it brings out a noteworthy thermal situation. During the eclipse, the satellite is in IDLE mode and the COM subsystem, being close to the external faces, is the first to cool down. When the communication mode is switched on, it receives a large amount of power from the batteries and most of it is dissipated as heat. The heat starts to heat the subsystem and must be evacuated. Even though the thermal links with its direct surroundings are limited, a thermal strap connects it to the anti-pitch face. This face is a highly emissive surface and can be used as a radiator. But what part of the heat does this radiator help evacuate?

To answer this question, let us have a look at the temperatures of the components at a given point in time. To be representative of the thermal situation described above, let us take a snapshot of the thermal situation at the 51^{st} minute of the orbit for the high-power mission case. This corresponds to the near end of the communication mode. It is done in Figure 3.19. The drawing is related to the design of the satellite (Figure 3.1) with the internal components (7 blocks) inside a black box (the structure) over which are located the 6 faces (grey plates). For 2D drawing purpose, the face 3 and 4 (velocity and anti-velocity) are placed slantwise. The temperature of each component is displayed. It can be seen that the COM subsystem is the hottest component and that the faces are the coldest, especially the zenith face which is oriented towards the deep space.

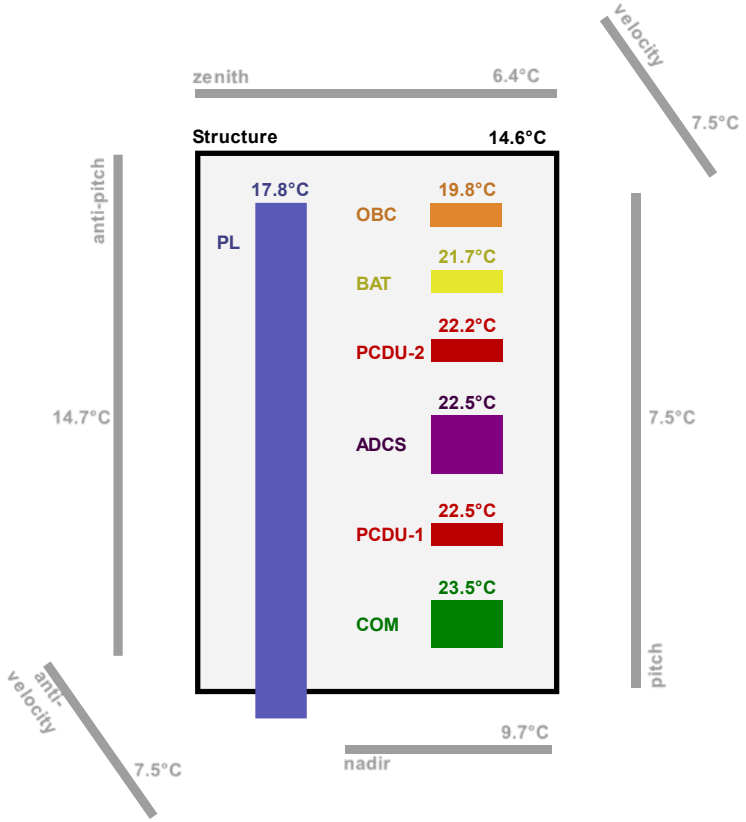


Figure 3.19 - Thermal situation at near end of communication mode (high-power case)

From that base, let us connect the components together and show the heat flows that take place inside the satellite. A map gathering them has been drawn in Figure 3.20. The heat flow between two components is the power they exchange in the form of heat. They are composed of the heat received by external radiation (yellow arrows), i.e. the incoming heat fluxes, the heat emitted by external radiation (blue arrows), the conducted heat (red arrows) which can be leaving or entering the components, and the power

dissipation (dashed green arrows) which is the electrical power dissipated in the components. Be aware that the global energy balance is time-dependent, and the sum of the leaving and entering heat flows is not equal to zero as the balance equation shows,

$$C\frac{\mathrm{d}T}{\mathrm{d}t} = Q_{in} - Q_{out} + Q_{int}$$

The difference between the leaving and the entering heat power is called the stored heat power, this power is related to the temperature variation of the component through its thermal capacity. A positive stored power means that the temperature of the component is increasing, a negative value means a decreasing temperature. The stored heat power of each component is displayed in black in Figure 3.20.

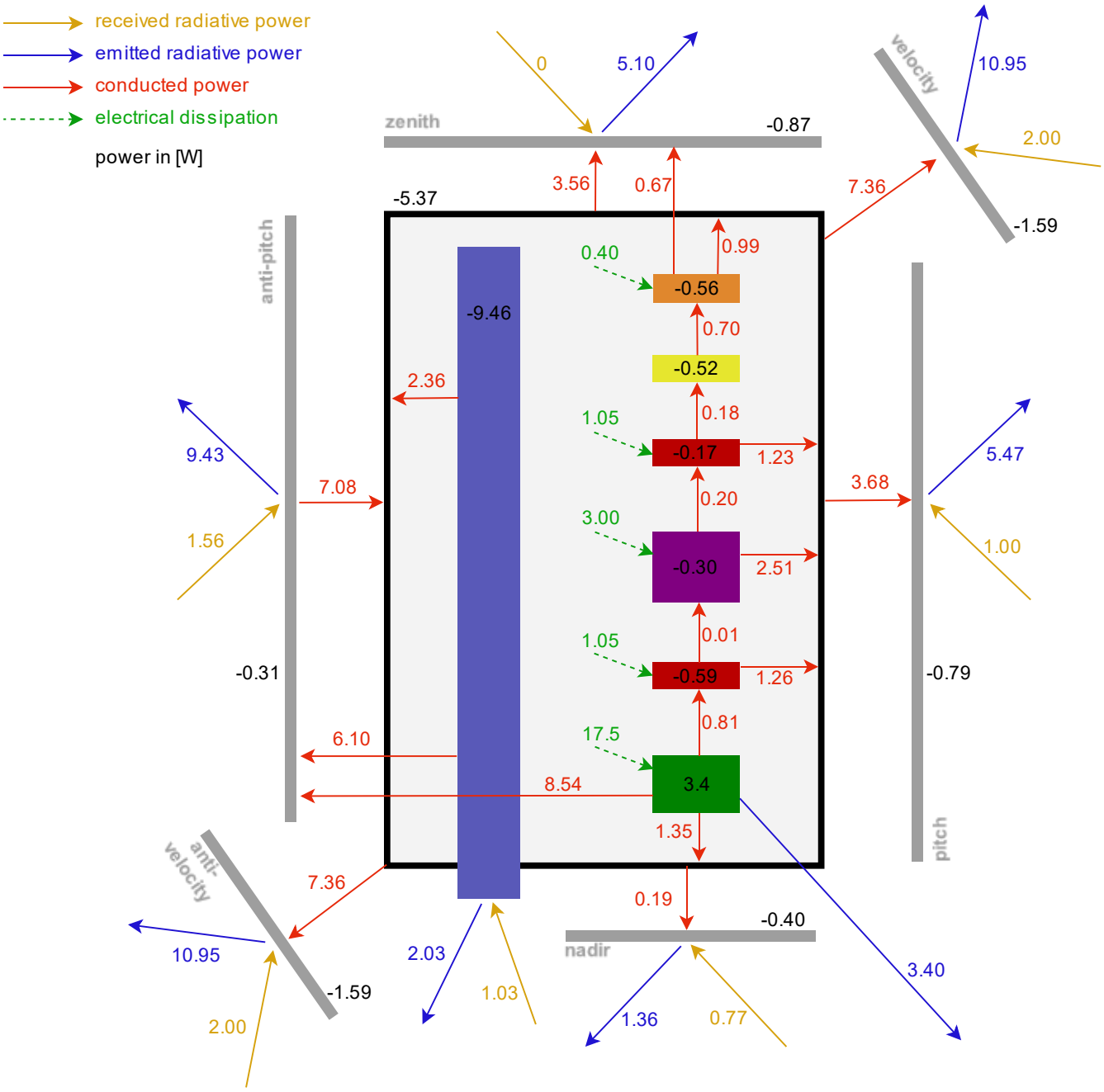


Figure 3.20 - Heat flow map at near end of communication mode (high-power case)

The stored heat power shows that all the components are getting colder except the COM subsystem. Its value also indicates the rate at which the temperature is varying. This consideration highlights the importance of the thermal inertia of the component in its temperature variation. Indeed, a component will heat twice as fast as another component showing the same stored power but having a thermal capacity twice as large. As an example, the stored power of the COM subsystem and the payload throughout the orbit along with their temperature is plotted in Figure 3.21 for the high-power case.

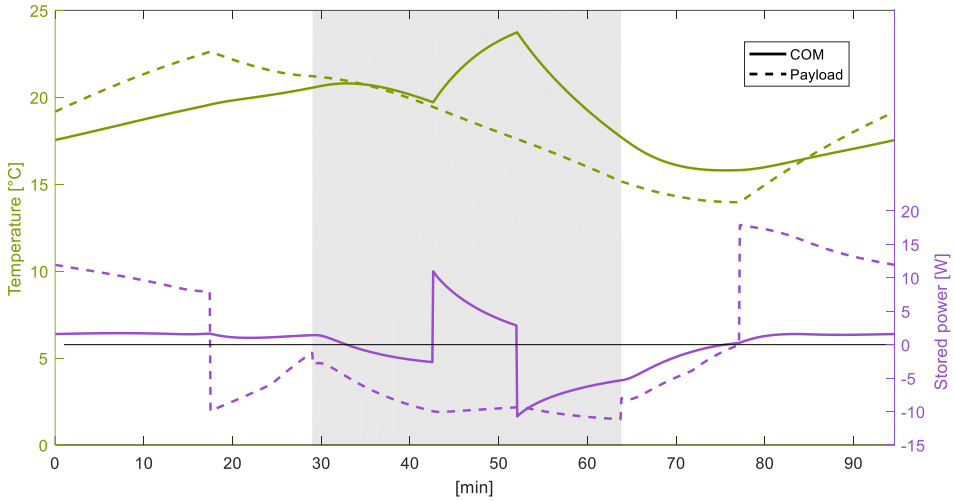


Figure 3.21 – Relationship between stored power and temperature for the COM subsystem and payload (high-power case)

From the map (Figure 3.20), it can be seen that the internal heat flows are small compared to the flows involving the external assembly (structure and faces). This is logic as the temperatures of the internal components are close to each other while the external assembly is colder during this eclipse time.

This map corresponds to one given time of the communication mode. Figure 3.21 shows the general behavior of the COM subsystem as a function of the time. During the preceding IDLE mode, the stored power is negative, and the COM subsystem temperature is decreasing. When the communication mode is switched on, the arriving power grows instantly but the subsystem is still cold. It results in a boost of stored power accompanied by a high temperature increase rate. As the communication mode goes on, the COM subsystem temperature rises, and the conductive links transfer more heat. This implies a decrease in its stored heat and thus a deceleration in the temperature increase rate. When the communication mode comes to an end, the COM subsystem sees its stored heat drastically drop along with its temperature.

Figure 3.22 stacks all the paths taken to discharge the heat of the COM subsystem during the communication mode: conducted to the PCDU (blue), the structure (red) and to the radiator (yellow), stored (green) and RF emitted (grey). The 17.5W of electrical power (see Figure 3.20 or Table 2) are distributed between those 5 paths. The first three are conductive heat transfers. The last is the useful part of the COM subsystem power consumption which is the RF radiations. The remaining power that cannot be evacuated is kept by the COM subsystem as stored heat power. In the beginning, the PCDU is still hotter and transfers heat to the COM subsystem, hence the negative value for the first minutes. As time goes, the conductive ways increase in efficiency and the stored power decreases. The graph also highlights that a considerable part of the heat going to the radiator goes back to the structure afterward. This fact can also be seen in the heat flow map (Figure 3.20). It leads us to the questioning: how is this heat finally radiated away from the spacecraft?

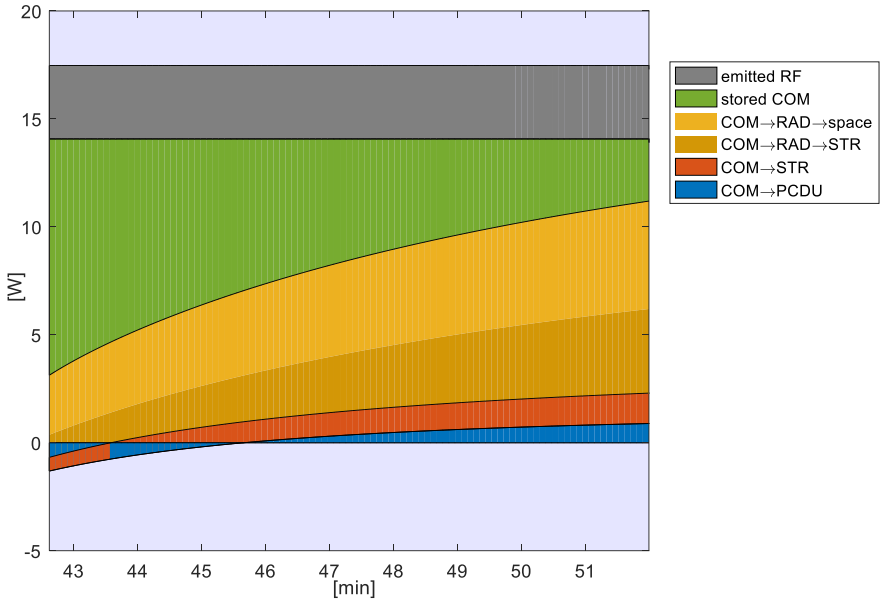


Figure 3.23 - COM heat discharge paths

In that concern, Figure 3.23 proposes to track the heat dissipated by the COM subsystem, i.e. 17.5 W, and to see which path is taken until it is radiated away by the external surfaces or stored. It is presented in the form of a Sankey diagram and takes place at the same given time of Figure 3.19 and Figure 3.20, i.e. 51st minute. Putting aside the power emitted in radio waves, the figure illustrates that only one-third of the heat is evacuated thanks to the radiator while more is sent out via the other faces through the structure.

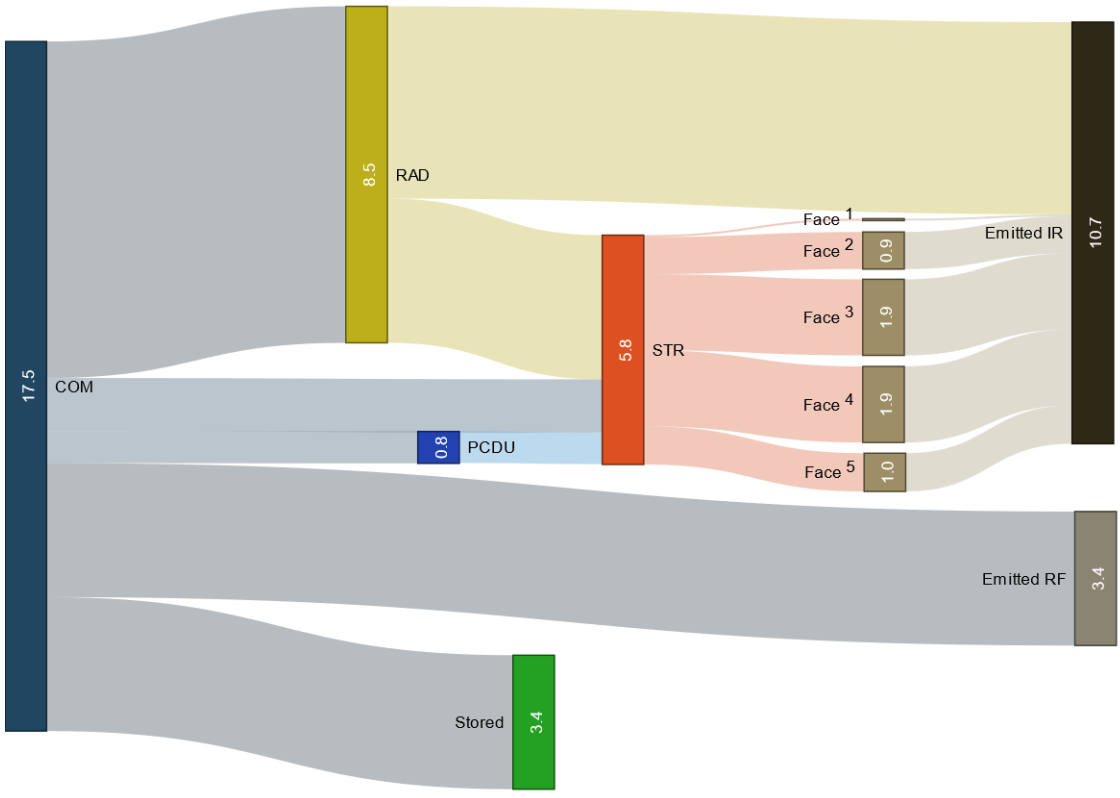


Figure 3.22 - Evacuation of the internal power of the COM during communication mode

This result questions the utility of placing the thermal strap between the COM subsystem and the radiator and not between the COM subsystem and the structure. Indeed, by running the simulation in that latter case, the results are similar with an even slightly better performance, the graphs are presented in Appendix E. However, this last result must be put into perspective because the faces, other than the radiator, are also significantly emissive (0.54 for the base panels against 0.81 for the radiator).

In this case of high-power mission, the power that the payload must evacuate when it is active is similar. However, it is of lesser impact because the payload has a larger thermal capacity that implies lower temperature changes with the same dissipation power. Moreover, the payload is more isolated from the structure and it is connected to the radiator via a twice as big thermal strap. This link to the radiator makes the heat evacuation sufficient.

The study of the COM subsystem case in this section has given a concrete example of the difficulty that can be encountered for evacuating heat outside of satellites.

3.6 Nodal Model Discussion

In this section, we look back over the results and we discuss the accuracy of the model.

Nodal Network Size

The nodal network primary parameter is by definition the number of nodes. We wish to examine the effect of reducing the number of nodes of our system. 14 nodes were considered is this chapter, let us simulate the model for:

- 9 nodes: 6 for the faces, 1 for the structure (str), 1 for the payload (PL) and 1 for the rest of the internal components (intern.).
- 3 nodes: 1 for the external assembly (str + faces), 1 for the payload (PL) and 1 for the rest of the internal components (intern.).
- 2 nodes: 1 for the external assembly (str + faces) and 1 for the internal components (intern. + PL).
- 1 node: the entire spacecraft.

The temperatures of the nodes for each case are plotted on Figure 3.24. Each case is compared with the base case of 14 nodes (light curves in the background).

One thermal node is defined as an isothermal subsystem characterized by a thermal capacity and thermal links relating it to the other nodes. Reducing the number of nodes of the system usually means to merge some nodes together. For example, in the 2 nodes system, the structure and the 6 faces are merged together into the first node, and the internal components are merged together into the second node. Merging 2 nodes together means to sum their thermal capacity and to consider the thermal link between them as perfect, i.e. infinite thermal conductance, making the new node isothermal and having a larger thermal inertia. By reducing the number of nodes, the average thermal inertia is increased and, thereby, the temperature of the nodes is damped and fluctuates less.

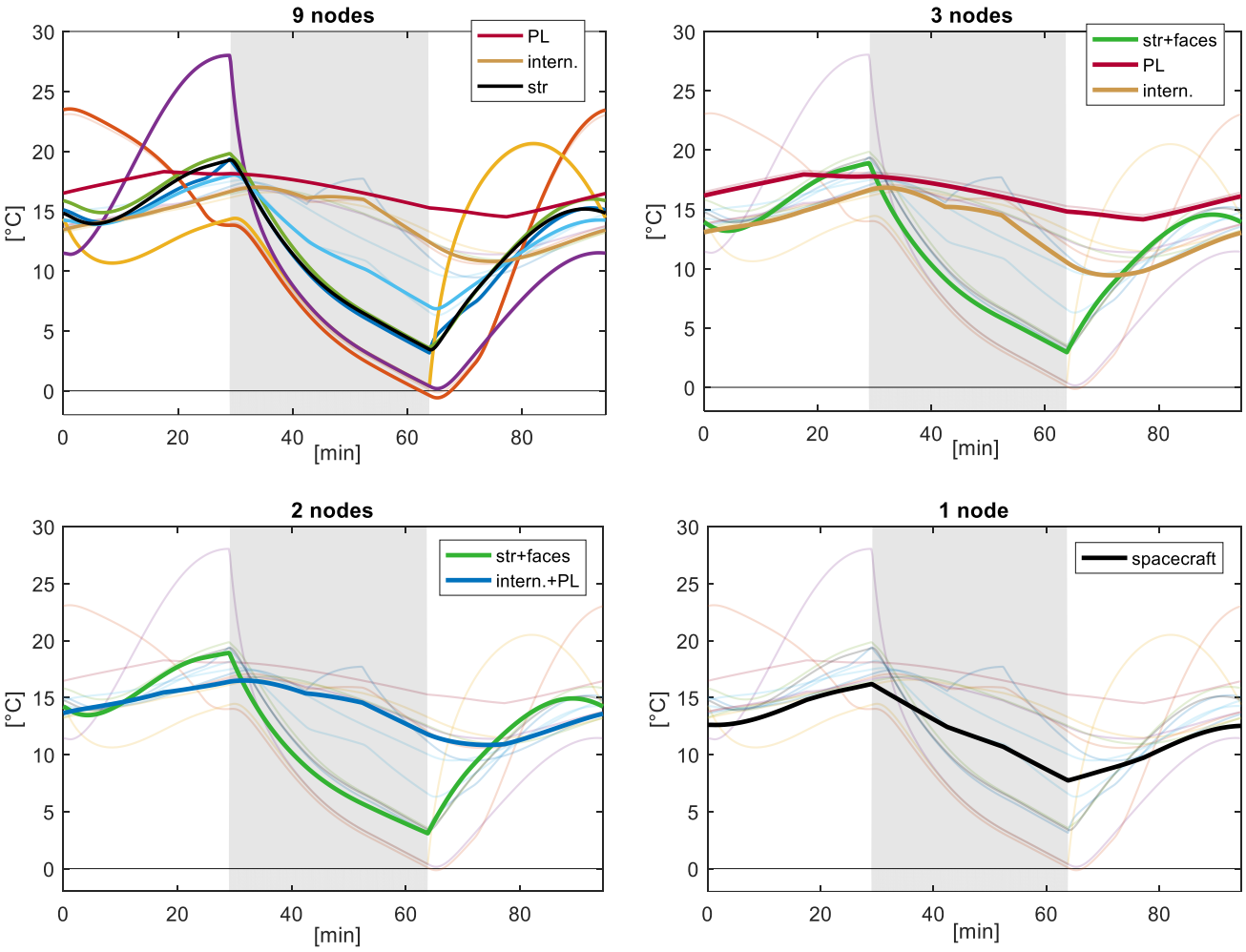


Figure 3.24 - Nodal network size comparison

The temperature fluctuation of the one-node system is not quite representative of the temperature fluctuation of each component. However, it is representative of the damped trend followed by the satellite. This consideration was highlighted in chapter 1 when the mass of the one-node model had to be chosen.

It can be seen that considering all the internal components (except the payload and the structure) as one thermal node as it is done in the 3-nodes case, gives a good approximation of their individual temperatures. The overall temperature is slightly colder due to fact that internal dissipations are directly conducted away. Another point is that the temperature increase of the COM subsystem is less marked. It makes us conclude that if the COM subsystem were made of several nodes instead of one, the increase of temperature would be greater. Indeed, the power is not equally dissipated inside, and some subcomponents will warm up more than others.

This reasoning applies to the whole system. A more refined nodal network would bring a wider range of temperatures. This fact can also be clearly seen between the case of one node for each face, and one node for the entire external assembly.

Structure Node Accuracy

Taking the point of view of this latter concern, it seems legitime to wonder if the consideration of only one node for the structure is accurate enough. Figure 3.25 shows the temperature gradient between the faces for 3 orbits for the low-power case. The temperature gradient is presented as vertical lines corresponding to the range of temperatures between the minimum and the maximum calculated for the 6 faces.

This figure indicates a constant temperature gradient between the panels for a maximum of 15°C. While the structure is considered isothermal, it is also well thermally coupled to each face. These two facts are hardly compatible. It can be concluded that the structure is not isothermal and is affected by the temperature gradient of the faces. Nevertheless, the maximum temperature gradient is not excessive and the thermal conductivity of the structure being high, it is an acceptable assumption. In addition, this assumption allows us to be more general in the analysis and less dependent on the exact configuration of the CubeSat.

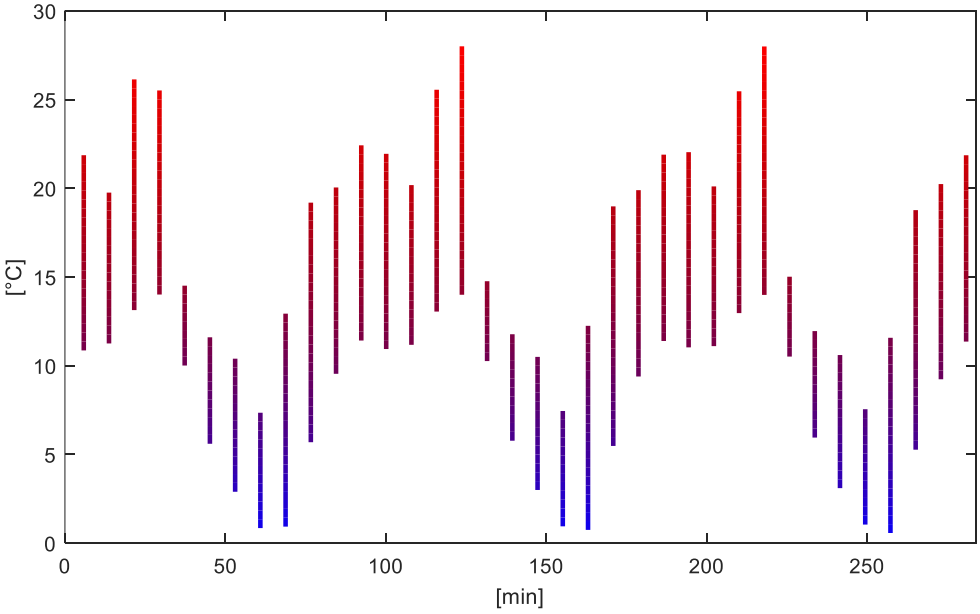


Figure 3.25 - Temperature gradient between faces (low-power case)

This section had for purpose to discuss the limitations of our model. In conclusion, this model of a few-nodes system has limitations, but is accurate enough with regard to the objectives of generality and simplicity established for this study case in the introduction of the chapter.

3.7 Conclusion

This chapter has provided a study case which brought out the thermal behavior of a CubeSat and its components. The studied CubeSat mission is the current most frequent mission, the Earth observation, and follows a common Sun-synchronous orbit.

Two different variants of this mission were presented and detailed: the low and high-power cases. The first one consists of a basic EO mission requiring low-power consumption, the second one, a high-resolution EO mission requiring high-power consumption. They were respectively designed as body-mounted and crossed-mounted satellites, the latter including deployable panels. These two configurations are typical among CubeSats, but also very dissimilar, hence the interest of studying both cases.

The thermal analysis has been conducted by dividing the whole CubeSat into 14 thermal nodes: 6 for the faces, 1 for the structure, 1 for the payload and 6 for the other internal components. The 14 nodes have been put under different external environmental conditions, referred to as cold and hot cases, to determine the extreme temperatures that they may experience during realistic situations. The main outcome of this analysis is the establishment of the temperature range of each component in comparison with their thermal requirement provided by chapter 2. It comes out that all components comply with their requirements for the low-power case. As for the high-power case, the payload reaches its lower-bound limit during the operational cold case. A proposition to remedy the problem was to implement an active thermal control in the form of electrical heaters located at the payload and coupled to a thermostat. The thermostat manages their activation at a critical temperature which includes a safety margin.

Further interpretations of the results, in the form of energetic or heat flows analyses, were also proposed. It allows the reader to grasp different aspects present in the thermal concerns of a CubeSat mission. For example, the potential difficulty to withdraw heat from the spacecraft. This latter aspect was presented through the study of the heat flows balance inside the satellite during the communication mode. It reported a limited aptitude of the radiator to evacuate the heat excess. The concept of stored power was also introduced and visually presented as an indicator of the temperature variation rate.

In addition, the relative importance of radiative and conductive heat transfer was evaluated. This comparative study made strong assumptions that fit the level of precision of the model. It was concluded that internal radiative exchanges can be neglected for such a general analysis.

Finally, the chapter ends by putting into perspective the realized analysis and showing its limitations. The desire to have as guidelines, generality, intuition and understanding, is accompanied by a lack of accuracy. The accuracy can be achieved by performing finite elements analyses; however, such analyses do not meet the previously mentioned aspects.

This chapter completed the introduction of the thermal behavior of a CubeSat by giving to the reader a concrete study case that has hopefully helped him acquire useful knowledge on the topic.

Conclusion

Technical Comment

This thesis was undertaken to provide an introduction to the thermal behavior of a CubeSat, which is the most common type of small satellite. The target reader is not familiar with satellite thermal concerns, it is why a didactic and general approach has been adopted.

The first part simplified the analysis by considering the CubeSat as a single thermal node, an isothermal sphere. It progressively increased in complexity: from a simple sphere seeing only the Sun, to a sphere coated with solar panels and equipped with internal electrical devices, that undergoes a cyclic thermal behavior. This analysis allowed us to cover and discuss numerous parameters that affect the temperature of the sphere. Finally, the sphere was turned into a cube in order to validate the consistency of the analysis for the shape of a CubeSat. This approach made it possible to draw conclusions for any CubeSat instead of a specific mission. We have learned, for example, that whatever the size and the coating of the sphere, it always tends to the same temperature during eclipses, or that, from a thermal point of view, solar panels only impact the distribution of the incoming heat over the orbit, not its total amount.

The second part presented more technical contents. After having been accustomed to the thermal environment of space, this part gave an overview of the satellite itself. The subsystems of a CubeSat were presented from a technical and thermal point of view. It enabled us to establish the thermal requirements of each component as well as the mass and power budget of a typical mission. We have learned, among others, that batteries and payloads were usually the most restrictive components in terms of temperature requirements, or that the communication subsystem requires considerable power, but only for a short time.

The third part merged the two previous parts into a concrete case. This study case had for objective to provide a more detailed thermal analysis. It considered today's most representative CubeSat, an Earth observation 6U CubeSat. This analysis has been simplified to remain consistent with the guidelines of this work. It decomposed the satellite into 14 thermal nodes and used basic programming, i.e. MATLAB, for simulations. This approach was intended to get away from complex software packages that provide more accurate simulations but lack generality and offer no understanding of the interprocess. This study case covered many topics, such as power balance or heat flows analyses, and, in particular, the temperature range of each component. This range, compared to the recommended temperature range, is the main result of any satellite thermal analysis as it constitutes the theoretical approval about its thermal concerns.

Personal Comment

The thesis is a major personal progress as it is the final test in any academic studies. It is why I have been advised to end this dissertation by a personal comment about what I have learned.

When I think of how I usually tackle problems, I realize that I have gained a lot with the approach taken in this work. The approach is general and forced me to extract the big picture of the topic. Making simplifications and focusing on the typical rather than the specific, allows us to be much more

representative and didactic, as well as to better understand. Many are the engineers who are stuck in a specific standpoint. They cannot provide an answer outside of their specific case or need to run simulations for any parameter variation instead of intuitively perceiving their influence. It applies to all areas, scientific or otherwise. Having an overview is a key element for understanding. However, I do not overlook specific analyses which are essential for accuracy in a given case.

The writing of the second chapter invited me to synthesize a lot of information. The web is full of data on CubeSats and it is a challenge to sort only the part that interests us. This part stressed the importance of synthesizing but also the heaviness of the documentation task in order to provide a representative and coherent content.

More technically, this thesis made me take a deep interest in the field of space and led me to learn a lot about CubeSats and satellites in general.

Overall, this experience has been a real benefit for me.

Appendix

A. Albedo Flux Empirical Formula

The albedo flux is still equal to,

$$G_a = a\, F_a\, E_s$$

With E_s the solar constant, a the albedo factor and F_a the view factor of the albedo flux.

F_a is composed of two terms. The first, F_E, accounts the distance from the surface of the Earth and the satellite's face attitude. The second considers the satellite's position, it will be maximal at subsolar point. To compute those terms, the formulas chosen come from [100] and [4] , this approach comes from [101].

$$F_E = r^{2.1}\, \left(\sin\left(\frac{\rho}{2}\right)\right)^e$$

$$e = 160.31r^6 + 723.36r^5 + 1380r^4 + 1394.6r^3 + 780.65r^2 + 226.81r + 21.232$$

With $r = \frac{R_e}{R_e+h}$ and ρ the angle between the normal of the surface element and the local zenith (=180° for a face pointing Earth).

$$F_a = F_E\, (\cos(0.9\,\theta))^{1.5}\, F_{ecl}$$

With θ the orbital position, F_{ecl} is a Boolean term representing the eclipse time (0 for eclipse time and 1 for daytime).

This represents one empirical formula for the albedo flux, there are many others that gives approximatively the same results.

B. Validation of the Internal Dissipation Approximation

Validation of the approximation of the effect of internal dissipation on temperature,

$$\Delta\bar{T} \cong \frac{Q_{int}}{4\,\bar{T}^3\,\sigma\,\epsilon\,A_{out}}$$

Approximation presented in section 1.6.

The validation consists to simulate the increase in mean temperature of the satellite presented in the case study (high-power case, chapter 3) as a function of the internal dissipations (considered constant throughout the orbit).

The averaged emissivity of the CubeSat is 0.57 (from Table 5) and its external area is 0.22 m^2 (6U CubeSat).

Figure 0.1 plots the simulated mean temperature increases of the CubeSat as a function of the internal dissipated power (assumed from the payload) in solid red line, and compares it with the approximated value given just above in dashed black line.

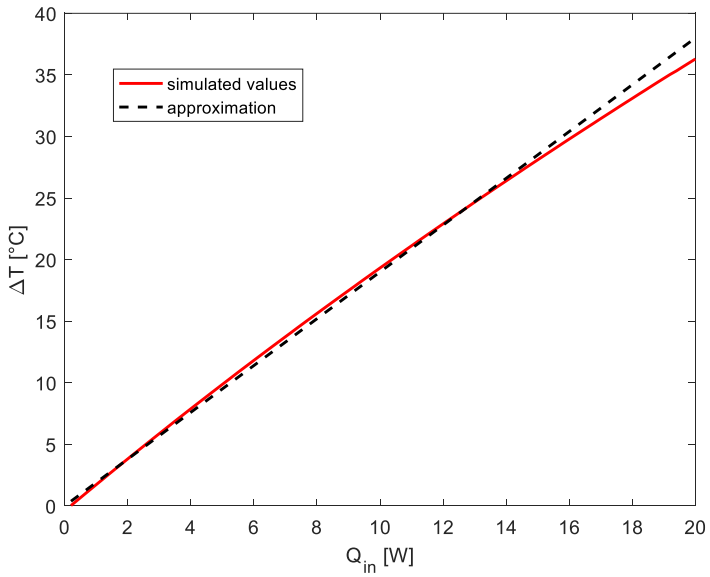


Figure 0.1 - Mean temperature increase in function of the internal dissipation

C. Complementary Graphs on the Fluxes and Temperature of a Cube

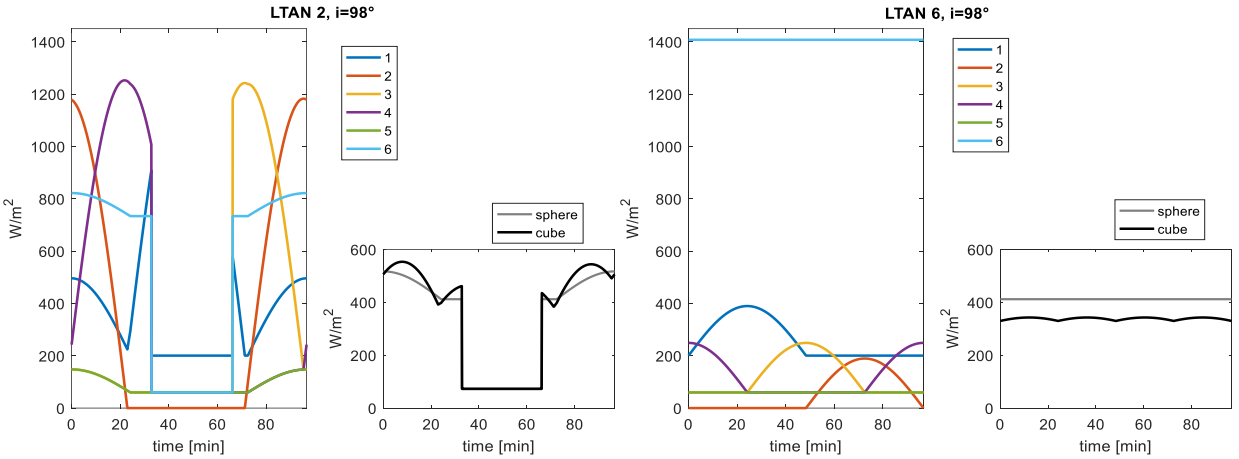


Figure 0.3 - Incoming flux on the faces of a cube, for different LTANs

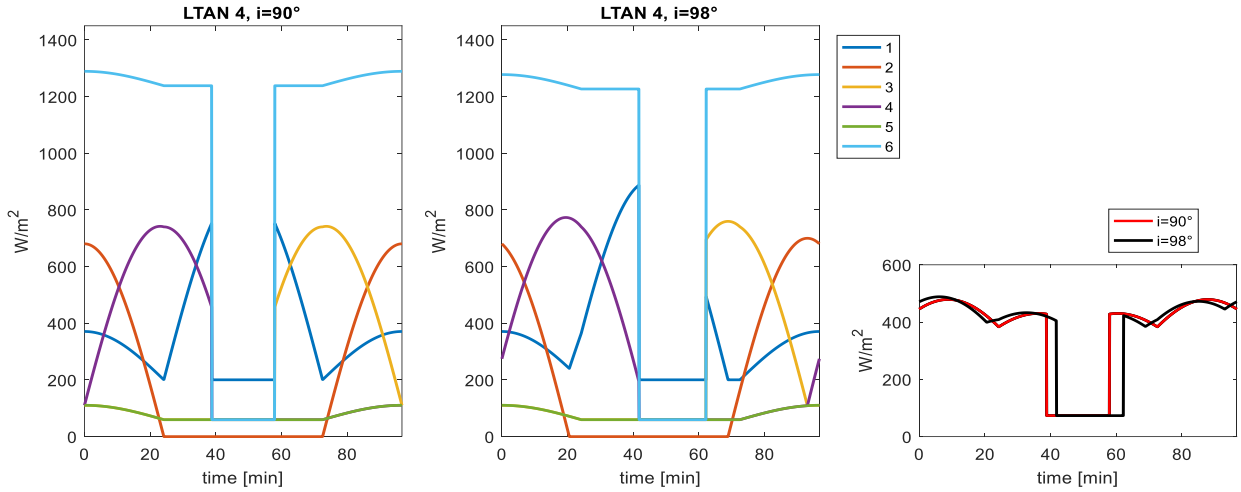


Figure 0.2 - Incoming heat flux on the face of a cube, influence of the inclination

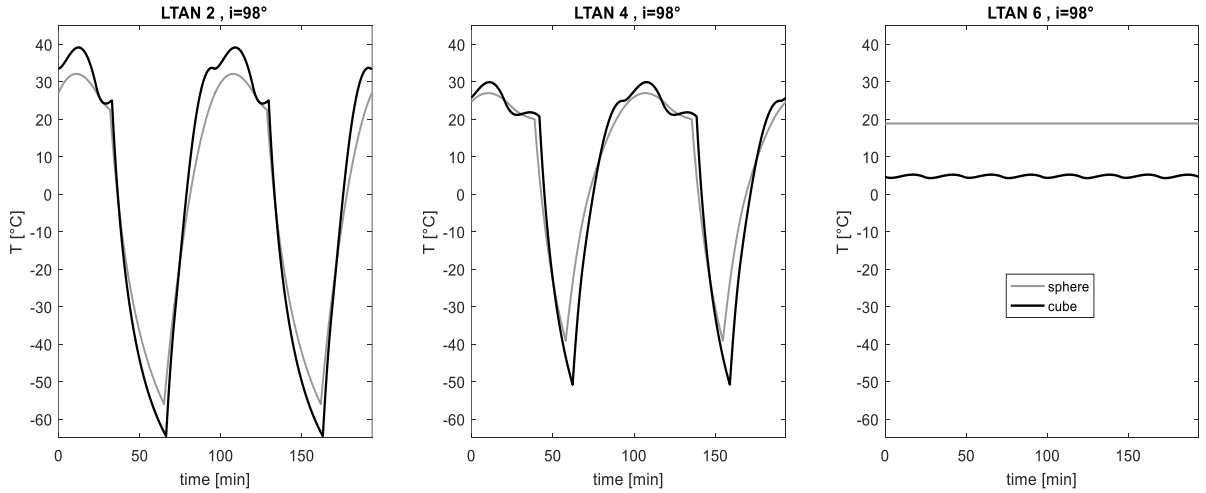


Figure 0.4 - Temperature evolution of a cube for different LTANs

D. Thermostat Directives for Active TCS

In the case operational cold case for high-power mission type, the temperature of the payload reaches its lower-bound temperature. The solution proposed in section 3.5.3 is the implementation of electrical heaters as an active thermal control for the payload.

Figure 0.5 presents the effect of different thermostat directives (m1, m2 and m3) for a same total energy consumption of the heaters. For similar results, the total installed power for electrical heaters is reduced by applying a powering during a longer period of time.

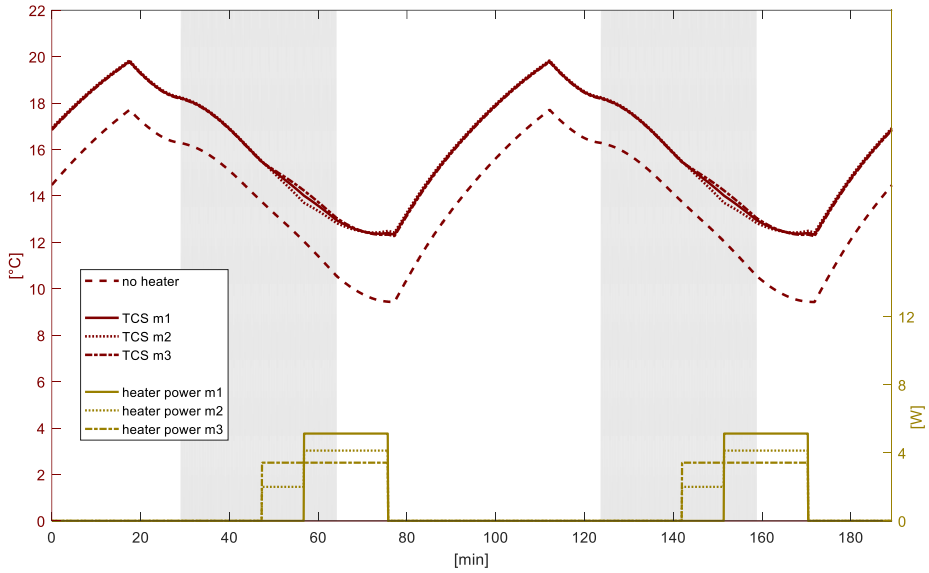


Figure 0.5 - Payload temperature and heaters consumption for different thermostat directives (high-power case)

E. Thermal Strap Location

The location of the thermal strap between the COM subsystem and the external assembly is addressed in section 3.5.4. Figure 0.6 plots the temperatures of interest of the satellite, in case of high-power, for two different configurations: in the top graph for a thermal strap linking the COM subsystem and the radiator and in the bottom graph for a strap linking the COM subsystem and the structure. The results are similar, one can even see a better management of the COM subsystem heat discharge in the second case.

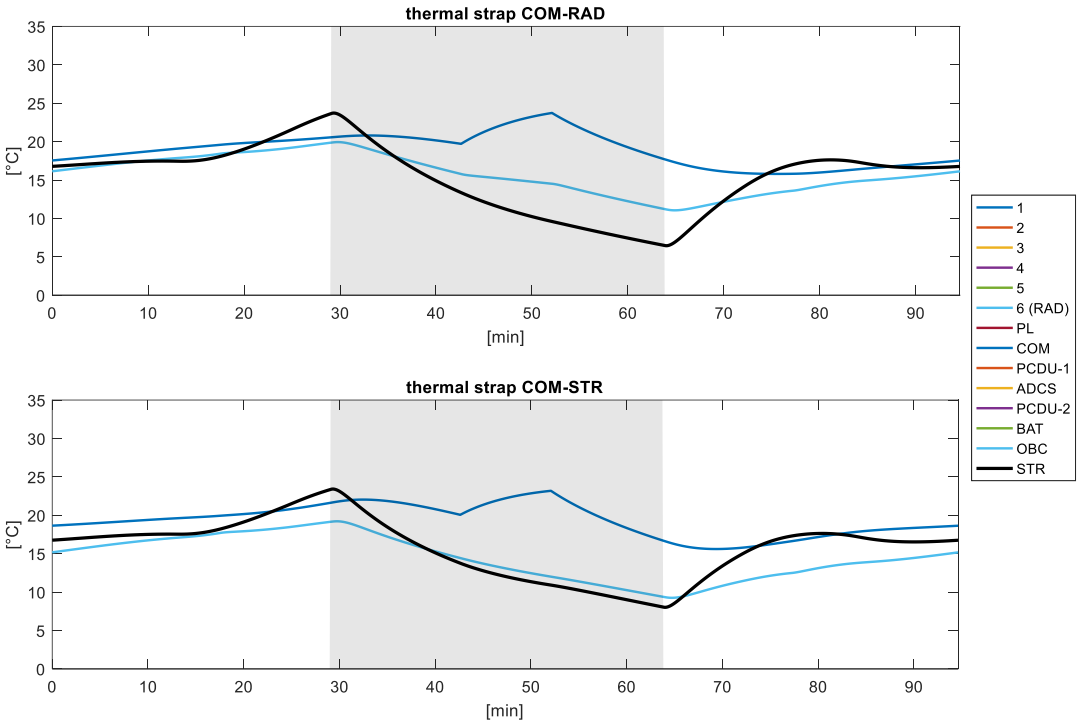


Figure 0.6 - Comparison of the COM thermal strap location (high-power case)

Bibliography

[1] E. Kulu, «Nanosatellite & CubeSat Database,» 10 June 2019. [Online]. Available: https://www.nanosats.eu/. [Accessed 1 July 2019].

[2] M. A. Swartwout, «CubeSat Database,» [Online]. Available: https://sites.google.com/a/slu.edu/swartwout/home/cubesat-database. [Accessed 1 July 2019].

[3] A. Space, «A Basic Guide to Nanosatellites,» [Online]. Available: https://alen.space/basic-guide-nanosatellites/. [Accessed 1 July 2019].

[4] D. Gilmore, «Spacecraft Thermal Control Handbook: Fundamental Technologies,» Aerospace Press, 2002.

[5] I. Martinez, «Spacecraft Thermal Control,» [Online]. Available: http://webserver.dmt.upm.es/~isidoro/. [Accessed 1 July 2019].

[6] R. Manley and P. Reynolds, «Climate Data Information - Albedo,» [Online]. Available: http://www.climatedata.info/forcing/albedo/. [Accessed 09 August 2019].

[7] J. Kaufman, «Properties and Characteristics of Aluminum and Aluminum Alloys,» ASM International, 2016.

[8] ISIS, «1-Unit CubeSat structure,» [Online]. Available: https://www.cubesatshop.com/product/1-unit-cubesat-structure/.

[9] M. A. Green, «Third Generation Phototvoltaics: Advanced Solar Energy Conversion,» *Springer,* n°112, 2003.

[10] GOMSpace, *NanoPower P110 datasheet,* 2018.

[11] DHV Technolgy, «CubeSat Solar panel DHV-CS-10,» [Online]. Available: https://www.cubesatshop.com/product/cubesat-solar-panels/.

[12] SpectroLab, *30.7% XTJ Prime datasheet,* 2018.

[13] AzurSpace, *Silicon Solar Space Cell S 32 datasheet,* 2016.

[14] EXA, «Deployable solar panels DSA/1A,» 2013. [Online]. Available: https://www.cubesatshop.com/product/solar-panels/.

[15] S.G.Bowden and C.B.Honsberg, «Photovoltaics Education Website, Effect of Temperature,» 2019. [Online]. Available: https://www.pveducation.org/pvcdrom/solar-cell-operation/effect-of-temperature.

[16] V. Khorenko et al., «BOL And EOL Characterization Of AZUR 3G Lilt Solar Cells For ESA Juice Mission,» 2016.

[17] N. Navarathinam, R. Lee and H. Chesser, «Characterization of Lithium-Polymer batteries for CubeSat applications,» *Acta Astronautica,* vol. 68, pp. 1752-1760, 2011.

[18] epec Engineered Technologies, «Battery Cell Comparision,» [Online]. Available: https://www.epectec.com/batteries/cell-comparison.html.

[19] NASA, «State of the Art Small Spacecraft Technology,» California, 2018.

[20] GOMSpace, *NanoPower Battery datasheet,* 2018.

[21] GOMSpace, *NanoPower BP4,* 2018.

[22] K. Li and K. J. Tseng, «Energy efficiency of lithium-ion battery used as energy storage devices in micro-grid,» chez *IECON 2015 - 41st Annual Conference of the IEEE Industrial Electronics Society*, 2015.

[23] P. Bugryniec, «CubeSat: The Need for More Power to Realise Telecommunications,» Sheffield, United Kingdom, 2016.

[24] X. Wang et al., «Effect of operation conditions on simulated low-earth orbit cycle-life testing of commercial lithium-ion polymer cells,» *Journal of Power Sources,* vol. 142, pp. 313-322, 24 March 2005.

[25] ClydeSpace, *Space Qualified Batteries datasheet,* 2011.

[26] I. Buchmann, «Battery University,» 2019. [Online]. Available: https://batteryuniversity.com/learn/.

[27] L. O. Valoen and M. I. Shoesmith, *The Effect Of PHEV And HEV Duty Cycles On Battery And Battery Pack Performance,* 2007.

[28] NanoAvionics, «Electrical Power System "EPS",» [Online]. Available: https://n-avionics.com/subsystems/cubesat-electrical-power-system-eps/.

[29] ClydeSpace, *CubeSate Power,* 2008.

[30] L Jasper et al, «HERMES, Colorado Space Grant Consortium (CoSGC),» 2008. [Online]. Available: https://spacegrant.colorado.edu/COSGC_Projects/co3sat/index.htm.

[31] CrystalSpace, «Crystalspace P1U "Vasik",» [Online]. Available: https://www.cubesatshop.com/product/crystalspace-p1u-vasik/.

[32] GOMSpace, *NanoPower P-series Datasheet,* 2014.

[33] Pumpkin, Inc., «CubeSat Kit, Datasheets, Linear EPS,» 2012. [Online]. Available: http://www.cubesatkit.com/content/datasheet.html.

[34] R. Mishra, «electronics cooling,» 2004. [Online]. Available: https://www.electronics-cooling.com/2004/02/the-temperature-ratings-of-electronic-parts/.

[35] ECE Paris school, «ECE3SAt - ADCS: Attitude Determination And Control System - Sensors ADCS,» 2017. [Online]. Available: http://www.ece3sat.com/cubesatmodules/adcs/.

[36] T. Lumbwe LwabanjiI, «Development of an onboard computer (OBC) for a CubeSat,» Bellville, 2013.

[37] J. M. Elliott, «The Thermal Design and Analysis of the CANX-4/-5 and NEMO-AM Nanosatellites,» Toronto, 2014.

[38] A. Farhat, J. Ivase, Y. Lu and A. Snapp, «Attitude Determination and Control System for CubeSat,» 2013.

[39] A. Slavinskis et al., «Attitude determination and control for centrifugal tether deployment on the ESTCube-1 nanosatellite,» *Proceedings of the Estonian Academy of Sciences,* vol. 63, p. 242–249, 2014.

[40] NewSpace, «NCTR-M002 Magnetorquer Rod,» [Online]. Available: https://www.cubesatshop.com/product/nctr-m002-magnetorquer-rod/.

[41] CubeSpace, «CubeWheel Small,» [Online]. Available: https://www.cubesatshop.com/product/cubewheel-small/.

[42] ClydeSpace, «High-Precision Attitude Determination and Control System (ADCS),» [Online]. Available: https://www.clyde.space/products/51-highprecision-attitude-determination-and-control-system-adcs.

[43] CubeSpace, «Cube ADCS,» [Online]. Available: https://www.cubesatshop.com/product/cube-adcs/.

[44] ISIS, «Magnetorquer Board Datasheet,» 2013. [Online]. Available: https://www.cubesatshop.com/wp-content/uploads/2016/06/iMTQ-Brochure-v1.pdf.

[45] Sinclair Interplanetary, «Reaction Wheels - 3 mNms Picosatellite Wheel,» 2018. [Online]. Available: http://www.sinclairinterplanetary.com/reactionwheels.

[46] NewSpace, «NSS Magnetometer,» [Online]. Available: https://www.cubesatshop.com/product/nss-magnetometer/.

[47] MAI, «MAI-SS Space Sextant - CubeSatShop,» 2017. [Online]. Available: https://www.cubesatshop.com/product/mai-ss-space-sextant/.

[48] M. Lankinen, «Design and Testing of Antenna Deployment System for Aalto-1 Satellite,» 2015.

[49] L. Abdul Halim et al., «A Review of Antennas for Picosatellite Applications,» *Hindawi - International Journal of Antennas and Propagation,* vol. 2017, 2017.

[50] ISIS, *ISIS VHF uplink/UHF downlink Full Duplex Transceiver brochure,* 2016.

[51] GOMSpace, *NanoCom ANT430,* 2018.

[52] GOMSpace, *NanoCom ANT2000 Datasheet,* 2017.

[53] NanoAvionics, «UHF Antenna,» [Online]. Available: https://n-avionics.com/subsystems/cubesat-uhf-antenna/.

[54] ClydeSpace, «CPUT S-Band Patch Antenna,» 2019. [Online]. Available: https://www.clyde.space/products/13-cput-sband-patch-antenna.

[55] NASA, *Iris V2.1 CubeSat Deep Space Transponder,* 2016.

[56] ClydeSpace, *CPUT VUTRX,* 2019.

[57] SpaceCom, «HiSPiCO S Band Transceiver 06-19,» 2019. [Online]. Available: https://www.iq-spacecom.com/images/downloads/HISPICO_Datasheet_06.2019.pdf.

[58] IMT, «Cubesat On-Board Computer,» 2016. [Online]. Available: http://www.imtsrl.it/obc-cubesat.html.

[59] CubeSpace, «Cube Computer,» 2016. [Online]. Available: https://www.cubesatshop.com/product/cube-computer/.

[60] ISIS, *On Board Computer (iOBC) Brochure,* 2014.

[61] XCAM, *C3D CubeSat Camera,* 2014.

[62] GOMSpace, *NanoCam C1U,* 2017.

[63] SCS Space, «SCS Gecko imager,» 2017. [Online]. Available: https://www.cubesatshop.com/product/scs-gecko-imager/.

[64] SAC, «Chameleon Imager,» 2018. [Online]. Available: https://www.cubesatshop.com/product/chameleon-imager/.

[65] ECSS, «Space engineering - Thermal design handbook - Part 6: Thermal Control Surfaces,» 2011.

[66] QIOPTIQ, Optical Solar Reflectors. [Online]. Available: http://www.qioptiq.com/space.html

[67] Sheldahl, «Product bulletin,» 2019. [Online]. Available: https://www.sheldahl.com/sites/default/files/2017-09/Radiator%20SSM_0.pdf.

[68] Thermotive, «Space Flight Heritage,» 2017. [Online]. Available: http://thermotive.com/thermalstraps.html.

[69] Thermal Space, «Highest Performance Thermal Straps for All Applications,» 2015-2016. [Online]. Available: https://thermal-space.com/thermal-straps/.

[70] Advanced Cooling Technologies, «Heat Pipes For Thermal Management,» 2019. [Online]. Available: https://www.1-act.com/innovations/heat-pipes/.

[71] Bergquist, «Thermal Interface Pad, Fibreglass, 0.9W/m · K 0.178mm,» [Online]. Available: https://befr.rs-online.com/web/p/thermal-pads/1692256/.

[72] J. Berg, *CryoCube-1: A Cryogenic Fluid Management CubeSat,* Cocoa Beach, FL: NASA Kennedy Space Center, 2013.

[73] Cryogenic Engineering Group, «Cryocoolers for space applications,» University of Oxford, [Online]. Available: http://www2.eng.ox.ac.uk/cryogenics/research/cryocoolers-for-space-applications.

[74] J. H. Henninger, «Solar Absorbance and Thermal Emittance of Some Common Spacecraft Thermal-Control Coatings,» *NASA Reference Publication 1121,* 1984.

[75] F. J. Franquiz et al., «Attitude Determination and Control System Design for a 6U CubeSat for Proximity Operations and Rendezvous,» Embry-Riddle Aeronautical University, Daytona Beach, FL, 32114, USA, 2017.

[76] B. Udrea, M. Nayak and F. Ankersen, «Analysis of the Pointing Accuracy of a 6U CubeSat Mission for Proximity Operations and Resident Space Object Imaging,» 2013.

[77] M. Pastena and J. Barrington-Brown, «Comparison of Magnetorquer,» 2010. [Online]. Available: http://mstl.atl.calpoly.edu/~bklofas/Presentations/SummerWorkshop2010/Barrington-Brown-magnetorquer.pdf.

[78] Berlin Space Technologies, «IADCS,» 2019. [Online]. Available: https://www.berlin-space-tech.com/portfolio/iadcs/.

[79] CubeSpace, «Cube ADCS,» [Online]. Available: https://www.cubesatshop.com/product/cube-adcs/.

[80] KULeuven, «KU Leuven ADCS,» [Online]. Available: https://www.cubesatshop.com/product/kul-adcs/.

[81] MAI, «MAI-400 ADACS,» 2016, [Online]. Available: https://www.cubesatshop.com/product/mai-400-adacs/.

[82] Spacefligh101.com, «Corvus-BC,» 2019. [Online]. Available: http://spaceflight101.com/meteor-m-2-1/corvus-bc/.

[83] Simera Sense, «xScape100 Technical specification sheet,» [Online]. Available: https://www.simera.com/wp-content/uploads/2018/07/Simera-Sense-xScape100-tech-data-sheet-230718A-1.pdf.

[84] L. C. Chang et al., «IDEASSat: The Ionosphere Dynamics Explorer and Attitude Subsystem Satellite,» chez *32nd Annual AIAA/USU Conference on Small Satellites - SSC18-WKIV-06*, 2018.

[85] U. Eren et al., «Design of a Flexible Nanosatellite Bus for Science Missions,» chez *AIAA SPACE*, Pasadena, California, 2012.

[86] C. Cupido, C. Nokes and A. Hamilton, «Ex-Alta 1 Design Overview Report,» 2014.

[87] L. Chang, «A Preliminary Design for the InSPiRESat-1 Mission and Satellite Bus,» 2016.

[88] A. Aslan et al., «BEEAGLESAT and HAVELSAT: Two 2U CubeSat's for QB50,» 2017.

[89] J. Straub, «OpenOrbiter: A Low-Cost, Educational Prototype CubeSat Mission Architecture,» *machines,* 24 january 2013.

[90] D. Schklar, «OUFTI-Next Nanosatellite: Feasibility Study and Mission Assessment,» 2017.

[91] Mitsubishi Gas Chemical, «High Performance FR-4 for Multi-layered PWB,» [Online]. Available: https://www.mgc.co.jp/eng/products/sc/fr4.html. [Accès le 31 July 2019].

[92] R. J. Boain, *A-B-Cs of Sun-Synchronous Orbit Mission Design,* 2004.

[93] E. Dmitriev, «CubeSat Smart Frame,» Grabcad, 2015. [Online]. Available: https://grabcad.com/library/cubesat-smart-frame-1.

[94] eoPortal Directory, «CANYVAL-X (CubeSat Astronomy by NASA and Yonsei using Virtual Telescope Alignment eXperiment),» 2018. [Online]. Available: https://directory.eoportal.org/web/eoportal/satellite-missions/content/-/article/canyval-1.

[95] PC/104 Embedded Consortium, «PC/104 Specifications,» 2001.

[96] EXA, «Deployable solar panels DSA/1A,» 2013. [Online]. Available: https://www.cubesatshop.com/product/solar-panels/.

[97] Sheldahl, «The Red Book - Thermal Control Overview,» [Online]. Available: https://www.sheldahl.com/technology/thermal-control-materials/the-red-book. [Accès le 31 July 2019].

[98] A. Kellens, «Thermal design of the OUFTI-Next mission,» Liège, 2018.

[99] A. Lidbeck and K. R. Syed, «Experimental Characterization of Li-ion Battery cells for Thermal Management in Heavy Duty Hybrid Applications,» Gothenburg, Sweden, 2017.

[100] I. Alet, «Contrôle thermique des engins spatiaux,» 1998.

[101] L. Jacques, «Thermal Design of the Oufti-1 nanosatellite,» 2009.

[102] P. Zarchan, «Engineering 360 - Satellite Thermal Control for Systems Engineers,» 1998. [Online]. Available: https://www.globalspec.com/reference/39126/203279/v-louvers.

[103] T. Tritt, «Thermoelectric Materials: Principles, Structure, Properties, and Applications,» *Encyclopedia of Materials: Science and Technology,* 2002.

[104] A. Silmi, «Grabcad,» 19 June 2015. [Online]. Available: https://grabcad.com/library/cubesatlego-1.

[105] J. Rossie, «AerospaceEd.org,» 2006. [Online]. Available: http://www.rossie.com/layer4x.jpg.

[106] G. Quinsac, «Les CubeSats,» 2018. [Online]. Available: http://sesp.esep.pro/fr/pages_nanosats/impression.html.

[107] P. Platzer, «exploded view of ArduSat,» 2012. [Online]. Available: https://commons.wikimedia.org/wiki/File:ArduSat3.png.

[108] P. Fortescue, G. Swinerd and J. Stark, Spacecraft Systems Engineering, 3 éd., Ltd London: John Wiley & Sons , 2003, p. 369.

[109] J. P. Mason, B. Lamprecht, T. N. Woods and C. Downs, «CubeSat On-Orbit Temperature Comparison to Thermal-Balance-Tuned Model Predictions,» 2017.

[110] C. Lafleur, «Spacecraft Encyclopedia,» 2014. [Online]. Available: http://claudelafleur.qc.ca/Spacecrafts-2014.html.

[111] Clodoweg, «La lumière des étoiles,» 19 September 2015. [Online]. Available: https://www.psaltery.org/wordpress/la-lumiere-des-etoiles/.

[112] S. Chandrashekar, «Thermal Analysis and Control of MIST CubeSat,» Stockholm, Sweden, 2017.

[113] M. CERF, «Low-Thrust Transfer Between Circular Orbits Using Natural Precession,» *Journal of Guidance Control and Dynamics 39,* March 2015.

[114] Y. A. e. a. Cengel, *Fundamentals of Thermal-Fluid Sciences,* McGraw-Hill, 2008.

[115] P. S. Anderson, «NASA Skunkworks Team Designs Advanced New 'Dellingr' CubeSat,» America Space, 2014. [Online]. Available: https://www.americaspace.com/2014/11/19/nasa-skunkworks-team-designs-advanced-new-dellingr-cubesat/.

[116] B. Anderson, C. Justus and G. W. Batts, «Guidelines for the Selection of Near-Earth Thermal Environment Parameters for Spacecraft Design,» 2001.

[117] Gunter's Space Page, «UBAKUSAT (UBAK-3U-SAT),» 2018. [Online]. Available: https://space.skyrocket.de/doc_sdat/ubakusat.htm.

[118] University of Leuven (Belgium), «The first billboard in space,» 2015. [Online]. Available: http://spacebillboard.com/mission/. [Accessed 1 July 2019].

[119] MyHeatSink, «Standard Heat Pipes,» 2019. [Online]. Available: https://myheatsinks.com/heat-pipe-solutions/standard-heat-pipes/.

[120] AASC, «Spacecraft Thermal Radiators,» 2019. [Online]. Available: https://www.aascworld.com/portfolio/thermal-radiator/.

[121] eoPortal, «Satellite Missions Database,» 2000-2019. [Online]. Available: https://directory.eoportal.org/web/eoportal/satellite-missions.

[122] Australian Space Academy, «Radio frequencies for space communication,» [Online]. Available: https://www.spaceacademy.net.au/spacelink/radiospace.htm.

[123] Pcbcart, «PCB Materials,» [Online]. Available: https://www.pcbcart.com/pcb-capability/pcb-materials.html.

[124] NewSpace, «NSS Fine Sun Sensor,» [Online]. Available: https://www.cubesatshop.com/product/digital-fine-sun-sensor/.

[125] Design World, «New Line of Flexible Heaters,» 2008. [Online]. Available: https://www.designworldonline.com/new-line-of-flexible-heaters/.

[126] GOMSpace, *NanoPower P60 Dock,* 2019.

[127] GOMSpace, *NanoPower P31u Datasheet,* 2019.

[128] ISIS, «ISIS 6U CubeSat,» 2018. [Online]. Available: https://www.isispace.nl/wp-content/uploads/2018/07/ISIS-6U-CubeSat-Brochure.pdf.

[129] Discover, Energy Corp., «http://www.heliant.it/images/FV/ev_temperature_effects.pdf,» 2015. [Online]. Available: http://www.heliant.it/images/FV/ev_temperature_effects.pdf.

[130] Parker, «How to Identify Quality Thermal Gap Fillers in Four Steps,» 2019. [Online]. Available: http://blog.parker.com/how-to-identify-quality-thermal-gap-fillers-in-four-steps.

[131] AMSAT-UK, «Help Track ISS CubeSats,» 2013. [Online]. Available: https://amsat-uk.org/2013/11/19/help-track-iss-cubesats/.

[132] Endurosat, «Custom C-Band Patch Antenna,» 2019. [Online]. Available: https://www.endurosat.com/cubesat-store/all-cubesat-modules/custom-c-band-patch-antenna/.

[133] ISIS, «CubeSat dipole antenna system,» 2010. [Online]. Available: https://www.isispace.nl/product/dipole-antenna-system/.

[134] IMT, *Cubesat Battery Pack.*

[135] ECM Space, «Applicable CubeSat sizes,» 2019. [Online]. Available: https://www.ecm-space.de/index.php/launch-adapters-h/cubesat-sizes.

[136] ITACA, «A Guide To Photovoltaic Panels,» [Online]. Available: https://www.itacanet.org/a-guide-to-photovoltaic-panels/photovoltaic-pv-cells/.

[137] T. Halt and A. Wieger, *Smallsats by the Numbers 2019 - Bryce Space and Technology,* 2019.

UNIVERSITÉ CATHOLIQUE DE LOUVAIN
École polytechnique de Louvain
Rue Archimède, 1 bte L6.11.01, 1348 Louvain-la-Neuve, Belgique | **www.uclouvain.be/epl**